DESIGN, MODELING, GUIDANCE AND CONTROL OF A VERTICAL LAUNCH SURFACE TO AIR MISSILE

A THESIS SUBMITTED TO
THE GRADUATE SCHOOL OF NATURAL AND APPLIED SCIENCES
OF
MIDDLE EAST TECHNICAL UNIVERSITY

BY

RAZİYE TEKİN

IN PARTIAL FULFILLMENT OF THE REQUIREMENTS
FOR
THE DEGREE OF MASTER OF SCIENCE
IN
ELECTRICAL AND ELECTRONICS ENGINEERING

SEPTEMBER 2010

Approval of the thesis:

DESIGN, MODELING, GUIDANCE AND CONTROL OF A VERTICAL LAUNCH SURFACE TO AIR MISSILE

Submitted by **RAZİYE TEKİN** in partial fulfillment of the requirements for the degree of **Master of Science in Electrical and Electronics Engineering Department, Middle East Technical University** by**,**

Prof. Dr. Canan Özgen _____
Dean, Graduate School of **Natural and Applied Sciences**

Prof. Dr. İsmet Erkmen _____
Head of Department, **Electrical and Electronics Engineering**

Prof. Dr. M. Kemal Leblebicioğlu _____
Supervisor, **Electrical and Electronics Engineering Dept., METU**

Dr. Özgür Ateşoğlu _____
Co-Supervisor, **Mechanical Engineering Dept., METU**

Examining Committee Members:

Prof. Dr. Mübeccel Demirekler _____
Electrical and Electronics Engineering Dept., METU

Prof. Dr. M. Kemal Leblebicioğlu _____
Electrical and Electronics Engineering Dept., METU

Prof. Dr. Aydan Erkmen _____
Electrical and Electronics Engineering Dept., METU

Prof. Dr. M. Kemal Özgören _____
Mechanical Engineering Dept., METU

Assist. Prof. Dr. Ali Türker Kutay _____
Aerospace Engineering Dept., METU

Date: _____

I hereby declare that all information in this document has been obtained and presented in accordance with academic rules and ethical conduct. I also declare that, as required by these rules and conduct, I have fully cited and referenced all material and results that are not original to this work.

Name, Surname: Raziye, Tekin

Signature:

ABSTRACT

DESIGN, MODELING, GUIDANCE AND CONTROL OF A VERTICAL LAUNCH SURFACE TO AIR MISSILE

Tekin, Raziye

M.Sc., Electrical and Electronics Engineering Department

Supervisor: Prof. Dr. M. Kemal Leblebicioğlu

Co-Supervisor: Dr. Özgür Ateşoğlu

September 2010, 153 Pages

The recent interests in the necessity of high maneuverability and vertical launching triggered namely the unconventional control design techniques that are effective at high angle of attack flight regimes. For most of missile configurations, this interest required thrust vector control together with conventional aerodynamic control.

In this study, nonlinear modeling and dynamical analysis of a surface to air missile with both aerodynamic and thrust vector control is investigated. Aerodynamic force and moment modeling of the presented missile includes the challenging high angle of attack aerodynamics behavior and the so called hybrid control, which utilizes both tail fins and jet vanes as control surfaces. Thrust vector and aerodynamic control effectiveness is examined during flight envelope. Different autopilot designs are accomplished with hybrid control. Midcourse and terminal guidance algorithms are implemented and performed on target sets including maneuverable targets. A different initial turnover strategy is suggested and compared with standard skid-to-turn maneuver. Comparisons of initial roll with aerodynamic and

thrust vector control are examined. Afterwards, some critical maneuvers and hybrid control ratio is studied with a real coded genetic algorithm. Rapid turnover for low altitude targets, intercept maneuver analysis with hybrid control ratio and lastly, engagement initiation maneuver optimization is fulfilled.

Keywords: Vertical Launch Surface to Air Missile, High Angle of Attack, Thrust Vector Control, Hybrid Control, Rapid Turnover, Skid-to-Turn, Initial Roll Maneuver, Maneuver Optimization, Optimal Hybrid Control Ratio.

ÖZ

DİK FIRLATILAN KARADAN HAVAYA BIR FUZENİN TASARIM, MODELLEME, GUDUM VE KONTROLÜ

Tekin, Raziye

Yüksek Lisans, Elektrik ve Elektronik Mühendisliği Bölümü

Tez Yöneticisi: Prof. Dr. M. Kemal Leblebicioğlu

Ortak Tez Yöneticisi: Dr. Özgür Ateşoğlu

Eylül 2010, 153 Sayfa

Yüksek manevra kabiliyeti gereksinimi ve dik fırlatma özelliği, yüksek hücum açılarında etkin olan geleneksel olmayan kontrol teknolojilerini tetiklemiştir. Bir çok füze uygulamalarında, bu istek aerodinamik kontrol ile birlikte itki vektör kontrol teknolojilerinin kullanımını gerektirmektedir.

Bu çalışmada, dik fırlatılan aerodinamik ve itki vektör kontrol teknolojilerine sahip bir füzenin doğrusal olmayan modellemesi ve dinamik analizi yapılmıştır. Aerodinamik kuvvet ve moment modellemesi, farklı davranışlara sahip yüksek hücum açısı aerodinamik özellikleri içermektedir. Bu model üzerinde itki vektör kontrol ve aerodinamik kontrolün etkinlik analizleri yapılarak, uçuş safhalarında etkinliklikleri belirlenmiştir. Aerodinamik ve itki vektör kontrol yüzeylerinin birlikte hareket ettirildiği (karma kontrol) kontrol tipi kullanılmıştır. Farklı otopilot tasarımları karma bu kontrol yapısı içerisinde hazırlanmıştır. Arafaz ve son güdüm algoritmaları modellenmiş ve manevra yapan hedefler de dahil olmak üzere çeşitli hedefler üzerinde performansları değerlendirilmiştir. Kayarak dönen füze yaklaşımı, ilk dönüş manevrası için değiştirilmiş ve farklı bir dönüş manevrası önerilmiştir. Sonrasında, kritik manevraları ve karma kontrol katsayısı gerçek

kodlu bir genetik algoritma ile eniyilenmeye çalışılmıştır. Eniyileştirme çalışmaları, alçak irtifadaki hedefler için hızlı dönüş manevrası, karma kontrol oranı ile birlikte yakalama manevrası ve son olarak da çarpışma manevrasına yönelik olarak yapılmıştır.

Anahtar Kelimeler: Karadan Havaya Dik Fırlatılan Füze, Yüksek Hücum Açısı, İtki Vektör Kontrol, Karma Kontrol, Hızlı Dönüş, Kayarak Dönen, İlk Yuvarlanma Manevrası, Manevra Eniyilemesi, Eniyi Karma Kontrol Oranı.

ACKNOWLEDGEMENTS

The author thanks to Prof. Dr. Kemal Leblebicioğlu for his guidance, advice, criticism, and insight throughout the thesis.

The author thanks to Dr. Özgür Ateşoğlu for his kind support, motivation and encouragement all the time. Even though he was not in Turkey during the last parts of the study, his comments were valuable.

The author thanks to the following individuals from Roketsan: Koray S. Erer for his support and criticism. İbrahim Kaya for his support in the preparation of the Appendix. Kazım Küçükturhan for his support and understanding. Dr. Yavuk Aka and Dr. Sartuk Karasoy for their support.

TABLE OF CONTENTS

LIST OF FIGURES

FIGURES

LIST OF TABLES

TABLES

LIST of SYMBOLS

X, Y, Z	Axes of earth fixed reference frame
x, y, z	Axes of body fixed reference frame
$\hat{C}^{(a,b)}$	Orthogonal transformation matrix that represents a transformation from frame F_b to frame F_a.
$\vec{u}_i^{(a)}$	i[th] unit basis vector of reference frame F_a
$\hat{C}^{(e,b)}$	Direction cosine matrix
ϕ, θ, ψ	Euler angles (in roll, pitch and yaw planes)
V_x, V_y, V_z	Velocity components in earth fixed reference frame
u, v, w	Velocity components in body fixed reference frame
p, q, r	Components of angular velocity in the body fixed reference frame with respect to the earth fixed reference frame
$\vec{F}$	Sum of all externally applied forces to the missile
$\vec{V}_M$	Total missile velocity
m	Missile mass
F_x, F_y, F_z	Components of total force acting on the missile expressed in the body frame
$\vec{M}$	Sum of all externally applied torques to the missile
$\vec{H}$	Angular momentum of the missile
$\breve{J}$	Inertia dyadic
$\hat{J}$	Inertia matrix
I_{xy}, I_{xz}, I_{yz}	Cross inertia terms
I_{xx}, I_{yy}, I_{zz}	Elements of inertia matrix

M_x, M_y, M_z	Components of moment acting on the missile expressed in the body frame
$F_{A_x}, F_{A_y}, F_{A_z}$	Aerodynamic force components
$M_{A_x}, M_{A_y}, M_{A_z}$	Aerodynamic moment components
$F_{T_x}, F_{T_y}, F_{T_z}$	Thrust force components
$M_{T_x}, M_{T_y}, M_{T_z}$	Thrust moment components
g_x, g_y, g_z	Body frame components of the gravitational acceleration
Q	Dynamic pressure
A	Cross sectional area of the missile
d	Missile diameter
ρ	Air density
ρ_0	Air density at sea level
h	Altitude
$\delta_a, \delta_{Ae}, \delta_{Ar}$	Aerodynamic control surface deflections (aileron, elevator, rudder)
δ_{Te}, δ_{Tr}	Thrust vector control surface deflections (elevator, rudder)
K	Hybrid control ratio
α	Angle of attack
β	Sideslip angle
γ	Flight path angle
M	Mach number
C_x	Axial force coefficient
C_y	Side force coefficient
C_z	Normal force coefficient
C_l	Rolling moment coefficient
C_m	Pitching moment coefficient
C_n	Yawing moment coefficient
C_D	Drag force coefficient

C_L	Lift force coefficient
ω_n	Natural frequency of a second order system
ζ	Damping ratio
N	Navigation constant
λ	Line-of-sight angle
ϕ_{com}	Roll angle command
θ_{com}	Pitch angle command
λ_{AZ}	Azimuth angle
λ_{EL}	Elevation angle
R_C	Closing distance
θ_T	Thrust deflection in pitch plane
ψ_T	Thrust deflection in yaw plane
ε	Look angle
AoA	Angle of attack
K1, K2, K3	Controller gains
DoF	Degree of freedom
TVC	Thrust vector control
FOV	Field of view
LTI	Linear time invariant
LTV	Linear time varying
PNG	Proportional navigation guidance
A	System matrix
B	Control matrix
C	Output matrix
x	State vector
VLSAM	Vertical Launch Surface to Air Missile
LOS	Line of Sight
DCM	Direction Cosine Matrix

CHAPTER 1

INTRODUCTION

Since their development in the early 1900's, missiles have become an increasingly critical element in modern warfare. A historical review of early missile development can be found in [1]. In general missile systems can be categorized into two classes: strategic or tactical. Strategic missiles are designed to travel long distances towards known, stationary targets. Tactical missiles track or intercept shorter range, maneuvering and non-maneuvering targets where its guidance and control technologies turn out to be more critical [2]. Strategic missiles primarily operate in exoatmospheric conditions while tactical missiles most commonly operate in endoatmospheric conditions. In modern warfare, new technologies are growing faster. As the capability of aircrafts are increasing, missile capabilities are increasing in parallel to their development. Tactical missiles require higher turn rates and larger maneuverability envelopes while reduced storage values. Hence, high angle of attack maneuver regime and lateral acceleration capability is increasing which leads to unconventional missile control technologies. Some advanced missiles combine classical control technologies with thrust vector control technologies and/or side jet technologies. The jet vane thrust vector control technique begins with German V-2 missile and it is still in progress with different types of thrust vector control technologies. Vertical launch missile systems are one of the applications of which use thrust vector control. Vertical launch of a tactical missile was performed at least as early as 1967 and since then has attracted interest in different areas. Vertical launch-MICA, Evolved Sea Sparrow, IRIS-T, Umkhonto and BrahMos are some of vertical launch missile systems which are

being developed on or in progress with different control technologies. As it can easily be guessed, vertical launch missile systems fall into the critical technologies; this explains why the literature on this topic is limited or almost nonexistent.

In trainable launcher missile systems, missile is pointed to the target with launcher. However, in vertical launch missile systems, guidance and control unit has to direct the missile to the target; thus, designing guidance and control units of vertical launch missile systems is very important. Guidance and control algorithms should have the capability to cover all of the space because of oncoming threats. The first and most important challenge these systems encounter is the high angle of attack behavior. Then, as these missile systems' reach high velocities in a very short time, their dynamics change very fast; this behavior requires additional control design effort. Before autopilot design, dynamics have to be analyzed carefully. For example, in many conventional systems, boost phase control is ignored even though it is critical for these systems. Guidance algorithm, mostly midcourse guidance algorithm has to be considered, because terminal guidance phase is usually done with the proportional navigation which is effective and easy to implement. But if, a further performance is required, terminal guidance phase has to be taken into account carefully.

1.1 Motivation

The main aim of this thesis comes from the rarity of literature in agile dynamics including the high angle of attack flight regime with aerodynamic and thrust vector control. As it is well known there are many studies on autopilot and guidance design of missiles, but many of them are point mass models, three degrees of freedom with limited aerodynamic database and with constant mass and inertia. So, many of the high order autopilot and guidance algorithms are easier to implement. However, it is not so easy to work with highly nonlinear dynamical systems with complex control capabilities. Control of agile dynamics is also a challenging issue.

There are some studies based on agile dynamics and control with different missile control technologies. [3] describes agile dynamics with thrust vector control and

reaction jet control systems. Even though the mathematical models are presented, control application and some of the keynotes are not mentioned. One of the other open issues in this study is that it mentions about the fact that acceleration autopilot in boost phase of the missile is not applicable, and so it is not preferred. [4] is about an application based reaction jet control system. In that study, autopilot is divided into three sections and high angle of attack regime is simplified. However, neither of the studies present full order aerodynamic database. [5] is an application paper of Evolved Sea Sparrow missile. In literature, [5] and [6] mention the angle of attack values during turnover maneuvers. [6] is the only published study available to the public on vertical launch turnover concept with a simplified mathematical model. So the values of some critical parameters, states, etc. in these papers, such as angle of attack, turn rates, thrust vector control effectiveness were very valuable during most of the phases of this thesis work.

There are published studies in the library of METU about thrust vector control. [7], [8] are master theses and [9] is a doctorate thesis. [7] was published in 1989 and it describes especially the thrust vector control technologies and [8] is based on secondary injection design and analysis process in computational fluid dynamics. However, the master studies mentioned are not exactly on the concept of system dynamics and control. [9] is on high angle of attack flight regime of fighter aircrafts and we have been motivated by this study mostly.

Even though the worldwide literature on thrust vector control and vertical launch systems is scarce, there are many countries with advanced military technologies working hard on the development of such systems. However there is limited or almost no study and not enough experience with thrust vector control systems yet in Turkey. So, vertical launch missile design with both aerodynamic and thrust vector control is considered in this thesis with the aim of being as realistic as possible. It was also very exciting to obtain rather significant results and present them. It is our hope that this thesis will lead to many new studies in this area in Turkey.

1.2. Contributions

In this thesis, a vertical launch missile design strategy with enhanced control capability is presented. Six degrees of freedom model of vertical launch missile with both tail fins as aerodynamic control surfaces and jet vanes as thrust vector control surfaces is described in details. Aerodynamic and thrust vector control surfaces are used as elements of the hybrid (using both the aerodynamic and thrust vector control surfaces simultaneously) control strategy.

In order to satisfy tactical requirements, high angle of attack regime is studied. An aerodynamic database including high angle of attacks ($-90 < \alpha < 90$) is generated. As the literature in this area is highly confidential and there is not available aerodynamic database, aerodynamic database is examined and presented in details.

Control effectiveness analysis of aerodynamic control and thrust vector control is performed and this analysis illustrated the known fact that low dynamic pressure results in less control effectiveness. [3] presents control effectiveness of RCS and aerodynamic control between 0.1 and 1 Mach, but it is not presented for jet vanes. There are no other works on the related issue to our knowledge.

Jet vanes and tail fins are coupled as in applications and a hybrid ratio selection method is presented. In the related parts of the study, real coded genetic algorithm is used to optimize hybrid control ratio and an approach to design the hybrid control ratio is suggested. In literature, hybrid control ratio suggestion and an optimization procedure is not presented and not examined.

There are many autopilot studies with different approaches, however as the flight, velocity profile and the angle of attack region is wide, we carried doubt about the possibility to have successive autopilots using classical control methods. In the thesis, it is demonstrated that this is quite possible.

A midcourse guidance approach is proposed after vertical launch, and illustrated with simulation results. This strategy is combined with proportional navigation guidance and effectiveness of the guidance algorithm on several targets is presented emphasizing that these methods can be useful for practical applications.

In addition to these, a different strategy is suggested during turnover from vertical launch. The suggested methodology depends on initial roll maneuver during vertical flight and after initial roll maneuver missile is controlled as in its standard form which is skid to turn. The suggested turnover strategy and its results are also new as far as we know in the open literature. Sharing all of the key points is also significant.

Finally an optimal guidance strategy is implemented for initial guidance phase. This strategy is related with different purposes of missile technology such as erodable or jettisoned jet vanes design process and it is shown that it is theoretically applicable. So, the presented values in the study such as 60 degrees of angle of attack, 350 degrees per second body rates, thrust deflection limit, actuator frequency are very significant.

The papers which are originated with this thesis are given below.

“Modeling and Vertical Launch Analysis of an Aero- and Thrust Vectored Surface to Air Missile”, at “AIAA 2010 GNC/AFM/MST/ASC/ASE” Conference which is about aerodynamic and dynamic modeling and results.

“Çevik Füze Dinamiği ve Denetimi Üzerine Temel İncelemeler”, at “Ulusal Havacılık ve Uzay Konferansı”, which is about the highly varying body rate dynamics and control.

“Hibrit Kontrollü - Dikey Fırlatılan Bir Hava Savunma Füzesinin Dinamiği ve Hızlı Dönüş Manevrası için Otopilot Tasarımı”, at “Otomatik Kontrol Ulusal Toplantısı 2010”, which is on mostly angle autopilot design and results.

“İleri Hız Değişiminin Füze Yanal Dinamiğine Etkileri Üzerine Bir İnceleme”, at “Otomatik Kontrol Ulusal Toplantısı 2010”, which is about acceleration dynamics of the nonlinear system.

“Bir Hava Savunma Füzesinin Dikey Fırlatma Fazının ve Etkin Dönme Manevralarının İncelenmesi”, at “5. Savunma Teknolojileri Kongresi”, which is carried on the pitch plane and comprise the parameters for turnover parameters and thrust profile selection.

The ongoing paper studies are about optimal rapid turnover for low altitude targets, intercept positioning maneuver analysis with optimal hybrid control ratio, and engagement initiation maneuver optimization. Lastly a mixed control strategy with all control deflections will be considered.

1.3. Outline

Chapter 2 is a brief overview on vertical launching, vertical launch surface to air missiles and control technologies on these missile systems. Chapter 3 describes the dynamical modeling of vertical launch missile including high angle of aerodynamics, thrust vector force and moments. In nonlinear modeling, aerodynamic forces, moments, gravity and parameters changing with respect to time such as mass, center of gravity, and inertia are included. Chapter 4 provides the final specifications and characteristics of the designed missile. Aerodynamic characteristics, thrust vector and aerodynamic control effectiveness, stability are analyzed in details. Chapter 5 is about autopilot design and performance results of the autopilots. Different autopilots such as angle, rate and acceleration are designed for different purposes also related with possible guidance strategies. Conventional guidance algorithms for midcourse and terminal phase are designed in Chapter 6. The midcourse guidance phase is similar to body pursuit guidance and proportional navigation guidance is modeled for the terminal guidance phase. Their performances are tested on different target sets, including low altitude, weaving and diving targets. Chapter 7 presents a different turnover algorithm together with

its analysis and comprises it with the turnover strategy expressed in Chapter 6. Chapter 8 is for the optimization processes for some maneuvers of vertical launch missiles with a real coded genetic search algorithm. These maneuvers are about optimal rapid turnover for low altitude targets, intercept maneuver analysis with optimal hybrid control ratio, and engagement initiation maneuver.

CHAPTER 2

A BRIEF OVERVIEW ON VERTICAL LAUNCH AND RELATED ISSUES WITH VERTICAL LAUNCH MISSILES

Vertical Launch System (VLS) is an arrangement for launching guided missiles vertically from a canister; see Figure 1, [10]. This maximizes weapon storage space and availability as well as minimizing complexity. The launch system is open to the sky which means missile is not pointed to the target or aligned. They rely on their guidance to align them once they have left the launch system. Typically, these systems are used aboard naval vessels (Figure 2), where space is tightly constrained and complex systems (such as moving launchers or reloading rails) are difficult to maintain.

Figure 1 Vertical Launch System [11]

Figure 2 Vertical Launch Concept for Naval Vessels [5]

Vertical launch prevents several attractive features over trainable launch systems. First, it provides more missiles at one firing process. Figure 3 shows a trainable launcher. Trainable launchers are capable of firing a limited missile before the launcher must be trained back to the reload position. This loss of time could be critical in the high density raid scenario. On the other hand, a vertically launched system utilizes missiles stored in clustered, sealed canisters above or below deck. The canisters serve as the firing platform for missiles as well as for shipping and handling. Thus, due to the vertical box launcher concept, the entire missile can be fired in a few seconds resulting in a substantial increase the number of missiles fired over trainable launchers.

Figure 3 Trainable Launcher [12]

A second advantage that vertical launch offers over trainable is the all aspect coverage. Trainable launchers require several installations on each side of the ship, since the ship's superstructure eliminates certain zones of fire from each launcher. This poses the problem of possible exhaustion in a saturation raid while the other systems, which are partially full, cannot be brought to bear on the threat. In a vertically launched system the missile is launched vertically and when clear of the ship's structure it is then commanded a pitch over into the target plane.

Although there are advantages of vertical launch systems, there are also disadvantages. One of these penalties is that vertical launch will tend to increase the time of the flight of the missile to the target over that of a trainable launcher. This could pose a serious problem for the engagement of a high speed sea skimming threat at close ranges [6].

A second potential problem associated with vertical launch is velocity loss. This is defined as the loss in missile velocity due to the turn over maneuver compared to the velocity of a trainable launched missile would achieve at the same time. This translates into reduced range and increased time to the target over that of a trainable launcher.

In order to have a meaningful missile configuration, short-medium range vertical launch missiles are searched and some missiles with technical specifications are shown in Table 1. The missiles given in Table 1 are mostly blunt nosed, have strakes on the nose which is directly related with the phantom yaw effect occurring with high angle of attack aerodynamics. Their velocities are between 2 and 3 Mach. Weight of the systems are about 116-170 kgs with diameters 150-180 mms. Their length varies between 1.8-3.3 meters. Their range is 10-40 kms [13], [14], [15], [16] and [17]. This search will be helpful for designing our generic vertical launch missile.

Table 1 VL Missile Characteristics

	IRIS-T	VL-Mica	MCT	Umkhonto IR	Archer
Mass (kg)	119	116	-	130	170
Diameter (mm)	150	160	135-180	180	115
Length (m)	3.25m	3.1m	-	3.320	2.9
Range (km)	25 -20	9-10	12	12-10	40-20
Velocity (Mach)	2-3 M	3 M	-	2.5	2.5

2.1. Control Technologies

One of the most important parts of a missile is the control system, because no matter how sophisticated the guidance system may be or how clever the autopilot is in compensating for the undesirable aerodynamic characteristics, they will be useless if the controls do not generate the required control forces to enable the demanded maneuvers. Traditionally, these control forces have been generated using moveable aerodynamic surfaces; however, increasing demand for more maneuverability has developed other control techniques, such as thrust vector techniques. In the following sections, aerodynamic control and thrust vector control methods will be explained.

2.1.1. Aerodynamic Control

There are basic configurations for aerodynamic control. Canards, wings and tail fins are the moveable surfaces which are used for aerodynamic control, see Figure 4. The comparisons of the three aerodynamic control surfaces can be found in [18]. Dynamic pressure is a measure of control effectiveness, and since dynamic pressure decreases as speed falls, and also with altitude, the result is that for a given deflection, the missile loses aerodynamic control effectiveness at high altitude and low speeds. Hence, unconventional control technologies which are called thrust vector control technologies are used at high altitude and low speed.

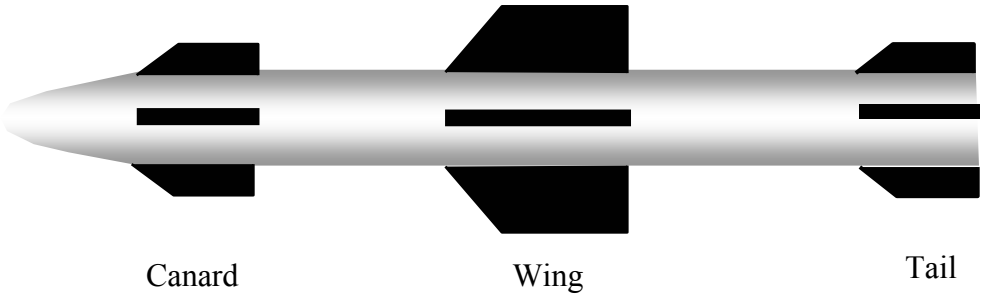

Figure 4 Aerodynamic Control Surfaces

2.1.2. Thrust Vector Control (TVC)

Thrust vector control is a technique whereby the moment required to turn the missile is generated by deflecting the primary thrust from centerline. Clearly this method is not dependent on dynamic pressure, and can therefore produce large control forces even at low speeds and high altitudes. Extremely high maneuverability can be achieved using TVC. There are numerous methods of thrust vectoring. In literature there are different approaches in classification of TVC mechanisms, but a simple classification can be seen in Figure 5. For detailed information about the thrust vector control technologies [5] and [19] can be investigated.

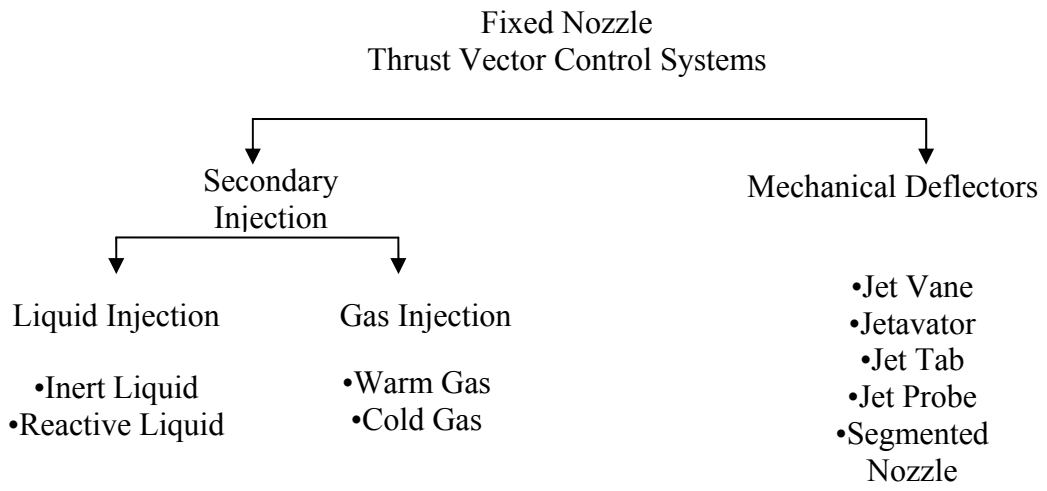

Figure 5 Thrust Vector Control Techniques

In the fixed nozzle TVC systems, main flow from the rocket motor is deflected at the exit plane using movable vanes or flaps, or by using fluid injection at nozzle wall. Fixed nozzle TVC systems are further divided into two groups as secondary injection and mechanical deflectors. Jet vane deflection is one of the most popular mechanical deflection methods. The jet vane TVC technique predates movable nozzle TVC, beginning with work on early liquid fuel rocket more than 70 years ago. The first operational application was with German V-2 missile. In this method, thrust vector control is accomplished by means of relatively small controlled vanes which are immersed in the exhaust stream. Figure 6 shows a demonstration of a jet vane test [20] where jet vanes are at the end of the nozzle.

This system is analogous to conventional aerodynamic control but with small aerofoil in a very fast moving propulsion jet stream. This system needs low actuation power and provides the control of roll, pitch and yaw angles. Suggested materials for vane are: tungsten, graphite, tungsten infiltrated with copper or silver, carbon reinforced by carbon-fiber and tungsten molybdenum alloys [21]. However, it is critical that the material of the vane should be resistant to abrasion and erosion. Therefore, tungsten infiltrated by copper or silver, and tungsten alloys is the most reliable materials.

Figure 6 Jet Vane

2.2. High Angle of Attack Aerodynamics

While low alpha dynamic analysis can be simplified, the high incidences achieved by modern combat aircraft and missiles created a need for more sophisticated analytical methods to be developed. These techniques are mainly concerned with the stability of the vehicle at high angles of attack. There are numerous aerodynamic phenomena associated with high angles of attack region which are non-existent or negligible at low incidence. This phenomenon can be summarized in time dependent effects, hysteresis, non-linearities and cross couplings.

2.2.1. Nonlinearities

At high angle of attack, many of the aerodynamics characteristics of the missile become a nonlinear function of the motion variables. This is contrary to Bryan's fundamental assumption of linearity, and means that the higher order terms of the multidimensional Taylor's expansion of the equation cannot simply be neglected [22]. Missile's static stability significantly changes with AoA. Figure 7 illustrates the changing pitch plane stability with AoA. A positive slope is unstable and a negative slope is stable. For the missile under investigation, aerodynamic control ends at or near 30 degrees AoA, and some form of alternate control is needed to fly at high angle of attack.

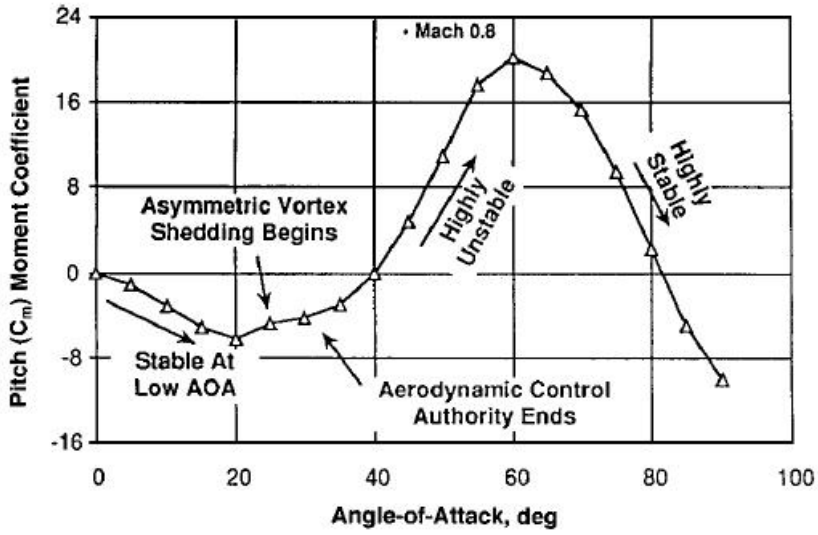

Figure 7 Missile Pitch Plane Stability Characteristics with AoA[3]

2.2.2. Aerodynamic Cross Coupling

Another very important effect of high angle of attack aerodynamics is the high degree of cross coupling which occurs due to asymmetric flow patterns. The conditions which may give rise to these cross coupling effects are briefly longitudinal aerodynamic forces and moments as a result of lateral motions or vice versa [23].

Asymmetric vortex shedding is a nonlinear phenomenon that must be addressed when considering high AoA flight. These asymmetric vortices can cause the nose to slice right or left and may require large control inputs to counter the effect. This phenomenon is often referred to as a phantom yaw and can be mitigated by addition of small strakes and/or nose bluntness [24]. Figure 8 is related with the above declaration. As seen, it is possible to reduce the aerodynamic cross coupling with stakes. From the point of view of controlling missiles, blunt nose is better than sharp nose as long as the missile nose shape is concerned.

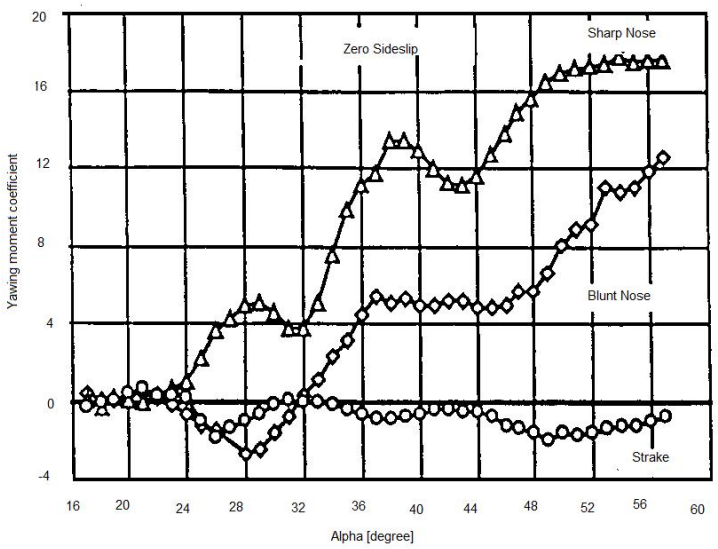

Figure 8 Configuration Redesign Reduces Asymmetric Vortex [20]

2.2.3. Hysteresis

Asymmetric vortex shedding and vortex burst are frequently responsible for aerodynamic hysteresis effects at high angle of attack. The double valued aerodynamic characteristics which occur are likely to produce significant effects on the dynamic response, particularly in oscillatory motion. On the other hand, the effects aerodynamic hysteresis on almost rectilinear motion to which the majority of the missile trajectory can be approximated, is likely to be quite small [25].

2.2.4. Time Dependent Effects

As mentioned previously many aerodynamic characteristics, aerodynamic characteristics depend not only the instantaneous values of the motion variables, but also on the time rate of change of these variables. The reason is primarily the convective time lag between changes in the flow field and that flow change being felt by the rear parts of the missile. The most important motion variables in this regard are the rates of change of incidence and the side slip angles $\dot{\alpha}, \dot{\beta}$ which are aerodynamically equivalent (in the first approximation) to translational accelerations in the same plane of motion (i.e., $\dot{w}, \dot{v}$). The acceleration derivatives

have been known of for a long time since the standard wind tunnel techniques of oscillation about fixed axes always yield composite derivatives such as $N_{\dot{\beta}}$. That is to say, oscillation about fixed axes will produce forces and moments with components due to both angular rates of rotation of the body, and rate of change of the angle of attack. In the past it was a common practice to ignore $\dot{\alpha}, \dot{\beta}$ effects and use the composite derivates in place of the purely rotary ones or to introduce a simple correction for them. At low angles of attack, the $\dot{\alpha}$ and $\dot{\beta}$ effects are usually negligible, and the errors introduced by this procedure enough to be justified. So, at higher angles of attack, however the effects become more substantial and can no longer be ignored or corrected for in a simple way.

CHAPTER 3

EQUATIONS OF MOTION

The dynamic equations of motion can be found from Newton's 2nd law of motion for rigid bodies which states that time rate of change of the momentum is equal to the net force applied on the body and time rate of change of the angular momentum is equal to the net moment applied on the body. In this chapter, reference coordinate frames and the dynamical modeling of the vertical launch surface to air missile which is designed for the thesis is described.

3.1. Reference Coordinate Frames

Two reference frames can be used to describe the motion of a missile, namely earth fixed coordinate frame and missile body coordinate frame. The earth fixed reference frame can be assumed to be inertial because the range of the missile is short compared to the radius of the earth and motion of the missile is much faster compared to earth motion [26]. The axes of the inertial reference frame are represented by X, Y and Z. Here X axis points towards north, Z axis points downwards to earth's center, and Y axis is the complementing orthogonal axis found by the right hand rule. Body fixed reference frame has its origin at the missile's center of mass and its axes are X_B, Y_B and Z_B. Earth and body reference coordinate frames are presented [27] as in Figure 9.

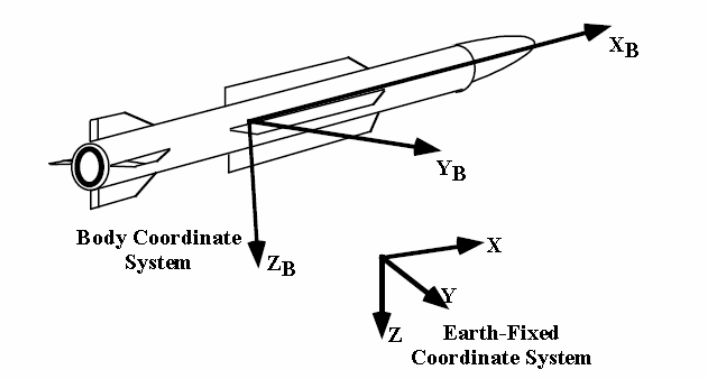

Figure 9 Earth and Body Axes

Any vector can be expressed in different coordinate frames as different column vectors. These column vectors can be related to each other by using linear transformations (rotations) between the specified coordinate frames. Such a transformation can be represented as

$$\overline{r}^{(a)} = \hat{C}^{(a,b)}\,\overline{r}^{(b)} \tag{3.1}$$

$\hat{C}^{(a,b)}$ is an orthogonal transformation matrix which represents a transformation from frame F_b to frame F_a. The following property exists for this orthonormal matrix

$$\hat{C}^{(a,b)} = \hat{C}^{(b,a)^{-1}} = \hat{C}^{(b,a)^{T}} \tag{3.2}$$

Let $\vec{u}_i^{\,(a)}$ and $\vec{u}_j^{\,(b)}$ be the i^{th} unit basis vector of reference frame F_a and j^{th} unit basis vector of reference frame F_b. Then the element at the i^{th} row and the j^{th} column of matrix $\hat{C}^{(a,b)}$ can be expressed as

$$\hat{C}_{i,j}^{\,(a,b)} = \cos(\theta_{i,j}) \tag{3.3}$$

where

$$\theta_{i,j} = \angle\left(\vec{u}_i^{\,(a)} \quad \vec{u}_i^{\,(b)}\right) \tag{3.4}$$

Using the above equalities, the transformation between the body and the earth axis can be written as

$$\begin{bmatrix} X \\ Y \\ Z \end{bmatrix} = \hat{C}^{(e,b)} \begin{bmatrix} x \\ y \\ z \end{bmatrix} \tag{3.5}$$

$\hat{C}^{(e,b)}$ is called the direction cosine matrix (representing the transformation from body frame to earth frame) and can be expressed uniquely using a set of Euler angles as

$$\hat{C}^{(e,b)} = \begin{bmatrix} \mathrm{c}\theta\,\mathrm{c}\psi & \mathrm{s}\phi\,\mathrm{s}\theta\,\mathrm{c}\psi - \mathrm{c}\phi\,\mathrm{s}\psi & \mathrm{c}\phi\,\mathrm{s}\theta\,\mathrm{c}\psi + \mathrm{s}\phi\,\mathrm{s}\psi \\ \mathrm{c}\theta\,\mathrm{s}\psi & \mathrm{s}\phi\,\mathrm{s}\theta\,\mathrm{s}\psi + \mathrm{c}\phi\,\mathrm{c}\psi & \mathrm{c}\phi\,\mathrm{s}\theta\,\mathrm{s}\psi - \mathrm{s}\phi\,\mathrm{c}\psi \\ -\mathrm{s}\theta & \mathrm{s}\phi\,\mathrm{c}\theta & \mathrm{c}\phi\,\mathrm{c}\theta \end{bmatrix} \tag{3.6}$$

where c and s are shorthand notations for cosine and sine functions. Direction cosine matrix (DCM) formulation is preferred to Euler angle formulation to avoid the singularity problem.

$$\hat{C}^{(e,b)} = \int \dot{\hat{C}}^{(e,b)} \tilde{\omega}^{(b)}_{(b/e)} \tag{3.7}$$

Although the quaternion formulation is computationally more efficient, it is not chosen because the DCM is more practical to interpret physically. Normalization of the DCM is not carried out after the integration because it is not required owing to the high simulation sample time (0.001 s) and the efficient integration algorithm (fourth order Runge Kutta).

3.2. Translational Dynamics

For the derivation of translational dynamic equations, following equality will be used.

$$\vec{F} = \frac{d}{dt}(m\vec{V})\Big|_E \tag{3.8}$$

Here, $\vec{F}$ represents the sum of all externally applied forces to the missile. $\vec{V}$ is the total missile velocity and m is the missile mass. $\Big|_E$ Indicates that the differentiations of the related vectors are done in the inertial frame. In the body frame Eq. (3.8) can be written again as

$$\vec{F} = \frac{d}{dt}(m\vec{V})\Big|_B + \vec{\omega} \times \vec{V} \tag{3.9}$$

where $\Big|_B$ indicates that the differentiation is done in the body frame. In the body frame, the relevant vectors will be represented by the following column vectors

$$\bar{F}^{(B)} = \begin{bmatrix} F_x \\ F_y \\ F_z \end{bmatrix},\ \bar{V}^{(B)} = \begin{bmatrix} u \\ v \\ w \end{bmatrix},\ \omega^{(B)}{}_{ang} = \begin{bmatrix} p \\ q \\ r \end{bmatrix} \tag{3.10}$$

The force equilibrium can be written:

$$\bar{F}^{(B)} = m(\dot{\bar{v}} + \tilde{\omega}\bar{v}) \tag{3.11}$$

where

$$\tilde{\omega} = \begin{bmatrix} 0 & -r & q \\ r & 0 & -p \\ -q & p & 0 \end{bmatrix} \tag{3.12}$$

Substituting vectors in Eq. (3.12) and Eq. (3.10) into Eq. (3.11) and making the necessary manipulations, the translational dynamic equations are found as

$$
\begin{aligned}
m\dot{u} &= F_x - q\,w + r\,v \\
m\dot{v} &= F_y - r\,u + p\,w \\
m\dot{w} &= F_z - p\,v + q\,u
\end{aligned}
\tag{3.13}
$$

where F_x, F_y, F_z are components of the total force acting on the missile expressed in the body frame, including aerodynamic, thrust (propulsive) and gravitational forces illustrated in Eq. (3.14) that all of them is expressed in details in the following sections.

$$
\overline{F}^{(B)} = \begin{bmatrix} F_x \\ F_y \\ F_z \end{bmatrix} = \begin{bmatrix} F_{A_x} + F_{T_x} + F_{G_x} \\ F_{A_y} + F_{T_y} + F_{G_y} \\ F_{A_z} + F_{T_z} + F_{G_z} \end{bmatrix}
\tag{3.14}
$$

3.3. Rotational Dynamics

For the derivation of rotational dynamic equations, following equality will be used.

$$
\vec{M} = \frac{d}{dt}(\vec{H})\Big|_E
\tag{3.15}
$$

Here, $\vec{M}$ represents the sum of all externally applied torques to the missile and Eq. (3.16) is the angular momentum of the missile.

$$
\vec{H} = \breve{J} \bullet \vec{\omega}_{ang}
\tag{3.16}
$$

where $\breve{J}$ is the inertia dyadic. In the body frame Eq. (3.15) can be written again as

$$
\vec{M} = \breve{J}\left\{ \frac{d}{dt}(\vec{\omega}_{ang})\Big|_B \right\} + \vec{\omega}_{ang} \times \breve{J} \bullet \vec{\omega}_{ang}
\tag{3.17}
$$

The inertia dyadic can be expressed in the body frame by the following matrix

$$\hat{J}^{(B)} = \begin{bmatrix} I_x & -I_{xy} & -I_{xz} \\ -I_{xy} & I_y & -I_{yz} \\ -I_{xz} & -I_{yz} & I_z \end{bmatrix} \tag{3.18}$$

By using the indications in equalities representation of total moment including aerodynamic and thrust moment equations in general form is

$$\bar{M}^{(B)} = \hat{J}\dot{\bar{\omega}} + \tilde{\omega}\hat{J}\,\bar{\omega} \tag{3.19}$$

The open form of moment equation is then like:

$$\begin{bmatrix} M_x \\ M_y \\ M_z \end{bmatrix} = \begin{bmatrix} I_x\dot{p} + qr(I_z - I_y) - I_{xy}(\dot{q} - pr) - I_{xz}(\dot{r} + pq) - I_{yz}(q^2 - r^2) \\ I_y\dot{q} + pr(I_x - I_z) - I_{xy}(\dot{p} + qr) - I_{yz}(\dot{r} - qp) - I_{xz}(r^2 - p^2) \\ I_z\dot{r} + pq(I_y - I_x) - I_{xz}(\dot{p} - qr) - I_{yz}(\dot{q} + rp) - I_{xy}(p^2 - q^2) \end{bmatrix} \tag{3.20}$$

where M_x, M_y, M_z are the components of the total moment acting on the body about its mass centre expressed in the body frame, including aerodynamic and thrust components, in Eq. (3.21). These moment symbols are defined in the following sections.

$$\begin{bmatrix} M_x \\ M_y \\ M_z \end{bmatrix} = \begin{bmatrix} M_{A_x} + M_{T_x} \\ M_{A_y} + M_{T_y} \\ M_{A_z} + M_{T_z} \end{bmatrix} \tag{3.21}$$

The body axis of the missile is taken to be coincident with the principle axis of inertia. Hence, product of cross inertia terms (I_{xy} , I_{xz} and I_{yz} is 0) vanish.

3.4. Forces and Moments

Forces that the system has can be categorized as aerodynamic forces, gravity forces and thrust forces and the moments as aerodynamic moments, thrust moments. These forces and moments are expressed in details in the following sections.

3.4.1. Aerodynamic Forces and Moments

In translational and rotational dynamic equations, force and moment components are not expressed clearly; instead it is just emphasized that they have aerodynamic, thrust and gravitational components. First of all, aerodynamic forces given at (3.22) are explained.

$$F^{(B)}_{aero} = \begin{bmatrix} F_{A_x} \\ F_{A_y} \\ F_{A_z} \end{bmatrix} = \begin{bmatrix} QSC_x \\ QSC_y \\ QSC_z \end{bmatrix} \tag{3.22}$$

where aerodynamic force coefficients are functions of Mach M, angle of attack and side slip $\alpha,\ \beta$ aileron, elevator and rudder deflection $\delta_a, \delta_e, \delta_r$, body rotational rates in pitch, yaw and roll axes p, q, r as given below:

$$\begin{bmatrix} C_x \\ C_y \\ C_z \end{bmatrix} = \begin{bmatrix} C_x(M,\alpha,\beta,\delta_a,\delta_e,\delta_r,q,r) \\ C_y(M,\alpha,\beta,\delta_a,\delta_r,p,r) \\ C_z(M,\alpha,\beta,\delta_e,q) \end{bmatrix} \tag{3.23}$$

In the thesis, since the missile under study is axi-symmetric and has cruciform geometry, instead of formulating the aerodynamic force coefficients as nonlinear functions of all independent flight variables, they are tabulated as shown. Thus, their dependencies on the flight variables are superposed and they are represented in a quasi-nonlinear fashion especially for the aerodynamic control surface deflections and body angular rates as below:

$$\begin{bmatrix} C_x \\ C_y \\ C_z \end{bmatrix} = \begin{bmatrix} C_{x0}(M,\alpha,\beta) + C_{x\delta_a}(M)\delta_a + C_{x\delta_e}(M)\delta_e \\ C_{y0}(M,\alpha,\beta) + C_{y\delta_a}(M)\delta_a + C_{y\delta_r}(M)\delta_r \\ C_{z0}(M,\alpha,\beta) \end{bmatrix} + \begin{bmatrix} C_{x\delta_r}(M)\delta_r + (C_{xq}(M)q + C_{xr}(M)r)d/(2V_T) \\ (C_{yp}(M)p + C_{yr}(M)r)d/(2V_T) \\ C_{z\delta_e}(M)\delta_e + (C_{zq}(M)q)d/(2V_T) \end{bmatrix} \tag{3.24}$$

The aerodynamic moments are also functions of dynamic pressure Q, final center of gravity $x_{c_{ref}}$, reference surface S and diameter d.

Aerodynamic moments are:

$$\bar{M}_{aero}^{(B)} = \begin{bmatrix} M_{A_x} \\ M_{A_y} \\ M_{A_z} \end{bmatrix} = \begin{bmatrix} QSdC_l \\ QSdC_m + (x_{c_{ref}} - x_c(t))F_{A_z} \\ QSdC_n - (x_{c_{ref}} - x_c(t))F_{A_y} \end{bmatrix} \tag{3.25}$$

where aerodynamic moment coefficients are functions of $M,\ \alpha,\ \beta,\ \delta_a,\ \delta_e,\ \delta_r,\ p,\ q, r$ as given below.

$$\begin{bmatrix} C_l \\ C_m \\ C_n \end{bmatrix} = \begin{bmatrix} C_l(M,\alpha,\beta,\delta_a,\delta_r,p,r) \\ C_m(M,\alpha,\beta,\delta_e,q) \\ C_n(M,\alpha,\beta,\delta_a,\delta_r,p,r) \end{bmatrix} \tag{3.26}$$

The tabulation of aerodynamic moment coefficients are very similar to aerodynamic force coefficients. The compact form for them is given at (3.27). Their dependencies on the flight variables are superposed and they are represented in a quasi-nonlinear fashion especially for the aerodynamic control surface deflections and body angular rates.

$$\begin{bmatrix} C_l \\ C_m \\ C_n \end{bmatrix} = \begin{bmatrix} C_{l0}(M,\alpha,\beta) + C_{l\delta_a}(M)\delta_a + C_{l\delta_r}(M)\delta_r \\ C_{m0}(M,\alpha,\beta) + C_{m\delta_e}(M)\delta_e \\ C_{n0}(M,\alpha,\beta) + C_{n\delta_a}(M)\delta_a + C_{n\delta_r}(M)\delta_r \end{bmatrix} + \begin{bmatrix} (C_{lp}(M)p + C_{lr}(M)r)d/(2V_T) \\ (C_{mq}(M)q)d/(2V_T) \\ (C_{np}(M)p + C_{nr}(M)r)d/(2V_T) \end{bmatrix} \tag{3.27}$$

Center of gravity change with respect to time is as

$$x_c(t) = x_{c_{init}} - \text{Imp}(t)(x_{c_{init}} - x_{c_{ref}})/\text{TotImp} \tag{3.28}$$

where $x_{c_{init}}$ is initial center of gravity of the missile, $x_{c_{ref}}$ is the mass of the missile at the end of the burn. Impulse and total impulse expressions are also:

$$\text{Imp}(t) = \int_0^t T(t')dt' \;\; \& \;\; \text{TotImp} = \int_0^{t_{boost}} T(t')dt' \tag{3.29}$$

Dynamic pressure in the equations (3.22) and (3.25) is expressed as

$$Q = \frac{1}{2}\rho V^2 \tag{3.30}$$

ρ is the air density and it changes with the altitude h, as

$$\rho = \begin{Bmatrix} \rho_0 \left(1 - 0.00002256\, h\right)^{4.256} ; h \le 10000m \\ 0.412\, e^{-0.000151\,(h-10000)} ; \;\; h > 10000m \end{Bmatrix} \tag{3.31}$$

Here ρ_0 is the air density at sea level (1.223 kg/m^3). Aerodynamic coefficients (C_i's ($i = x, y, z, l, m, n$)) usually depend on the speed of missile configuration and time history. But, according to the experimental results they are found to be functions of α, β, mach, body rates (p, q and r), $\dot{\alpha}, \dot{\beta}$, aerodynamic control surface deflections ($\delta_a, \delta_e, \delta_r$), centre-of-gravity changes and whether the main propulsion system is on or off (plume effects).

Throughout the flight, some flight angles are introduced to describe the motion of the missile. These angles are the angle of attack (α) and the sideslip angle (β). Using the total velocity of the missile, α and β can be expressed as

$$\alpha = arctan\left[\frac{w}{u}\right] \;\; \& \;\; \beta = arcsin\left[\frac{v}{V}\right] \tag{3.32}$$

3.4.2. Thrust Forces and Moments

Thrust vector control forces and moments are modeled using a time varying thrust that is deflected with jet vanes. It is assumed that jet vanes are coupled to each others, so thrust deflection is obtained only in pitch and yaw planes. Furthermore, the second assumption is that the jet vanes are not inside the nozzle but at the outside of the nozzle and they are not closed with a shroud. These specifications render to use yaw and pitch planes decoupled and provides linear modeling between jet vane deflection and thrust deflection. For further information [28], [29], [30], [31], [32] and [33] can be searched.

The relation between jet vane deflection and total thrust deflection which is usually function of δ_{T_e} and δ_{T_r} such as in [34];

$$\theta_T = f(\delta_{T_e}, \delta_{T_r})\delta_{T_e} \;\&\; \psi_T = f(\delta_{T_e}, \delta_{T_r})\delta_{T_r} \tag{3.33}$$

This relation has been taken a constant number for the theses, 0.5, that means if jet vanes are actuated to 20 degree total thrust has 10 degree for deflection. This definition will be directly related with autopilot design. 10 degree thrust deflection is the maximum deflection that is observed when jet vanes are used [35]. Also, thrust vector control modeling can be examined in the Appendix. These assumptions are supported with linear theories. However, linear theory is not a final decision; it says that these assumptions are not far from reality. Thus, the resulting thrust forces are:

$$\bar{F}_T^{(B)} = \begin{bmatrix} F_{T_x} \\ F_{T_y} \\ F_{T_z} \end{bmatrix} = \begin{bmatrix} T\cos(\theta_T)\cos(\psi_T) \\ T\sin(\psi_T) \\ -T\sin(\theta_T)\cos(\psi_T) \end{bmatrix} \tag{3.34}$$

where T is the total thrust, θ_T is the thrust deflection in pitch plane and

$$\vec{M}_{thrust} = \vec{l}_T \times \vec{F}_{thrust} \tag{3.35}$$

where $\vec{l}_T$ is the moment arm of TVC. It is the distance between the center of gravity of the missile and thrust vector unit center of gravity and it is a critical design criteria and l_x, l_y and l_z are the components of $\overline{l}_T^{(B)}$.

$$\overline{M}_T^{(B)} = \begin{bmatrix} M_{T_x} \\ M_{T_y} \\ M_{T_z} \end{bmatrix} = \begin{bmatrix} 0 & -l_z & l_y \\ l_z & 0 & -l_x \\ -l_y & l_x & 0 \end{bmatrix} \begin{bmatrix} F_{T_x} \\ F_{T_y} \\ F_{T_z} \end{bmatrix} = \begin{bmatrix} -T\,l_y\,s(\theta_T)\,c(\psi_T) - T\,l_z\,s(\psi_T) \\ T\,l_z\,c(\theta_T)\,c(\psi_T) + T\,l_x\,sin(\theta_T)\,c(\psi_T) \\ -T\,l_y\,c(\theta_T)\,c(\psi_T) + T\,l_x\,s(\psi_T) \end{bmatrix} \quad (3.36)$$

3.4.3. Gravity Forces

Gravity forces are also the forces acting on the missile. Body frame force components of the gravitational acceleration can be expressed as follows:

$$\overline{F}_{Gravity}^{(B)} = \begin{bmatrix} F_{G_x} \\ F_{G_y} \\ F_{G_z} \end{bmatrix} = mg \begin{bmatrix} -\sin\theta \\ \sin\phi\cos\theta \\ \cos\phi\cos\theta \end{bmatrix} \quad (3.37)$$

Unless otherwise stated, gravity compensation will be included as a part of the guidance design process. Thus, during the derivation of linear autopilot models, gravity terms can be neglected.

CHAPTER 4

MISSILE CHARACTERISTICS

In this section, modeled vertical launch surface to air missile is analyzed in details. Firstly, physical parameters are given. After then, aerodynamic characteristics is presented with related figures. Later, propulsion characteristics with thrust vector control will be expressed. Finally, velocity and range profiles will be exhibited within ballistic flight trajectory.

4.1. Physical Parameters

As the given agile missiles have a blunt nose with strakes, the designed missile has a geometrical shape given in Figure 10. VLSAM has two control surfaces, one is tail fin and the other one is jet vane. Its physical properties are given in Table 2 whose body fineless ratio is 16.5, which is high like agile missiles. As expected, inertia is also high like high body fineless ratio missiles [35].

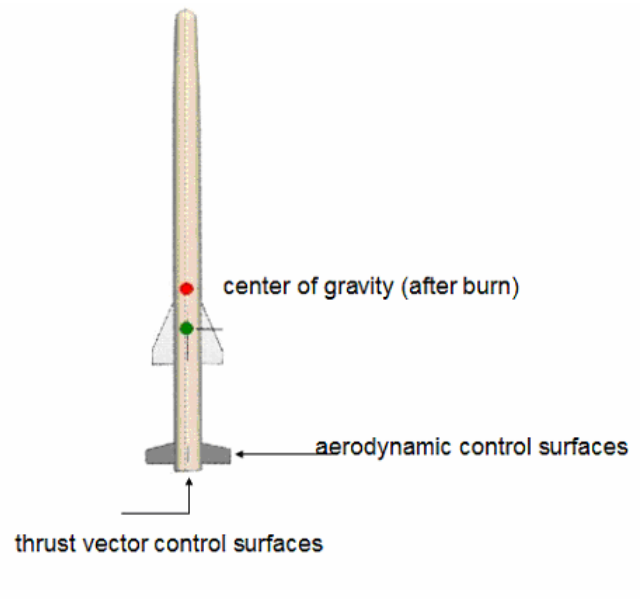

Figure 10 Generic VLSAM

Table 2 VLSAM parameters

Diameter	0.2 m
Length	3.3 m
Mass	135 kg (before burn)
I_{yy}	133.06 (before burn)
I_{xx}	1.27 (before burn)
x_{cg}	1.94 (before burn)

4.2. Aerodynamic Characteristics

The high angle of attack maneuvers of surface to air missiles, i.e. vertical launch, interception, etc, bring the necessity to the demand of the modeling of the aerodynamic forces and moments in wide angles of attack ranges. Thus, in this study, on the contrary to the investigated literature in which there is limited aerodynamic data with limited numerical parameters, a new and complete aerodynamic data base, over a wide range of angle of attack values, is generated. In

order to generate the necessary aerodynamic force and moment coefficients a semi-empirical aerodynamic estimation tool, i.e. Missile DATCOM, is used. The software is developed in 1985 and enhanced over the years to involve the increasing need for high angle of attack flight regimes. This is also presented by means of comparison of Missile DATCOM's aerodynamic parameter estimation capability, at high angles of attack, with certain wind tunnel test results for different missile configurations.

Although Missile DATCOM is revised and enhanced for high angle of attack values, for the sake of accuracy and reliability on the aerodynamic coefficients, it is generally proposed to be used up to values for which $|\alpha| \leq 40^{\circ}$. This is also carried out in this study and the aerodynamic coefficients are estimated by Missile DATCOM for $|\alpha| \leq 40^{\circ}$ flight regime. However, in order to complete the aerodynamic data set, the generated aerodynamic data set is tailored and extrapolated to $|\alpha| \leq 90^{\circ}$ flight regime by using the study done in the related previous literature between [36] and [45]. Analyses of the current aerodynamic database and the comparisons with literature are presented.

Figure 11 shows C_x versus alpha at various velocities. As seen, sign of C_x changes at about 30 or 50 degrees of alpha which is different from conventional missiles because conventional missiles usually do not need alpha higher than 20 degrees.

Figure 12 shows Cm versus alpha at various velocities. As mentioned in previous chapters, there is one main point which is about the stability of missile. About 30 and 40 degrees of alpha C_m passes from stable region to highly unstable region. Afterwards, about 50 and 70 degrees of alpha, it is again stable. This stability change will be extremely important in designing autopilots.

Figure 13 and Figure 14 show lift and drag coefficients versus alpha at various velocities. If the figures are analyzed, drag and lift coefficients changes drastically at velocities 1 and 1.4 mach. Afterwards, at low and high velocities, the coefficient

are relatively small. Figure 15 is the ratio of lift and drag coefficients which are important for analyzing agility of designed missile. For further information, [35] can be looked through. Figure 16 shows the comparison of coefficients. Left hand side of the graph shows the thesis's lift and drag coefficient, and the right hand side is a coefficient figure from [4] which claims that the approach in the thesis is right. Although the database is created without the aim of being similar to any database, the result is important that the generated database is extremely ordinary from the related studies.

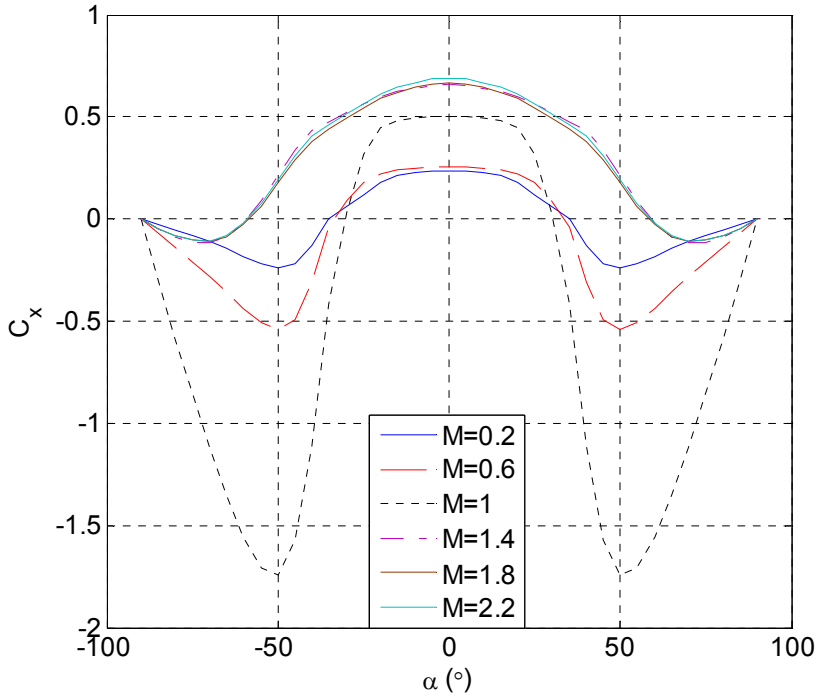

Figure 11 C_x Curve wrt. Alpha for Various Velocities

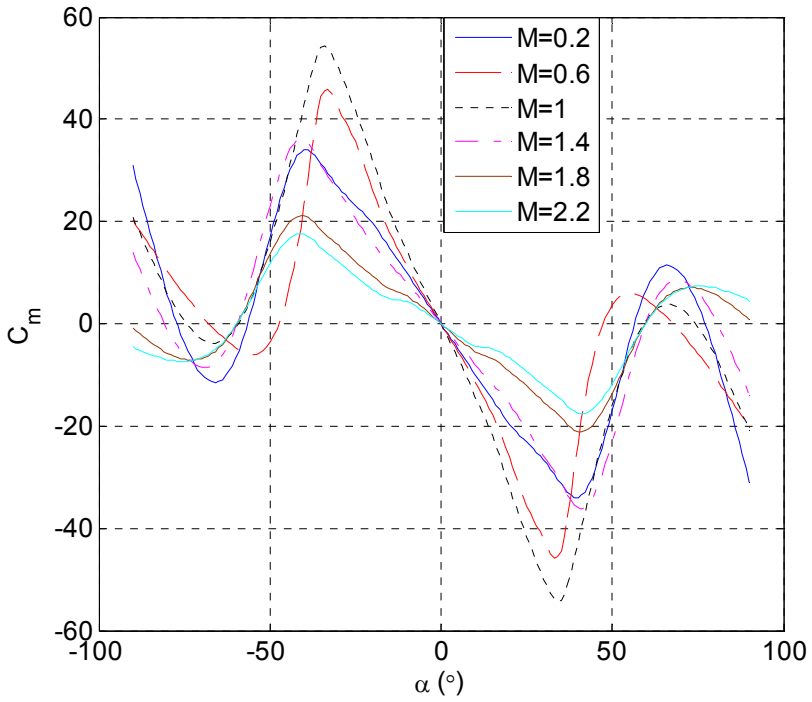

Figure 12 C_m versus Alpha for Various Velocities

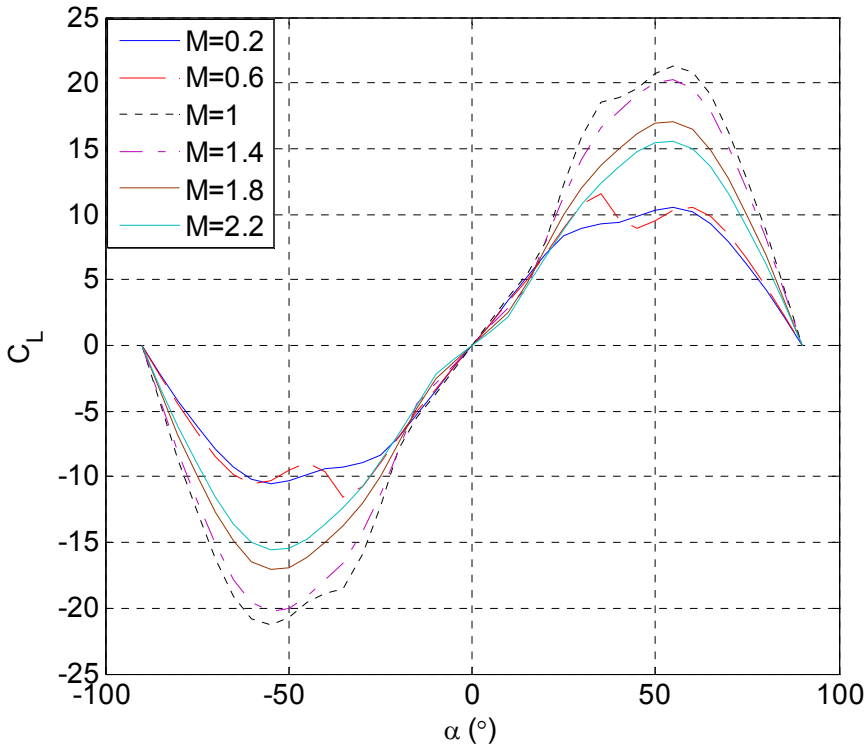

Figure 13 C_L Coefficient versus Alpha

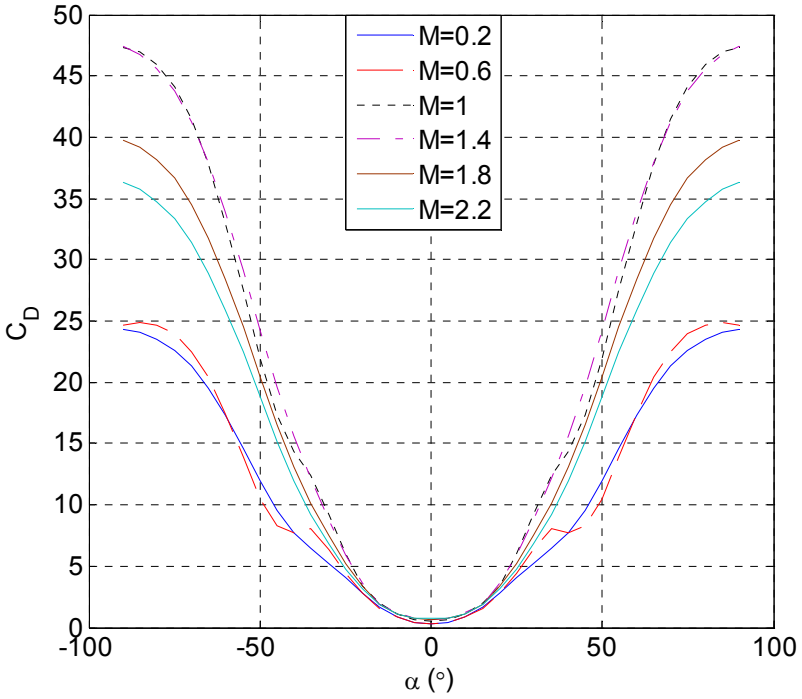

Figure 14 C_D Coefficient versus Alpha

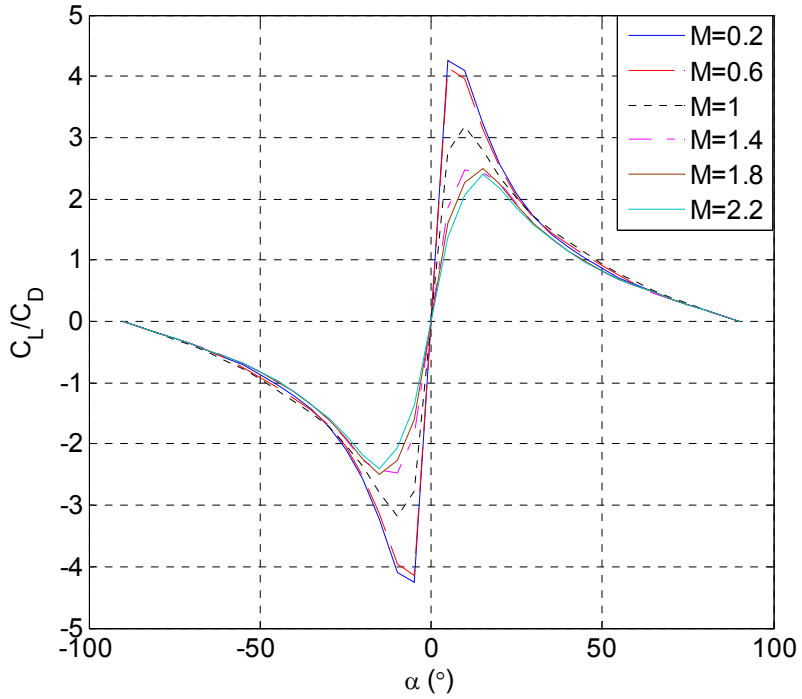

Figure 15 C_L/C_D versus Alpha

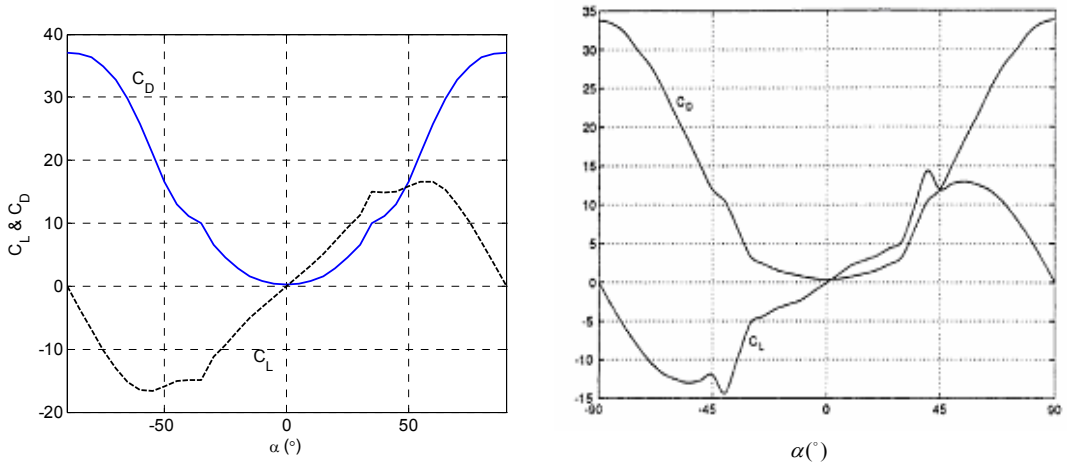

Figure 16 C_L - C_D Coefficient versus Alpha Comparison at Mach=0.8

4.3. Propulsion Characteristics

Most of VLSAM missiles use solid rocket motor with boost/sustain or all boost thrust profile. A typical thrust profile for these systems which has only boost motor is shown in Figure 17, and has a sharp rise, followed by a period of approximately constant thrust, with a sharp drop off at burnout.

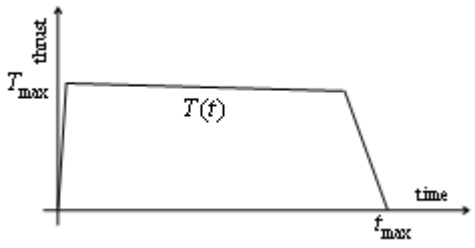

Figure 17 Typical Thrust Profile

For simplicity, the thrust profile is usually approximated by a constant thrust for a designated time. Designated time and thrust force is related with the Mach number that the missile has to reach and its weight. Time to reach to the maximum thrust

force is a critical point, if it is a long time (1-1.5 s), turn over maneuver is hard to achieve because velocity and dynamic pressure increases, and TVC effectiveness decreases. Hence, thrust profile design is a critical issue. Detailed study about effects of motor properties to quick turnover can be found at [46]. From the analysis which is carried on [46], thrust force which consists of only boost motor is 35.000 N and total thrust time is 3.5 seconds is considered. The chosen thrust profile takes missile velocity up to 2.5 Mach which is desired to be reached as in many missile systems presented in Table 1.

4.4. Thrust Vector Control Characteristics

All TVC systems are limited in the maximum thrust deflection angle. This angle is defined as the angle between the effective thrust line and the centerline of the missile. There are some parameters related to vane deflection angle, vane characteristics such as material, geometry, thickness, nozzle exhaust velocity, temperature. The total deflected thrust angle is related to many design parameters, such as shape of the jet vane, placement of the vane into the nozzle, exhaust Mach number etc. [35] shows the maximum deflection of the total thrust with various thrust vector control technologies. For the sake of simplicity, in the thesis, the relation with elevation angle and vane deflection angle is chosen 0.5 which can be stated like $\theta_T = 0.5\delta_e$. This relation means that 20 degrees of jet vane deflection will obtain 10 degrees of thrust deflection. Thrust vector control modeling in the Appendix has more details on this subject.

Another critical subject when dealing with jet vane technology is the vane material. As the vanes are mounted at the end of nozzle, vane material has to be chosen related with the algorithm requirement. If thrust vector capability is desired to be used during the time motor burns, vanes should not dissolve or should erode inconsiderable. Hence, these specifications are related with material problems. Vane material is enduring and thrust vector control has sufficient linear characteristics in the small angle of deflections. In the thesis, it is assumed that jet vane erosion is negligible which is possible.

4.5. Speed Characteristics

To analyze the ballistic velocity and trajectory, missile is launched with 50 degrees of initial theta angle. Maximum velocity of the missile is 2.5 Mach as seen in Figure 18. As there is not sustain motor, velocity decreases after boost motor is over. The position graph of the missile in this condition is also given in Figure 18. Within this ballistic flight, missile reaches more than 20000 meters range and 7500 meter altitude.

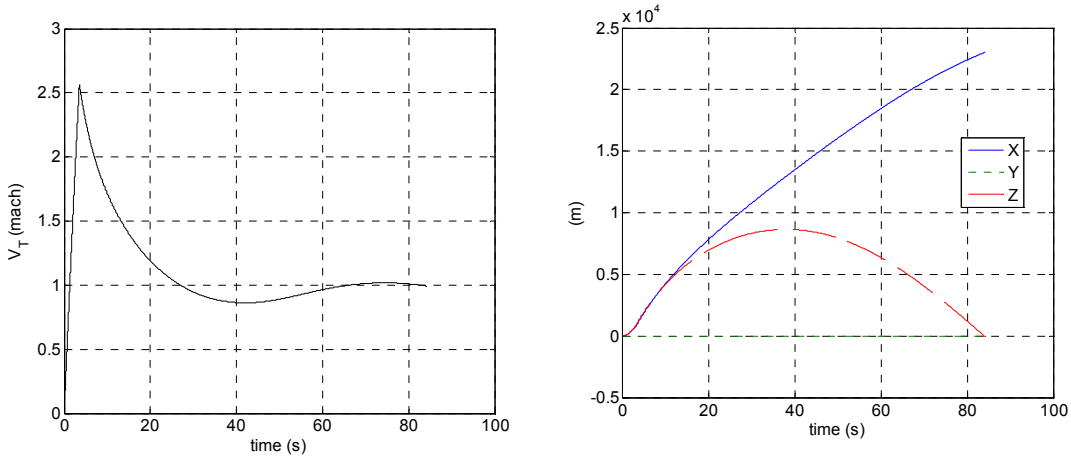

Figure 18 Ballistic Velocity Profile and Trajectory

4.6. Linearized Missile Analysis

The linearized systems stability gives opinion on the nonlinear system stability. Moreover, autopilots are designed for the linear systems mostly. So, linearized missile dynamics are analyzed. In most of the cases the linearization of the flight vehicles are done by decoupling the longitudinal and lateral motions. Thus, the linearized dynamics are investigated separately for different planes of motion. This is generally a good and simple approach that can be used for the flight vehicles that have relatively low angle of attack flight regimes and do not show significant time varying characteristics. However, here, the missile under study is also modeled to fly at high angle of attack flight regimes and has coupling effects between the

planes of motion it is necessary to carry out the linearization coupled in both planes of motion.

In this study the linearization of the nonlinear missile dynamics is done especially for vertical launch, including the thrust, and the vertical climb, after the engine burn-out, phases and the controls are locked. Thus, the trim flight conditions are chosen as

- $\alpha = \beta = 0^\circ$
- $p = q = r = 0^\circ / s$
- $\delta_a = \delta_e = \delta_r = \delta_{Te} = \delta_{Tr} = 0^\circ$
- $\theta = 90^\circ$.

θ is given for visualization purposes, it is not related with Euler angle singularity. Hence, the linear dynamics can be represented in the state space form. The aerodynamic and the thrust vectoring surface deflections are the control inputs ($\Delta\overline{u} = \overline{u}$) and all of the flight variables are the outputs ($\Delta\overline{y} = \Delta\overline{x}$) of the system:

$$\Delta\dot{\overline{x}} = A\Delta\overline{x} + B\overline{u} \tag{4.1}$$

Here, A is system matrix, B is control matrix and *u* vector represents thrust vector control and aerodynamic control inputs and the states are velocity, alpha, beta, roll, pitch and yaw rates as given;

$\Delta\overline{x} = \left[\Delta U\ \alpha\ \beta\ p\ q\ r\ \phi\ \Delta\theta\right]^{\mathrm{T}}$ and $\overline{u} = \left[\delta_a\ \delta_e\ \delta_r\ \delta_{Te}\ \delta_{Tr}\right]^{\mathrm{T}}$.

It shall be noted that, except ΔU and $\Delta\theta$, Δ sign is not used for other state variables for which the trim conditions are taken to be zero, i.e. the deviations from the trim conditions are equal to the values of the states themselves.

Linearization is done for two phases. Missile is vertically launched and a linearization time interval is decided as 20 seconds. The first 3.5 seconds of the vertical flight is defined as phase 1, and there is thrust in this phase. In the first phase, mass, inertia, velocity, center of gravity is changing with respect to time. The second phase is where there is no thrust. Mass, center of gravity and inertia is constant; the only changing missile parameter is its velocity. Both of the linearization conditions for Phase I and II are given in Table 3 and Table 4.

Table 3 Phase I Linearization Parameters

Time (s)	Altitude (m)	Velocity (Mach)	Dynamic Pressure (kg/m^3)
0.3	11	0.21	3230
0.65	52	0.47	1610
1.01	126	0.74	38770
1.36	232	1.01	70760
1.72	370	1.27	110530
2.07	540	1.53	156710
2.43	739	1.79	208060
2.78	969	2.04	262860
3.14	1227	2.28	319300
3.5	1514	2.52	375930

Table 4 Phase 2 Linearization Parameters

Time (s)	Altitude (m)	Velocity (Mach)	Dynamic Pressure (kg/m^3)
4	1929	2.44	335170
5.77	3276	2.16	22123
7.55	4462	1.95	155240
9.33	5529	1.79	113590
11.11	6502	1.66	85490
12.88	7395	1.55	65680
14.66	8222	1.45	51230
16.44	8989	1.36	40390
18.22	9702	1.28	32090
20	10367	1.21	25710

After linearization process, stability analysis of the system is carried on. Eigen values of *A* are seen in Figure 19. It has two parts, one is the thrust phase and the other part is when there is no thrust force. In phase II, as the velocity decreases immediately, the poles of the system approaches to the imaginary axes. In Table 4, the last value of the velocity is 1.21 mach which means the linearization process is being done for less 1.21 Mach. However, missile has to hit the target before its velocity decreases to critical values with respect to the target. Although analysis for lower velocity profile is not shown, it is clear that missile stability is decreasing parallel to its velocity.

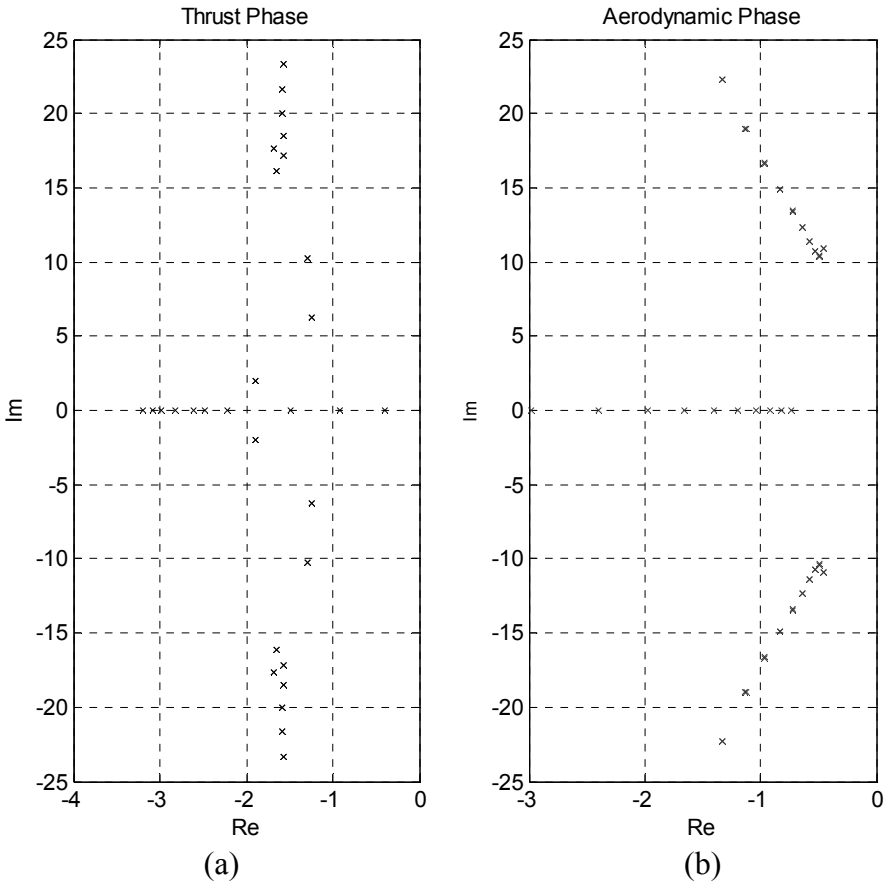

Figure 19 Eigen Values of Thrust (a) and Aerodynamic (b) Phases

Here, a state space representation at Mach = 0.27, altitude = 52 meter with two control inputs is given. As it is seen, cross coupling terms depending on the angle of attacks is included in linear equations. More state space representations are presented at [34].

$$\begin{bmatrix} \dot{\alpha} \\ \dot{\beta} \\ \dot{p} \\ \dot{q} \\ \dot{r} \end{bmatrix} = \begin{bmatrix} -2.91 & 0.211\text{e-}3 & 0 & 0.997 & 0 \\ 0.211\text{e-}3 & -2.91 & 0 & 0 & -0.997 \\ 0.77\ \text{e-}1 & 0.77\text{e-}1 & -0.571 & 0 & 0 \\ -12 & -0.49\text{e-}2 & 0 & -0.216 & 0 \\ -0.49\text{e-}2 & 12 & 0 & 0 & -0.216 \end{bmatrix} \begin{bmatrix} \alpha \\ \beta \\ p \\ q \\ r \end{bmatrix} + \begin{bmatrix} 0 & -0.089 & 0 \\ 0 & 0 & 0.089 \\ -148 & 0 & 0 \\ 0 & -10.6 & 0 \\ 0 & 0 & 10.6 \end{bmatrix} \begin{bmatrix} \delta_a \\ \delta_{Ae} \\ \delta_{Ar} \end{bmatrix} + \begin{bmatrix} -2.76 & 0 \\ 0 & 2.76 \\ 0 & 0 \\ -342 & 0 \\ 0 & 342 \end{bmatrix} \begin{bmatrix} \delta_{Te} \\ \delta_{Tr} \end{bmatrix} \tag{4.2}$$

Afterwards, nonlinear and linear system comparison is carried on. During the comparison it is a very important task to schedule the linear dynamics with respect to desired flight parameters. In general, the scheduling is done with respect to the dominant flight parameters that are changing very rapidly when compared to the other ones in such a way that they affect the coefficients of the linear and also nonlinear system. A frequently used scheduling method, in missile flight dynamics linearization, is carrying out the scheduling with respect to Mach number. However, in the first phase velocity is changing with respect to time. Moreover, center of gravity, inertia and mass is changing with respect to time. So, first phase is scheduled with respect to time. Velocity scheduling is applied for the second phase. Then, a deflection command set is applied for both of the phases and nonlinear simulation. The angle of attack and pitch rate responses of the two systems are shown in Figure 20. As seen, for a 1 degree of deflection of jet vanes and tail fins, the systems' responses are very close which claims the linearization is approximately true.

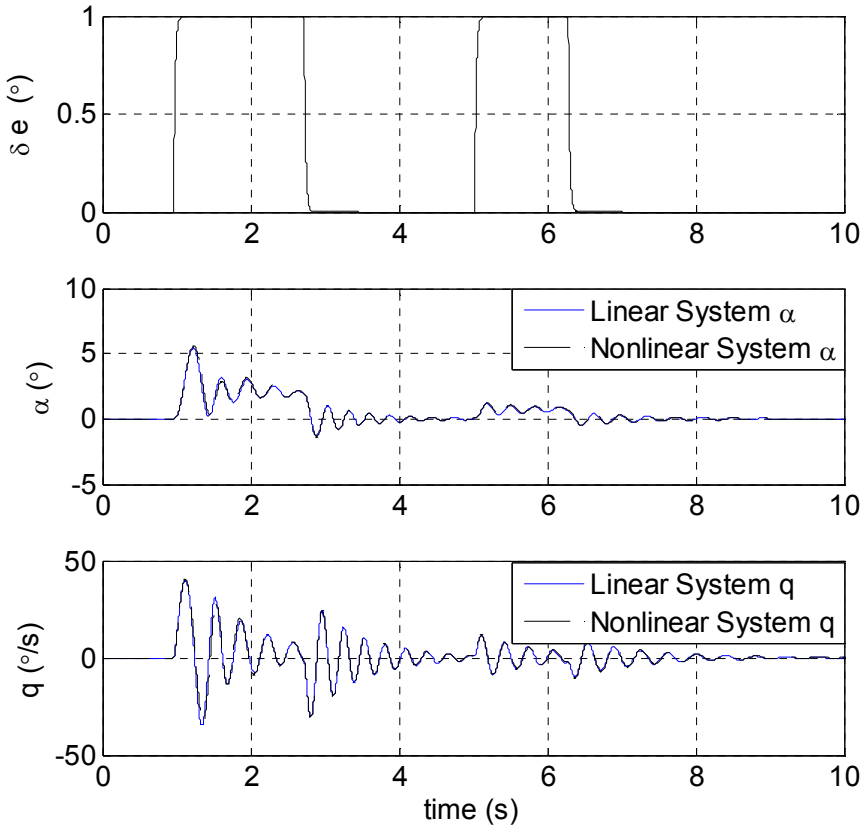

Figure 20 Linear-Nonlinear Response Comparisons

4.7. Thrust Vector & Aerodynamic Control Effectiveness Analysis

Thrust vector control and aerodynamic control approaches are compared to analyze the effectiveness of two control capability. Thus, control effort sharing can be obtained in a manner. Thrust vector control characteristics are independent of the flight condition. It is directly related with the thrust level with respect to time. Aerodynamic control characteristics depend on flight conditions like velocity, altitude, dynamic pressure. However, they are alternatives of each other and the designer have to know the control capability of thrust vector and aerodynamic control during flight. The comparison of two control capability (reaction jet and aerodynamic control) is given in [3]. [3] illustrates the comparison in different

altitudes. Here, it is preferred to make comparison during vertical launch which is the main property of the missile.

As defined in [34] a state space model for the missile dynamics can be written as

$$\dot{x} = Ax + B_A u_A + B_T u_T \tag{4.3}$$

where aero and thrust vector control inputs enter the system dynamic through B_T and B_A matrices. Control effectiveness can be analyzed by computing the ratio of these matrices throughout the flight envelope. So, the ratio of control inputs (aerodynamic and thrust vector control) for angle of attack dynamics; and the flight envelope is illustrated in Figure 21 as an example. As seen in Figure 21, thrust vector control is more effective than aerodynamic control where velocity and dynamic pressure are low. As velocity increases, so the dynamic pressure, the ratio of the control capability decreases. After 1 Mach, control effectiveness is close to 1 which means aerodynamic control is as effective as thrust vector control. In the end, where thrust is over, thrust vector control is no more available.

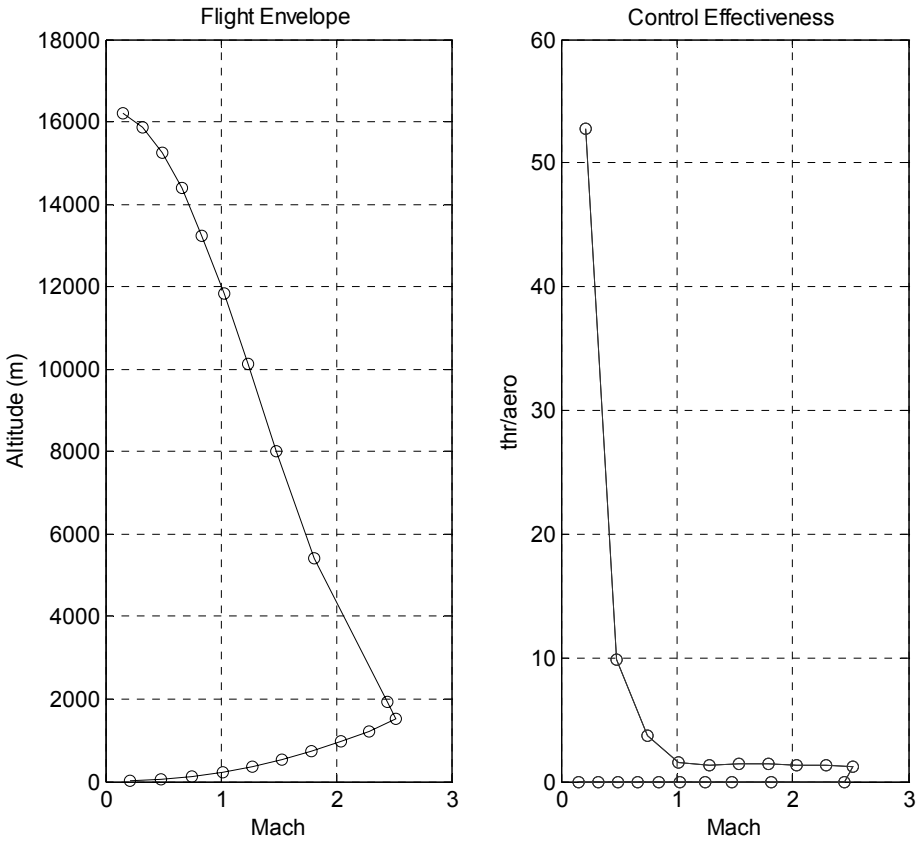

Figure 21 Control Effectiveness of Thrust/Aero Control

The problem is that if there is a mechanical connection between these control surfaces which means they are actuated by the same actuator system, what the ratio should be or what advantages of actuating the control surfaces separately are. If this problem is formulated, the overall state equations can be defined as where B_A is aerodynamic control, B_T is thrust vector control inputs. If hybrid control is selected the state equation can be written such as:

$$\dot{x} = Ax + (B_A + KB_T)u \tag{4.4}$$

And the control input is then:

$u = \left[\delta_a \;\; \delta_e \;\; \delta_r\right]^T$ where $\delta_e = \delta_{Ae} = \delta_{Te} / K$ and $\delta_r = \delta_{Ar} = \delta_{Tr} / K$.

The point is deciding to actuate the control surfaces (jet vanes and tail fins) separately or coupled. As a design procedure, it can be decided to actuate control surfaces separately. However, in literature, missiles which use tail fins and jet vanes as control surfaces usually chose coupled actuating systems which is called hybrid control [13], [14] and [47]. Figure 22 shows the hybrid control actuator of ESSM missile; here both jet vanes and tail fins are actuated by one electromechanical actuator.

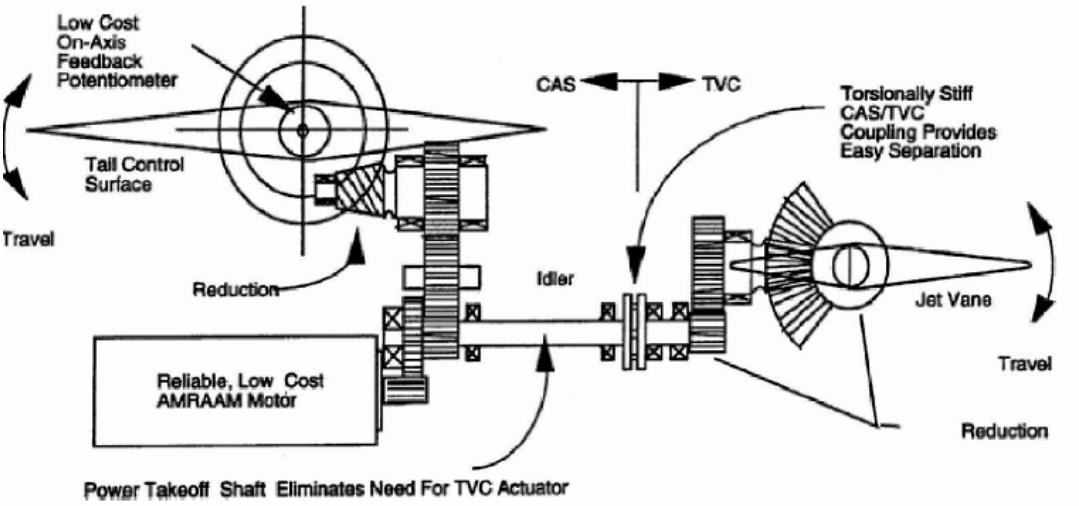

Figure 22 ESSM TV-Aero Control Hybrid Control Actuator [5]

As both of the control surfaces are at the end of the missile, these control surfaces are coupled to each other in order to packaging and power advantages. So coupled usage of the control surfaces is preferred. This ratio is also a design period result. It can be optimized with the known parameters like, control effectiveness, mechanical design parameters, limited space, power needing, mass for actuator etc. which is another study subject. However, as this study is not focused on optimization of the coupling ratio, for the sake of simplicity, the ratio is taken where the control inputs relatively same maneuvers, it is preferred 0.87 which means thrust vector control surfaces are less actuated. This will also minimize the amount the thrust loss; however in the thesis thrust loss is not a lot, less than % 1; however in real applications thrust loss is more than % 1.

CHAPTER 5

AUTOPILOT DESIGN

There are nonlinear controller design methods for agile, highly varying dynamical systems. [48] discusses control strategies for high angle of attack missiles, and presents comparison of linear and nonlinear control approaches. [49] is an autopilot design study for IRIS-T missile which is based on robust control theory. [50] is similar to the study in [49]. [4] is a sliding mode control strategy for air-to-air missiles. [51] is a brief application of classical autopilot structures working on high angle of attack. [52] and [53] are studies of autopilot designs on adaptive control theory. [52] discusses the controller design problem of the same application with a similar approach. It considers some periods as time varying systems and suggests a solution for this kind of highly varying dynamic systems. [54] is a master thesis on bang – bang controllers for VLSAM; however it is a very brief study without any detailed analysis. As seen, it is possible to find many different autopilot structures. However, before high level autopilot structures, it is decided to understand and analyze the capability of classical approaches and gain scheduling method in such systems and it is decided to start autopilot design with classical approaches.

Autopilot designs are been considered in the scope of existing feedback sensors on missiles such as gyros and accelerometers. Hence, body rates, angle and acceleration autopilots are studied on. Autopilots are designed for the linearized systems. Then, the autopilot structures are implemented into the nonlinear mathematical model and the gains are scheduled which is mostly done practically. The autopilots are activated after 0.2 seconds from launch, in order to be sure that

missile is at least at 5 meters height from the launcher. Missile is accelerated for 3.5 seconds and its velocity changes from 0 to 900 m/s (2.5 Mach) in 3.5 seconds. After 3.5 seconds, its velocity is decreasing rapidly. Moreover center of gravity, mass and inertia are also changing with respect to time, but constant after boost motor burns.

Due to the rapid change in velocity and dynamic pressure, plant parameters change rapidly. Beside these changes, desired angle of attack regions are also too wide as it is VLSAM. Consequently, autopilots must be as robust as possible towards these changes. As high angle of attack maneuvers are studied, cross couplings and nonlinear behaviors also occur [51].

As a first step, cross couplings between the two motions can be considered as disturbances and the autopilot should be capable of reducing the sensitivity of the missile to those disturbances for an acceptable level. Outputs of autopilot module are the desired deflection commands which will be realized by tail and jet vane deflections. These commands will be the input to the missile dynamics.

In the following part, body rate, angle, and acceleration autopilots are presented. After each autopilot design is completed, its performance is tested in the nonlinear simulation environment that includes nonlinear autopilot module (formed by gain scheduling method) and nonlinear missile model. Autopilots are tested with reference command signals.

5.1. Pitch Autopilot Design

In the derivation of autopilot model that will be used within the application of control system, equations of motion should also be linearized around equilibrium flight (trim) points. As mentioned in the linear missile analysis, because of cross coupling dynamics, agile missile dynamics are not decoupled for pitch, yaw and roll planes. However, if the coupling terms are taken into account as disturbance, some of standard approaches (short period approximation) can be applied. In this section, a linearization procedure is performed. First of all, for a skid-to-turn

missile, aiming to have no roll rate and keeping roll angle at a constant steady state value, and also decoupling pitch and roll-yaw plane state equations result in taking roll rate approximately zero.

In short period approach, one of the main assumptions is missile's velocity is not changing. However, in boost phase, missile is highly accelerating and the assumption is not completely true [55]. As control is critical in boost phase where it lasts for 3.5 seconds, velocity change has to be taken into account. If derivation of angle of attack is examined, rate of change of the velocity (acceleration of the missile) is seen to be included in the equations (4.5) and (4.6).

$$\dot{\alpha} = \frac{\dot{w}u - w\dot{u}}{u^2} = \frac{\dot{w}}{u} - \frac{\dot{u}}{u}\alpha \tag{4.5}$$

It is assumed that $\dot{u}$ and u are constant at the linearization instant so the Eq. (5.1) becomes:

$$\dot{w} = \dot{U}\alpha + U\dot{\alpha} \tag{4.6}$$

Using the linearized forms of aerodynamic coefficients given in the previous section, linear dynamic equations are obtained as follows:

$$\dot{q} = \frac{QSd}{I_{yy}}\left(C_{m_\alpha}\alpha + C_{m_q}\frac{d}{2U}q\right) + \left(\frac{QSd}{I_{yy}}C_{m_{\delta_e}} - K\frac{Tl_x}{I_{yy}}\right)\delta_e \tag{4.7}$$

$$\dot{\alpha} = \frac{1}{U}\left(\begin{array}{l}\left(\frac{QS}{m}C_{z_\alpha} - \dot{U}\right)\alpha + \left(C_{z_q}\frac{QS}{m}\frac{d}{2U} + U\right)q \\ + \left(\frac{QS}{m}C_{z_{\delta_e}} - K\frac{T}{m}\right)\delta_e\end{array}\right) \tag{4.8}$$

As a simplification, equations (7.6)-(7.7) can be stated as

$$\dot{q} = M_\alpha\alpha + M_q q + M_{\delta_e}\delta_e \tag{4.9}$$

$$\dot{\alpha} = (Z_\alpha - \frac{\dot{U}}{U})\alpha + (Z_q + 1) + Z_{\delta_e}\delta_e \tag{4.10}$$

The stability derivatives used in the equations (4.9) and (4.10) are:

$$\begin{aligned} M_\alpha &= \frac{QSd}{I_{yy}} C_{m_\alpha},\ M_q = \frac{QSd^2}{2I_{yy}U} C_{m_q}, \\ M_{\delta_e} &= \frac{QSd}{I_{yy}} C_{m_{\delta_e}} + K\frac{Tl_t}{I_{yy}} \end{aligned} \tag{4.11}$$

$$\begin{aligned} Z_\alpha &= \frac{QS}{mU} C_{Z_\alpha},\ Z_q = \frac{QSd}{2mU^2} C_{Z_q}, \\ Z_{\delta_e} &= \frac{QS}{mU} C_{z_{\delta_e}} + K\frac{T}{mU} \end{aligned} \tag{4.12}$$

where K is the hybrid control ratio. State space representation is then:

$$A = \begin{bmatrix} Z_\alpha - \frac{\dot{U}}{U} & 1 + Z_q \\ M_\alpha & M_q \end{bmatrix} \quad B = \begin{bmatrix} Z_{\delta e} \\ M_{\delta e} \end{bmatrix} \tag{4.13}$$

In the following section controller design process will be presented. Dynamical system analyses are critical for understanding of all systems. Thus, before controller design, system dynamics must be understood well. Firstly, change in parameters of A and B matrices are examined. As seen in Figure 23 and Figure 24, stability derivatives change rapidly within the time of boost phase. Especially changes of M_α and $M_{\delta e}$ are so drastic. Moreover, trend of the changes are not linear; it is seen that around the time 1.5 second there is a peak change. This change can be related with transonic region aerodynamic characteristics. After 1.5^{th} second, parameters change with another tendency which is because of transonic region behavior [51]. As seen in Figure 23 and Figure 24, most of the coefficients reach a peak value at 1.5^{th} second where velocity is 1.15 Mach.

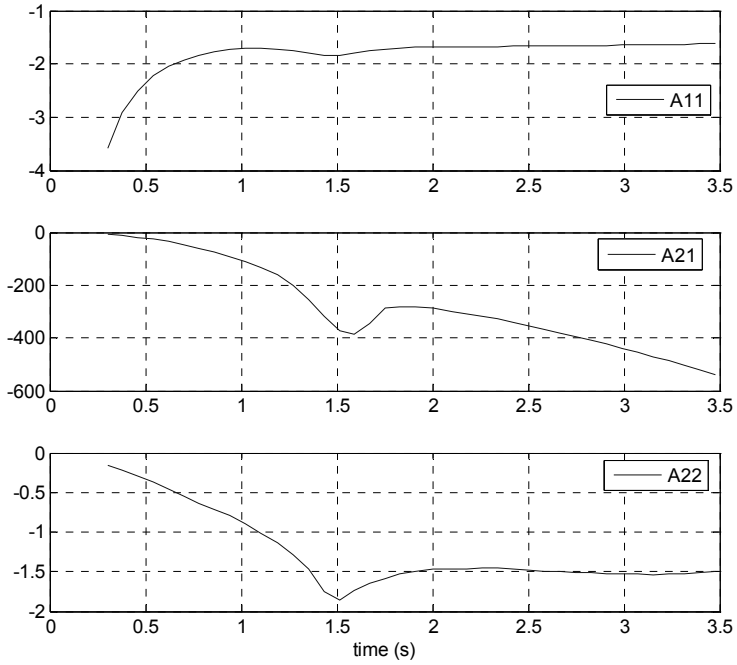

Figure 23 State Equations' Parameter Variations

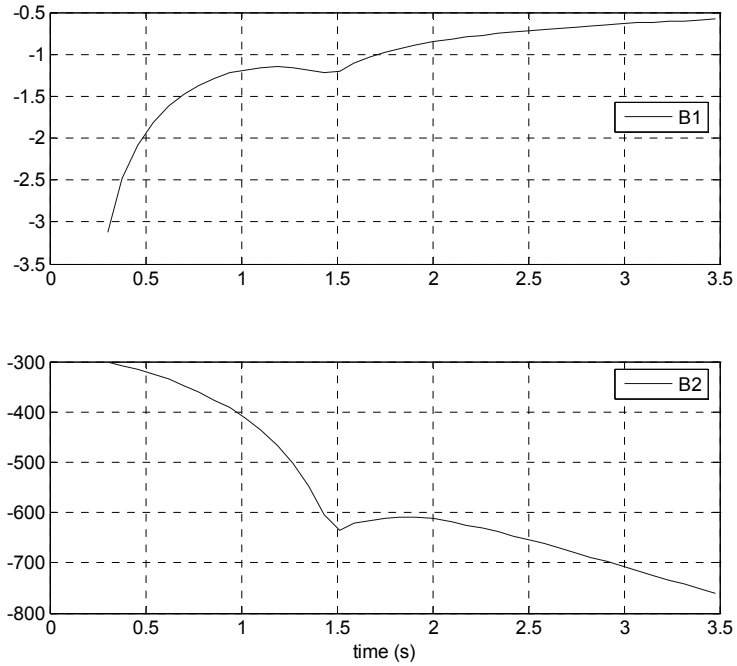

Figure 24 Control Parameters' Variations

In addition to varying parameter analyses, pitch rate natural frequency and damping coefficient changes are analyzed. Firstly, the transfer function of pitch rate with respect to hybrid elevator deflection (thrust vector and aerodynamic control where hybrid control ratio is 0.87) is obtained which is given in Eq. (4.14) and (4.15):

$$\frac{q(s)}{\delta_e(s)} = \frac{M_{\delta e}s - (Z_\alpha - \dot{U}/U)M_{\delta e} + M_\alpha Z_{\delta e}}{s^2 - s(M_q + Z_\alpha - \dot{U}/U) + (Z_\alpha - \dot{U}/U)M_q - M_\alpha - Z_q M_\alpha} \quad (4.14)$$

$$w_n = \sqrt{(Z_\alpha - \dot{U}/U)M_q - M_\alpha - Z_q M_\alpha}, \quad \xi = \frac{(M_q + Z_\alpha - \dot{U}/U)}{2w_n} \quad (4.15)$$

Then, natural frequency and the damping coefficient of the system for the boost phase are given in Figure 25 and Figure 26. One of the main issues in natural frequency and damping coefficient change is, as velocity increases natural frequency of the system increases with similar trend of the velocity profile. Damping coefficient decreases highly when velocity increases. Figure 27 shows the DC gain of the system during the boost phase. In the early stages of the flight time, its value is high. Immediately after the initial phase, its value decreases rapidly like an exponential function. Figure 28 is the pole zero map of the pitch rate dynamics. It can be examined better with the location of the poles and zeros. The same transonic region system behavior can also be seen in pole-zero map. This behavior was not recognized so clearly when boost phase is divided into 10 discrete time steps ($\Delta t = 0.35$ s). It is recognized during the autopilot design process. Although the linear controllers' performance was good, linear time varying responses were not as good as expected. In order to analyze poles and zeros in more details, boost phase is divided into 40 discrete time intervals ($\Delta t = 0.0875$ s) and controllers are designed for 40 plants.

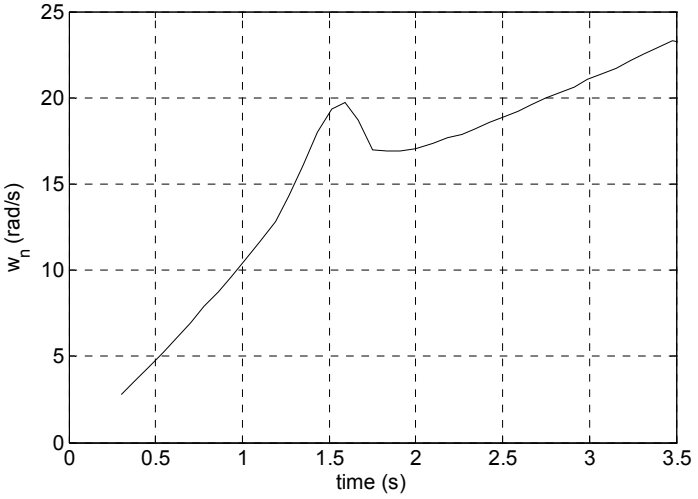

Figure 25 Natural Frequency of Pitch Rate Dynamics

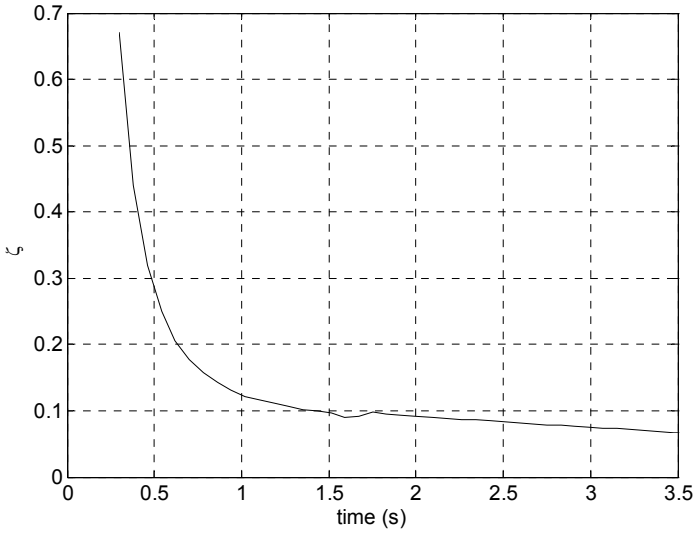

Figure 26 Damping Coefficient for Pitch Rate Dynamics

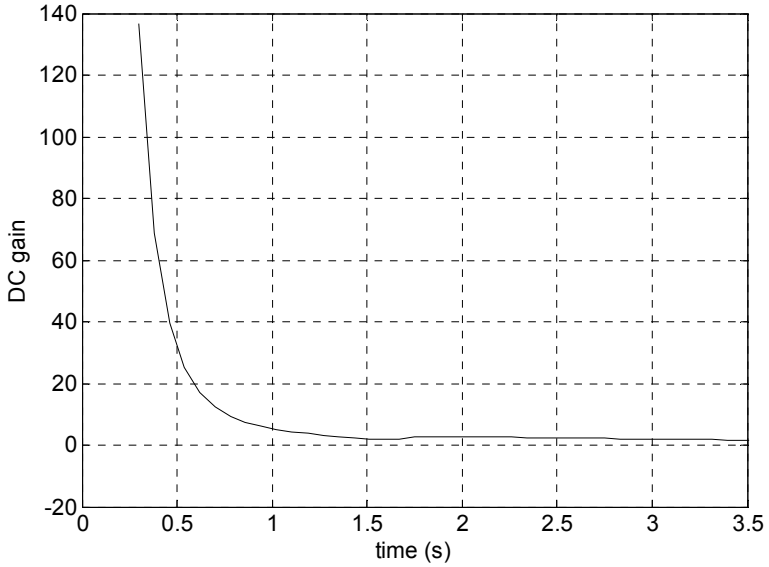

Figure 27 DC Gain of Pitch Rate Dynamics

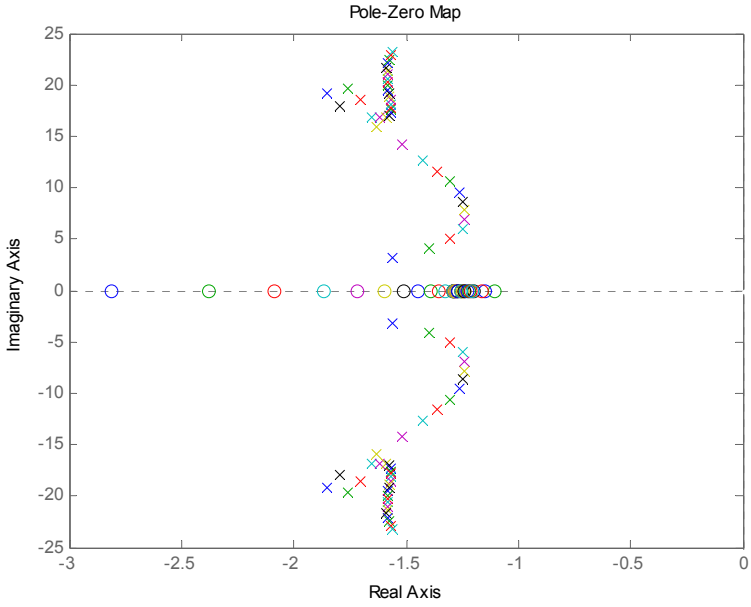

Figure 28 Pole Zero Map of Pitch Rate Dynamics

5.1.1. Pitch Rate Autopilot Design I

In this section, pitch rate is controlled with classical pitch rate controller. This type of controller is widely used in missile autopilots. Structure of the controller is given in Figure 29. Controller includes a zero and an integrator to inhibit steady state error. The state space representation and the parameters of the matrices are given in the previous section, so transfer function representation is not given again.

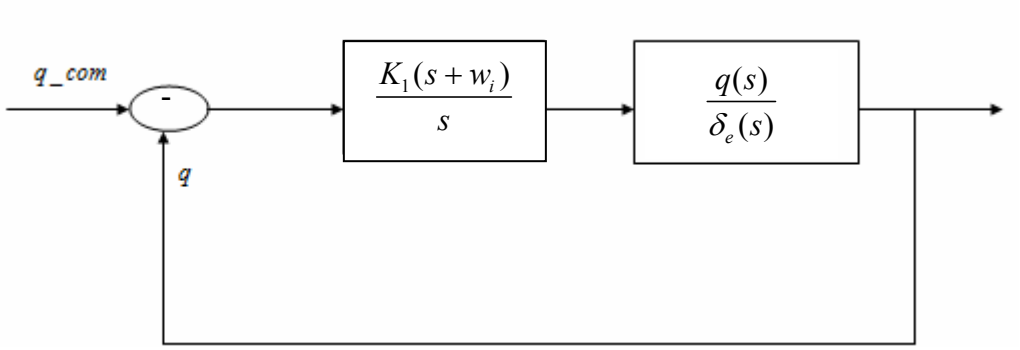

Figure 29 Pitch Rate Controller Structure I

It is obvious that the dominant pole placement technique cannot be applied with two free parameters. So, the parameters can be determined by time or frequency characteristics. Zeros of the controllers are placed in root locus and performance is examined for all frozen linear plants. The gains of the autopilot are given in Table 5. The responses of 10 linear time invariant plants and the deflections are seen in Figure 30. Settling time is less than 1 second in general and system behavior is like a first order system. These gains are scheduled with respect to time in the nonlinear simulation. The nonlinear simulation response and deflection is given in Figure 31. In all nonlinear simulation, nonlinear first order control actuator dynamics (w:300 rad/s) is included.

Table 5 Gains of the Controller for 10 LTI Systems at Δt=0.35s

	K_I	w_i
LTI 1	0.168	1.15
LTI 2	0.26	2.185
LTI 3	0.364	2.898
LTI 4	0.4	4.14
LTI 5	0.46	2.76
LTI 6	0.48	3.45
LTI 7	0.44	3.68
LTI 8	0.48	3.91
LTI 9	0.5	4.14
LTI 10	0.52	4.37

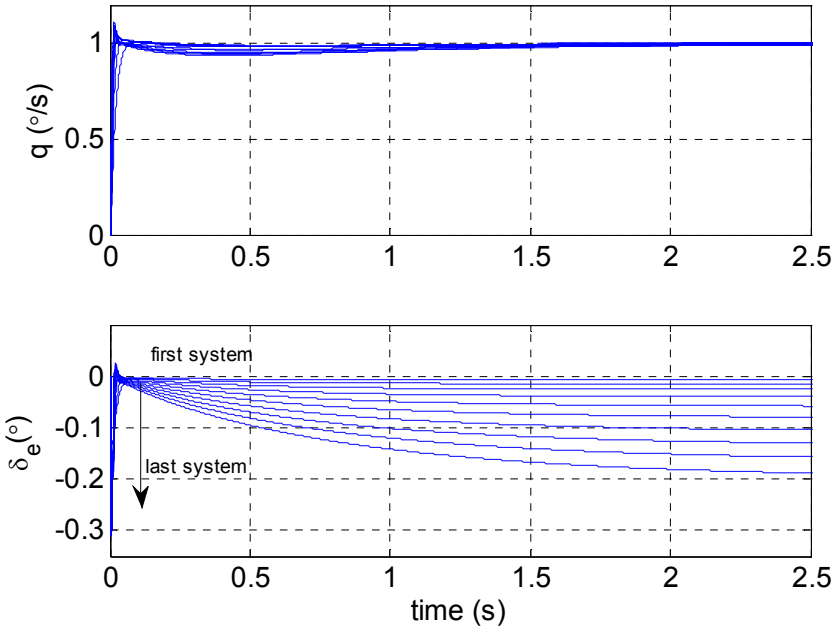

Figure 30 LTI Plants and Deflections I

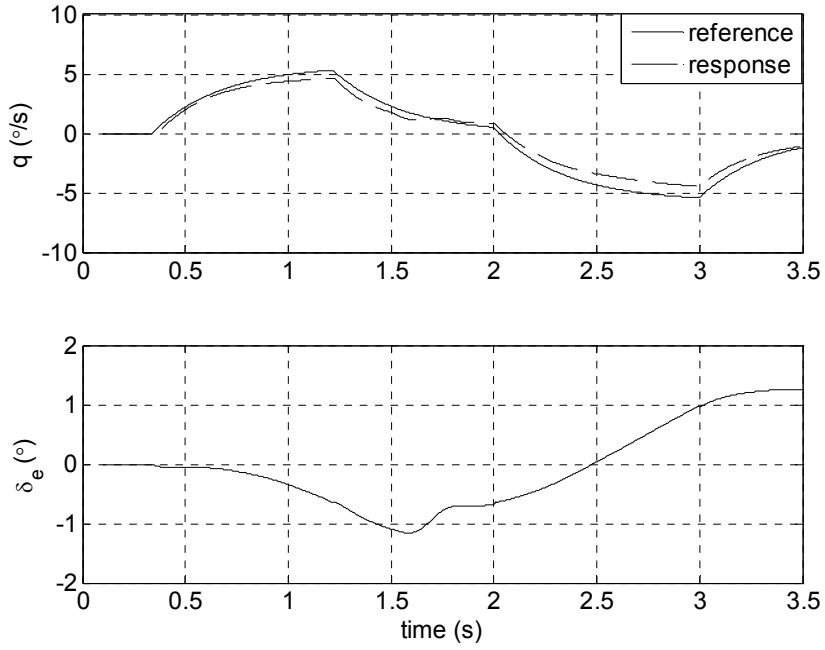

Figure 31 Pitch Rate Response and Deflection I (Nonlinear Simulation)

5.1.2. Pitch Rate Autopilot Design II

To analyze another control structure for the pitch rate dynamics, autopilot structure with state feedback is studied on. The A and B matrices of the pitch dynamics are given for the boost phase in Figure 23 and Figure 24. In this design procedure, a state feedback and feed forward gain is preferred. One of the desired poles is placed at the zero of the open loop system to improve the transient response and the other pole is placed at 1.25 times of w_n (Figure 25) of the linearized systems because of actuator time constant. The design procedure is applied to 40 linear time invariant plants (Δt=0.0875 s). The feed forward gain and state feedback gains are illustrated in Figure 32 and Figure 33. The responses of each plant and the deflections are seen in Figure 34. The responses of the LTI plants are quite well. However, when the plants are changed with respect to the linearized time schedule, response of the plant (linear time varying plant) varies. Interestingly, step response is not as good as LTI responses, see Figure 35. The second step of performance analysis of the design is using the autopilot in nonlinear simulation. As the feed-

forward gain is used in autopilot structure, the response will get worse whenever system is away from the linearization points. Figure 36 is the comparison of LTV plant and nonlinear plant with an approximately symmetric signal. Autopilot response is acceptable. But, it is hard to say it for the response in Figure 37. For related deflection angles, see Figure 38. This result directs a designer to find another autopilot structure.

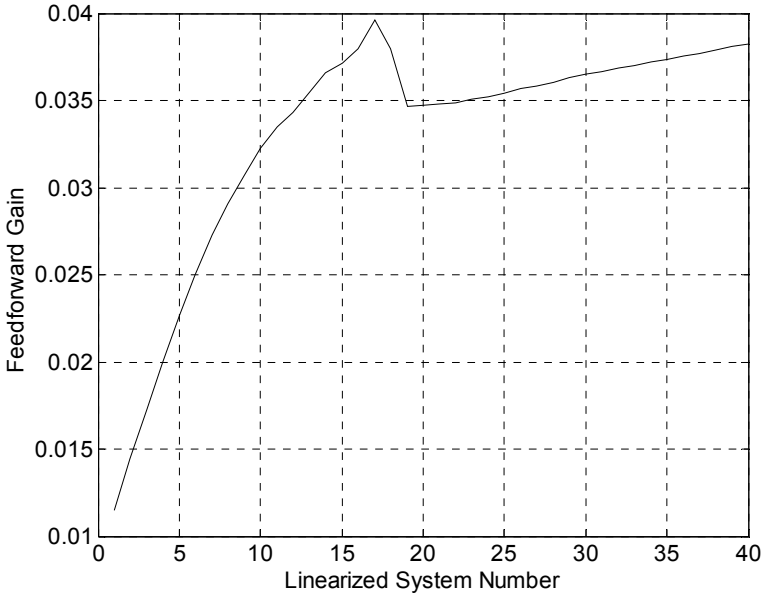

Figure 32 Feedforward Gain for the Linearized Systems

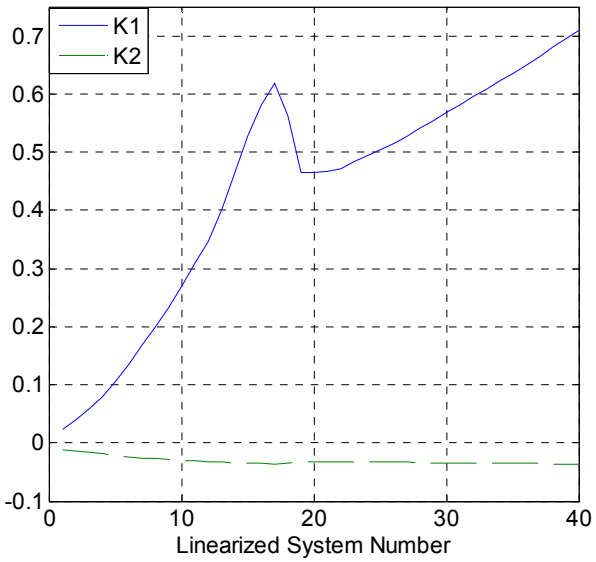

Figure 33 State Feedback Gains

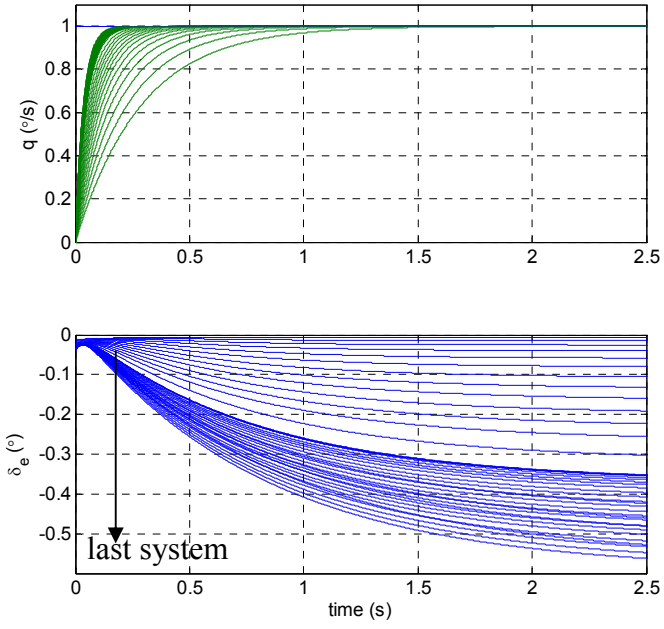

Figure 34 LTI Plants Responses to Unit Step and Deflections II

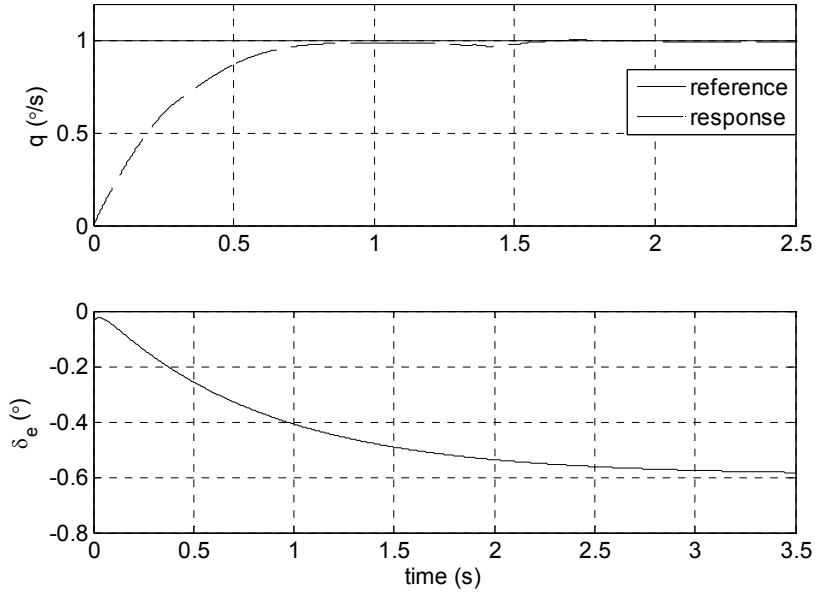

Figure 35 LTV Plants Response and Deflection II

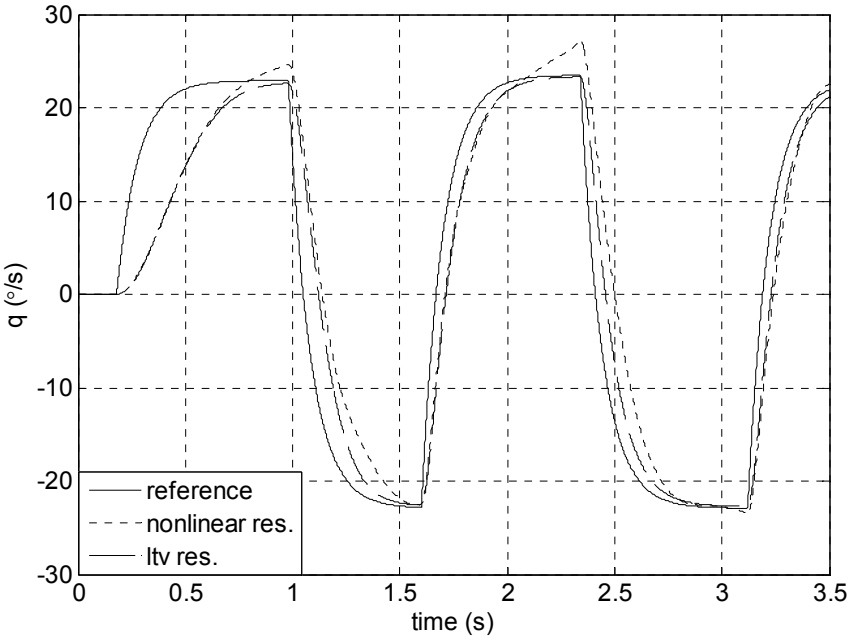

Figure 36 Autopilot Response to Symmetric Reference Input

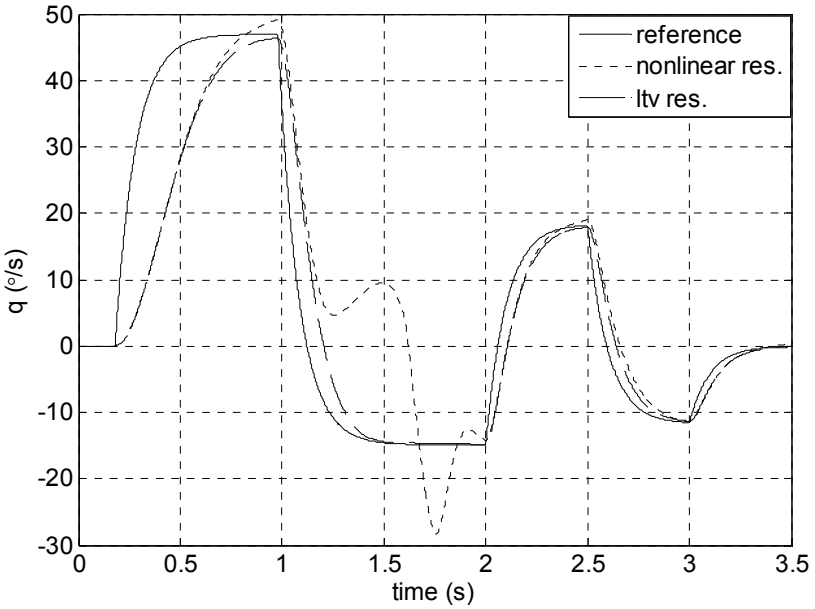

Figure 37 Autopilot Response to non-Symmetric Reference Input

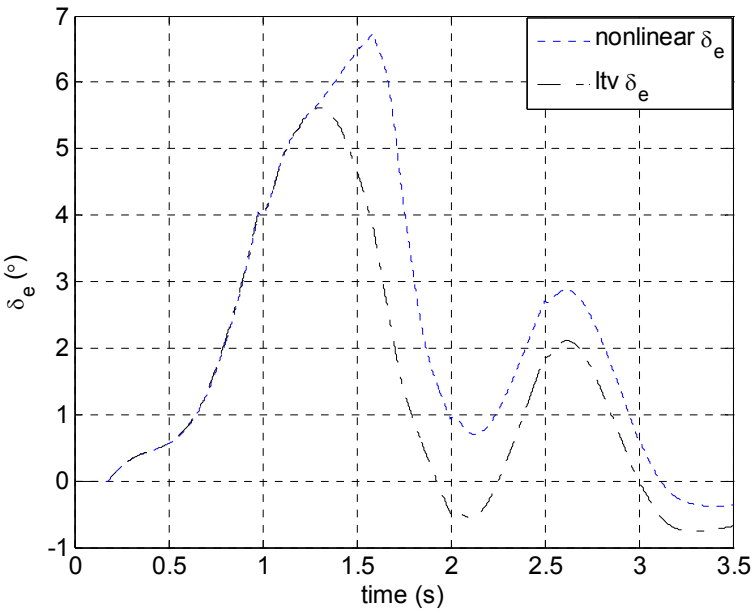

Figure 38 Deflection Angles

5.1.3. Pitch Rate Autopilot Design III

As controlled pitch rate dynamics is a type-one system and zeros of the system affects the transient response, practical suboptimal tracker method is studied on. In this section, practical suboptimal control structure with application to pitch rate dynamics will be held. The mentioned control structure and the necessity behind integrating the error is briefly described at [56].

By integrating the error dynamics to the system dynamics, the new state space representation is obtained as:

$$\begin{bmatrix} \dot{x} \\ \dot{\xi} \end{bmatrix} = \begin{bmatrix} A & 0 \\ -C & 0 \end{bmatrix} \begin{bmatrix} x \\ \xi \end{bmatrix} + \begin{bmatrix} B \\ 0 \end{bmatrix} u + \begin{bmatrix} 0 \\ I \end{bmatrix} r,\ y = C x \tag{4.16}$$

where

$$\dot{\xi} = q_{com} - q \tag{4.17}$$

and the control input is

$$u = -\begin{bmatrix} K2 & K3 \end{bmatrix} x + K1\xi \tag{4.18}$$

Overall gain matrix which can be chosen with pole placement method is:

$$K_T = \begin{bmatrix} K2 & K3 & -K1 \end{bmatrix} \tag{4.19}$$

For the boost phase of the system, one of the poles is placed at the zero of the system. The other poles are placed to the natural frequency and 1.3 times of the natural frequency of the linear systems. The state feedback gains are illustrated in Figure 39. Closed loop responses of linear systems and the elevation commands are illustrated in Figure 40. The slowest one of the linear systems (0.3 seconds after vertical launch) settles down before 2 seconds and the maximum deflection angle is 0.6º. To analyze the performance of the overall system during the boost phase,

linear time varying model is used with the given control structure. The controller's parameters are also changed and interpolated with respect to time. In this structure which will be the behavior of vertical launch system, the response and the deflection of the system is given in Figure 41. As seen, the step response of the system is not the like the ones given in Figure 40. This is a direct consequence of dealing with a highly varying system result whose parameter changes are given in Figure 23 and Figure 24, [52]. In order to analyze the final performance of the controller, controller structure is embedded into the nonlinear simulation and a reference input is given to the nonlinear system. The reference input, LTV and nonlinear system responses are given in Figure 42 and the deflections of LTV and nonlinear system is in Figure 43. It is clearly seen that the nonlinear response is not as satisfactory as expected which shows that it is not possible to have the desired responses with pure gain scheduling.

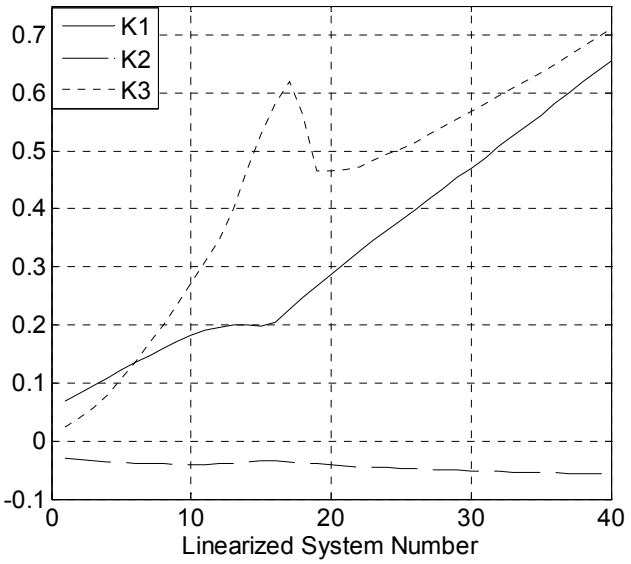

Figure 39 Gains of the Controller

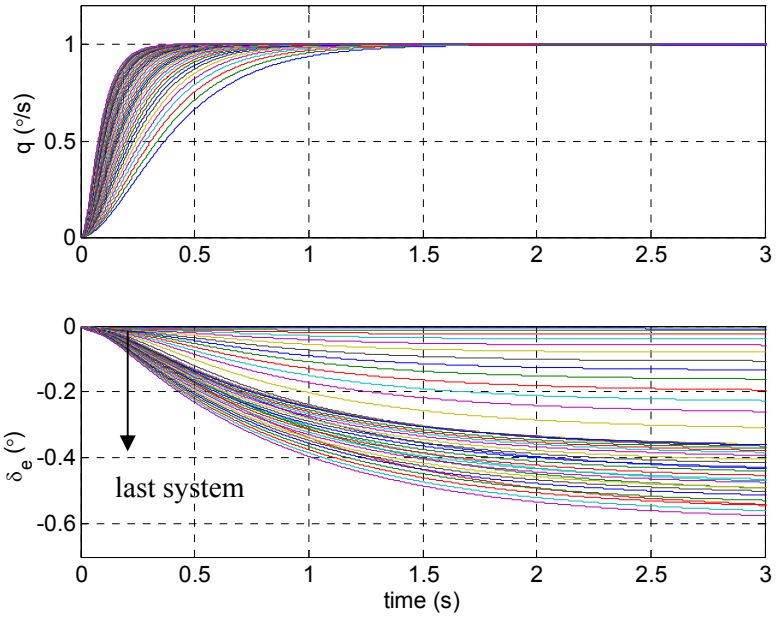

Figure 40 LTI Responses and Deflection Angles III

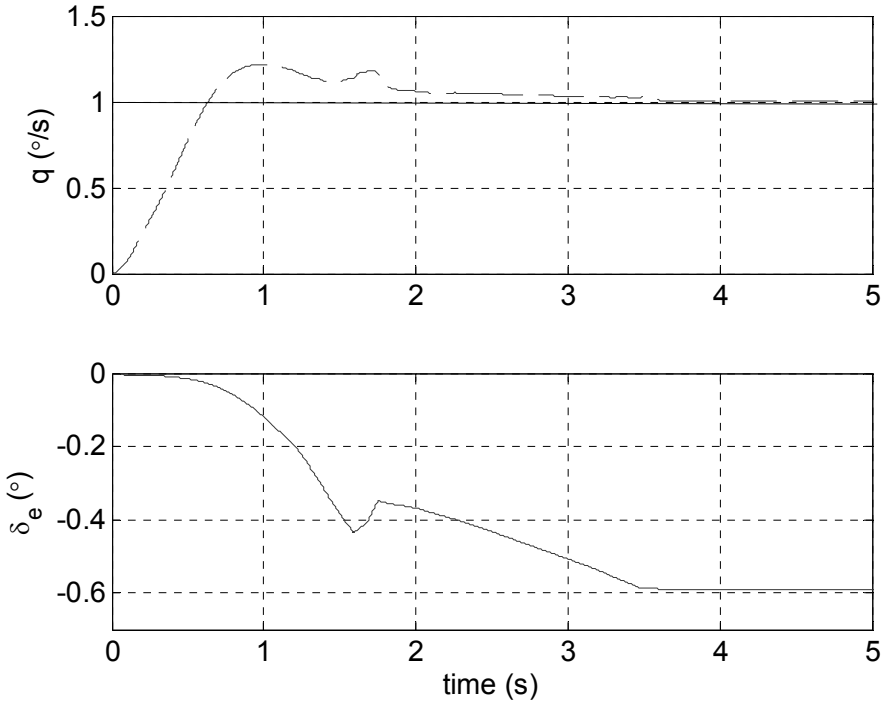

Figure 41 LTV Response and Deflection Command III

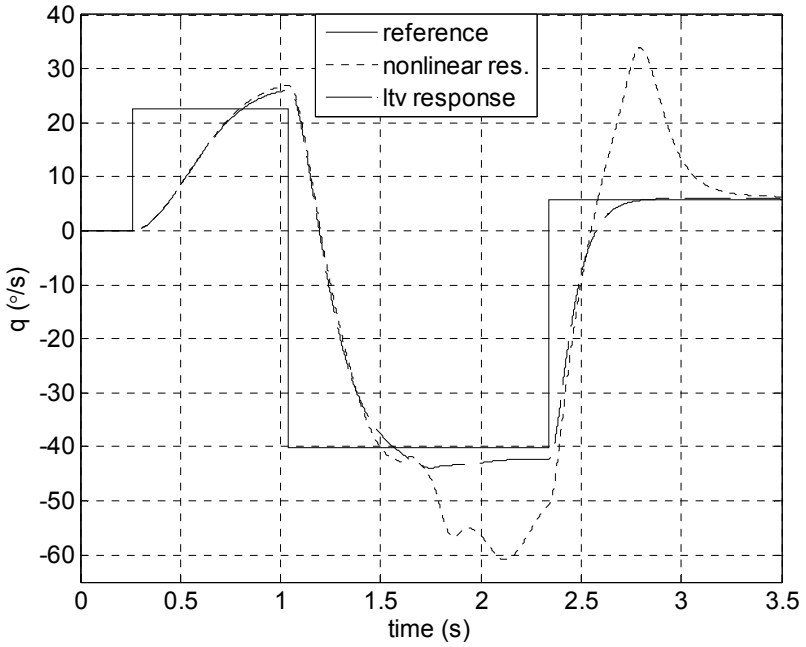

Figure 42 Nonlinear and LTV Responses

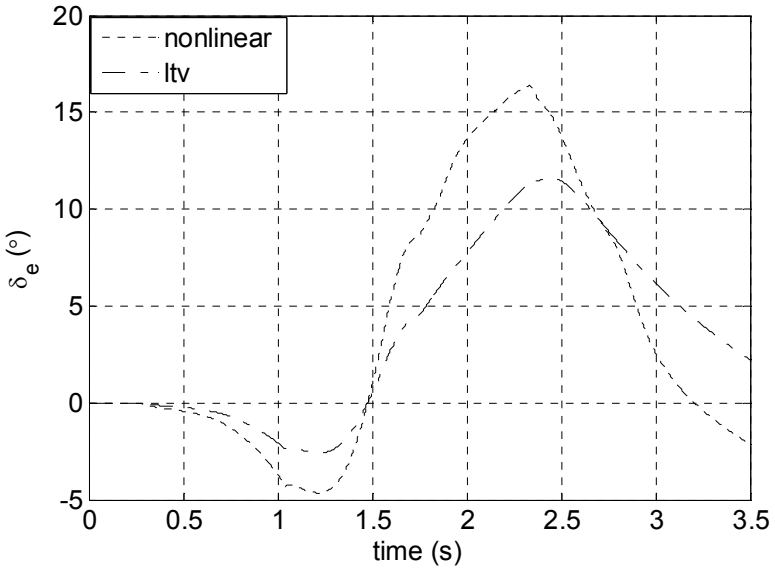

Figure 43 Nonlinear and LTV Systems Deflections

5.1.4. Pitch Angle Autopilot

The autopilot structures which are studied till now are mostly based on state feedback which needs alpha estimation and they do not have sufficient performance as desired. So that, another control type of pitch channel is considered. The body pitch angle, θ, is controlled. The main advantage of this controller is that the highly changing pitch rate is damped in the inner loop, and θ is controlled with the outer loop. θ autopilot loop is seen in Figure 44. The saturation seen in Figure 44 is for commanding pitch rates which are practically possible. In this study, pitch rate saturation is considered as 350º/s and it is a realistic value for air defense missiles [58].

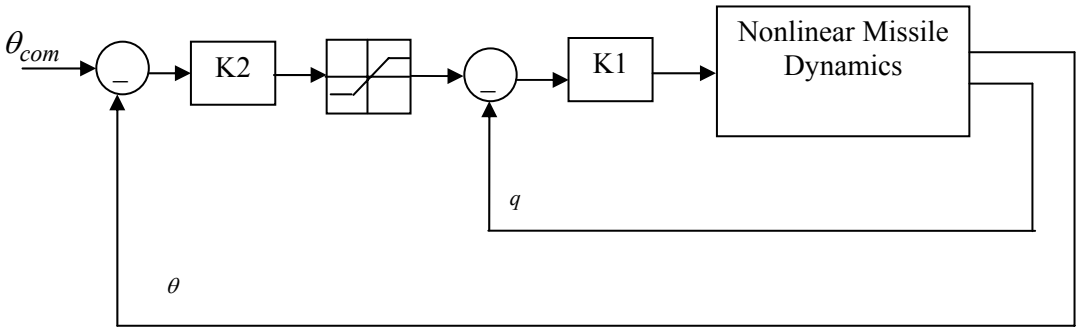

Figure 44 Theta Autopilot Loop

First, the controller structure given in Figure 44 is demonstrated for the linearized systems. Controllers' gains are chosen to have a settling time less then or close to 1 second with respect to the natural frequency of the linearized systems. The first one of linearized systems which is:

$$\frac{\theta(s)}{\delta_e(s)} = \frac{324.8\,s + 677}{s(s^2 + 2.602\,s + 26.93)}$$

has the gains $K2 = 10$ and $K1 = 0.19$. And the last system which is

$$\frac{\theta(s)}{\delta_e(s)} = \frac{761.5\,s + 917.5}{s(s^2 + 3.12\,s + 543.4)}$$

has the gains $K2 = 37$ and $K1 = 0.58$. The two linearized systems' response to a step input can be seen in Figure 45. Afterwards, the controller is embedded into the nonlinear simulation and scheduled with respect to time. Desired command and response with deflection is seen in Figure 46. In this scenario, missile is vertically launched and after it reaches 5m altitude, and control starts. For one second, zero command is sent to turnover the missile. Then this command is changed to pitch up till 2.5 seconds and finally for the last second command is directionally reversed. As seen, the turnover maneuver is successfully accomplished. The autopilot performance to turnover the pitch up - pitch down maneuvers are quite well within the varying parameters profile given in Figure 47 where angle of attack is changing between 0 and 60 degrees, velocity is accelerated from 0 to 2.5 Mach during 3.5 seconds.

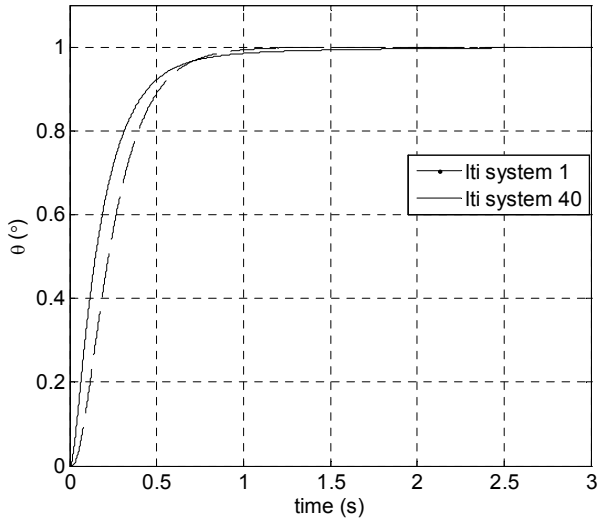

Figure 45 LTI Responses

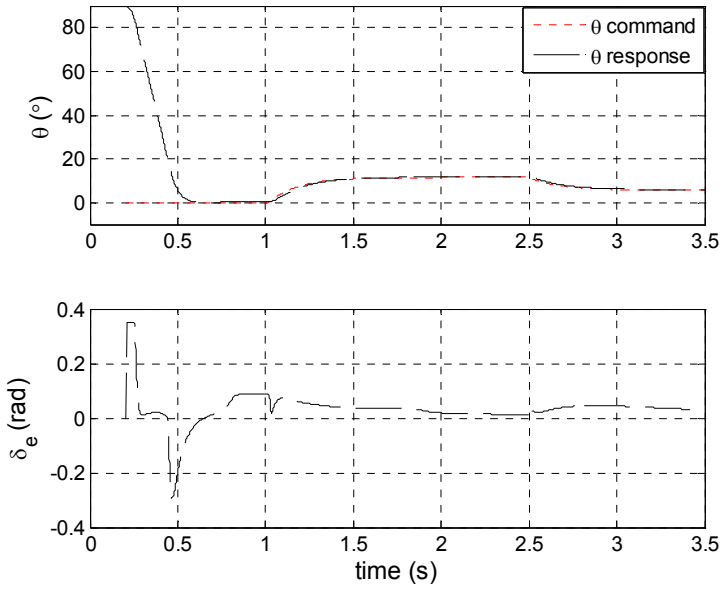

Figure 46 Nonlinear Simulation Response and Deflection

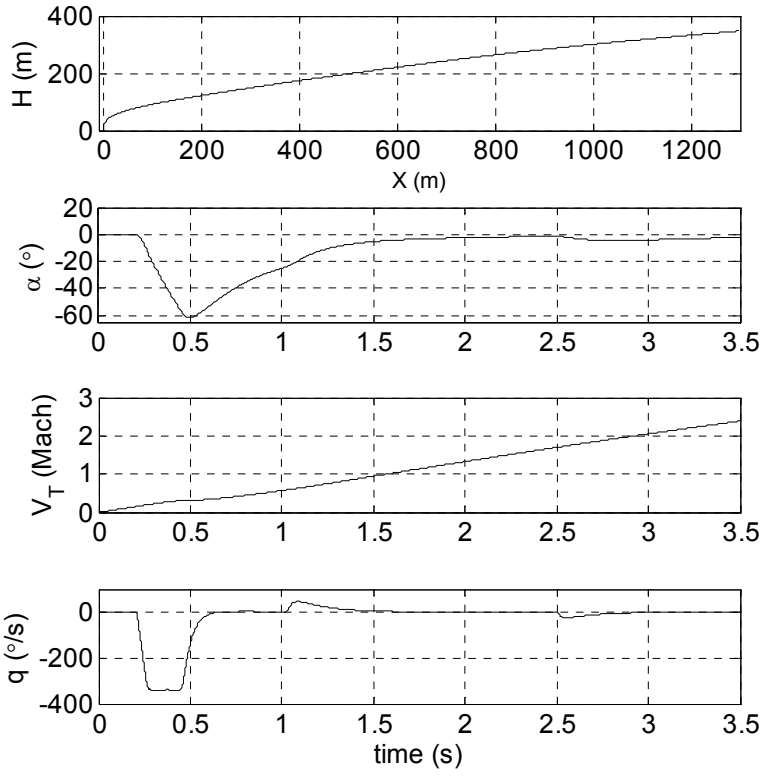

Figure 47 Altitude, Angle of Attack, Velocity, Pitch Rate During the Maneuver

5.1.4.1. Missile Turn Over Capability Analysis with Angle Autopilots

In an effort to determine the capability of hybrid controlled VLSAM, 3 scenarios are formed. In all of the scenarios, missile starts the turnover maneuver from different altitudes. In each turnover altitude, theta commands are applied until 3.5 seconds. In the first scenario, θ starts from 90 degrees, a θ command of 45 degrees is applied till the boost motor is over. Figure 48 shows the variation of altitude and downrange of missile during 45 degrees of continuous theta command. In the second scenario, θ starts from 90 degrees, and then a θ command of 0 degrees is applied till the boost motor is over. Control commands are started to be sent at different altitudes. The minimum turnover altitude is more than 150 meters and the maximum turnover altitude is more than 400 meters as seen in Figure 49. In the third scenario, a θ command of -45 degrees is executed. Figure 50 shows the minimum downrange with minimum altitude capability of the missile. If the missile starts the turnover maneuver at 5 meters altitude, it can approach 200 meters range within an altitude of 50 meters. But if, it starts turning at 100 meters altitude, it can approach 500-600 meters downrange within an altitude of about 270 meters.

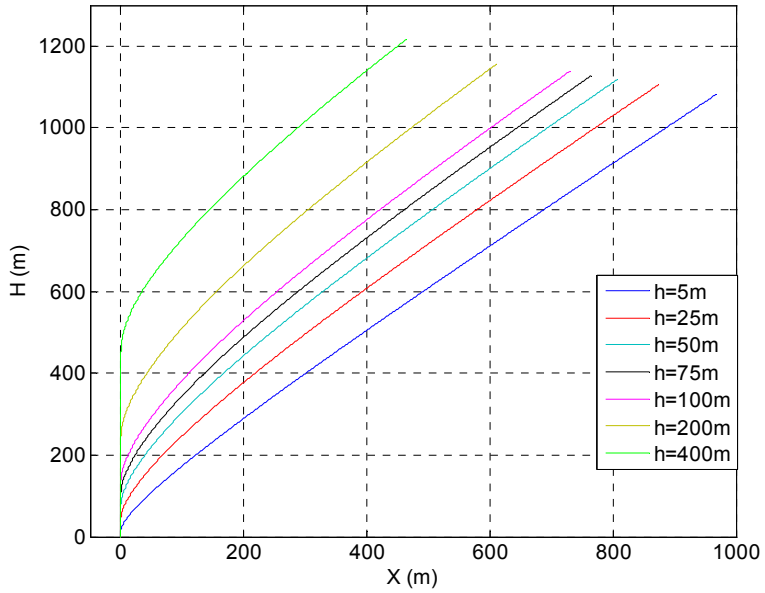

Figure 48 X-H Graph at θ_F = 45º wrt. to Various Initial Turnover Altitudes

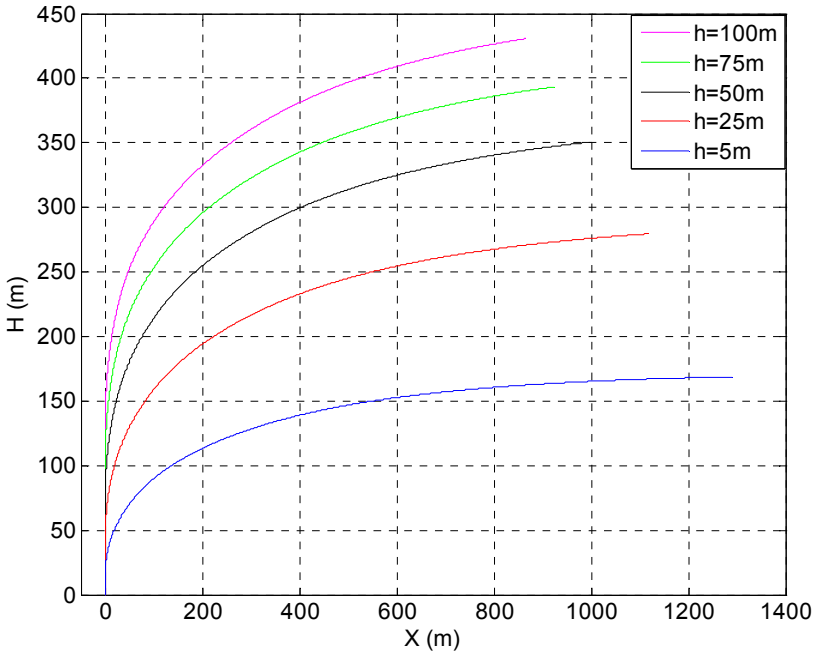

Figure 49 X-H Graph at θ_F = 0º wrt. Various Initial Turnover Altitudes

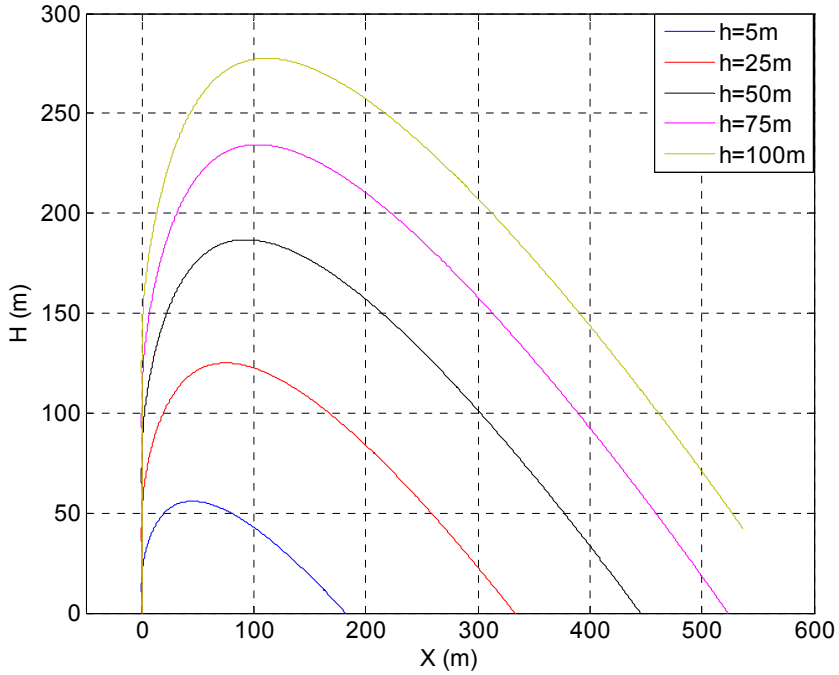

Figure 50 X-H Graph at θ_F =- 45º wrt. Various Initial Turnover Altitudes

5.2. Roll Autopilot Design

Using the linearized forms of aerodynamic coefficients as in the previous section, linear dynamic equations for the roll plane are obtained as follows:

$$\dot{p} = \frac{Q S d}{I_{xx}} \left(C_{l_\alpha} \alpha + C_{l_\beta} \beta + C_{l_p} \frac{d}{2U} p + C_{l_{\delta_a}} \delta_a \right) \tag{4.20}$$

$$\dot{\phi} = p \tag{4.21}$$

In equations (7.8)-(7.9), the stability derivatives used are:

$$\begin{aligned} L_p &= \frac{Q S d^2}{2 I_{xx} U} C_{l_p}, \; L_\beta = \frac{Q S d}{I_{xx}} C_{l_\beta}, \\ L_\alpha &= \frac{Q S d}{I_{xx}} C_{l_\alpha}, \; L_{\delta_a} = \frac{Q S d}{I_{xx}} C_{l_{\delta_a}} \end{aligned} \tag{4.22}$$

$$I_{xx}\dot{p} = L_p p + L_{\delta a}\delta a + L_\alpha \alpha + L_\beta \beta \tag{4.23}$$

If the terms connected with attack angles α and β are treated as disturbances the roll rate derivative can be rewritten as:

$$I_{xx}\dot{p} = L_p p + L_{\delta a}\delta a \tag{4.24}$$

where transfer function is expressed as:

$$\frac{p(s)}{\delta_a(s)} = \frac{L_{\delta a}}{sI_{xx} - L_p} \tag{4.25}$$

Pole of the transfer function in equation (4.25) with respect to mach and altitude for thrust phase is given in Figure 51. Rise in velocity directly results decrease in time constant.

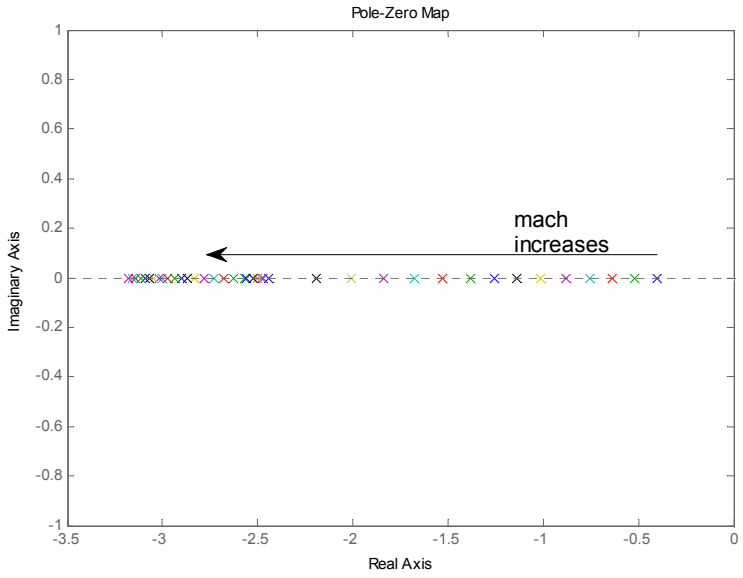

Figure 51 Pole Zero Map of Roll Channel

5.2.1. Roll Angle Autopilot

Roll angle control is performed with the same approach as in the theta control. The angle of sideslip and attack components are taken into account as disturbances. Roll commands are desired to be realized as soon as possible within actuator limitations. Firstly, controller structure given in Figure 52 is demonstrated for the linearized systems. Controllers gains are chosen to have a settling time changing from 1 to 5 seconds with respect to the natural frequency of linearized systems. The first linearized system is:

$$\frac{\phi(s)}{\delta_a(s)} = \frac{49.9}{s(s + 0.402)} \quad .$$

It has the gains $K2 = 0.8$ and $K1 = 0.02$. The last system is

$$\frac{\phi(s)}{\delta_a(s)} = \frac{2810}{s(s + 3.18)}$$

having the gains $K2 = 2$ and $K1 = 0.04$. The step responses of the first and fortieth systems are shown in Figure 53. Controller's gains are updated for all of the linearized systems. Afterwards, the controller is embedded into the nonlinear simulation. Desired command, response and deflection are seen in Figure 54.

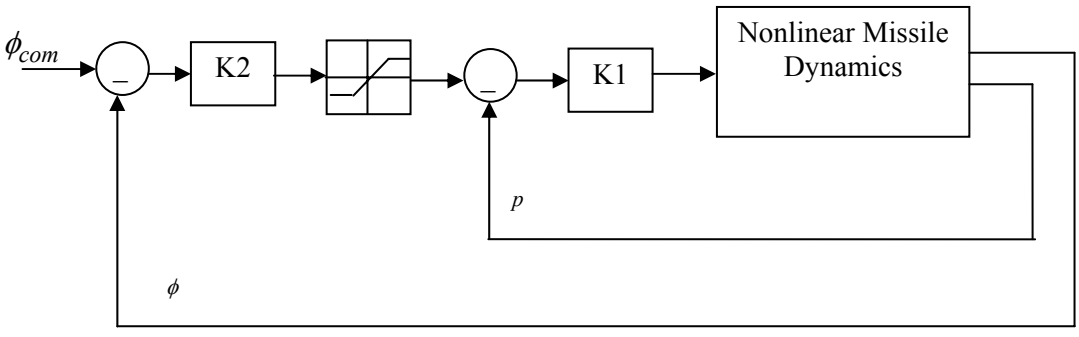

Figure 52 Roll Angle Control Structure

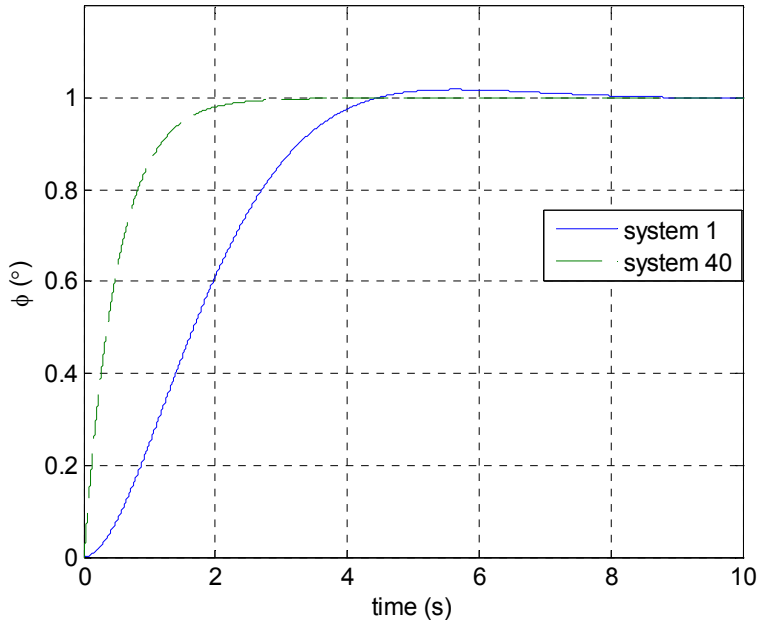

Figure 53 LTI Responses

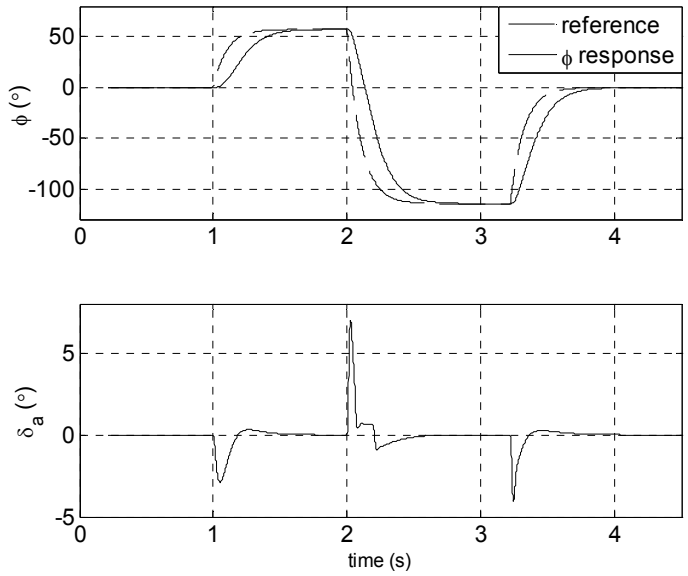

Figure 54 Roll Angle and Deflection Angle (nonlinear simulation)

5.2.2. Roll Rate Autopilot

In roll plane, another control parameter is the roll rate, *p*. High angle of attacks' effects are omitted. So, the same transfer functions without the integrator which are given in the roll angle autopilot and the pole-zero maps given in Figure 51 are valid for the roll rate dynamics.

In order to control the roll rate, the controller structure in Figure 55 is applied to the linearized systems. The controllers for the first and the last linearized boost phase systems are given below:

$$C_1 = \frac{0.051s + 0.02}{s} \text{ and } C_{40} = \frac{0.023s + 0.04}{s}.$$

Step responses of closed loop systems can be seen in Figure 56. Overall settling time is less than 1.6 seconds. After controllers' gains are scheduled with respect to time in the nonlinear simulation environment, a reference command is send to the roll channel which is given in Figure 57. Both controllers' response and aileron deflection command is quite well. Roll angle for the achieved roll rate is also given in Figure 57.

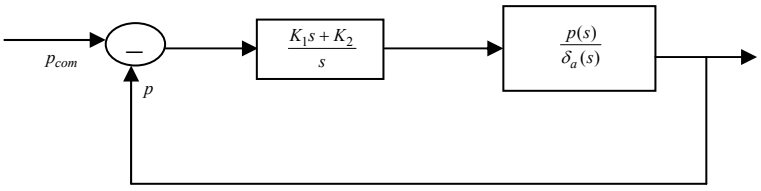

Figure 55 Roll Rate Controller Structure

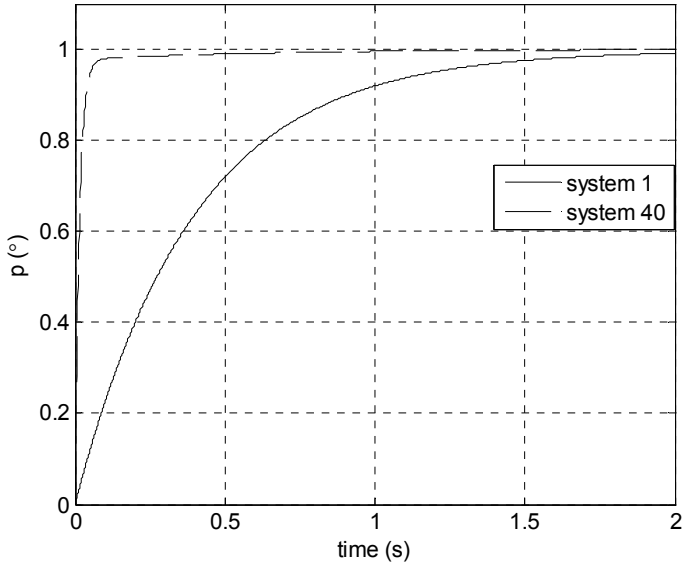

Figure 56 LTI Responses of Roll Rate Control

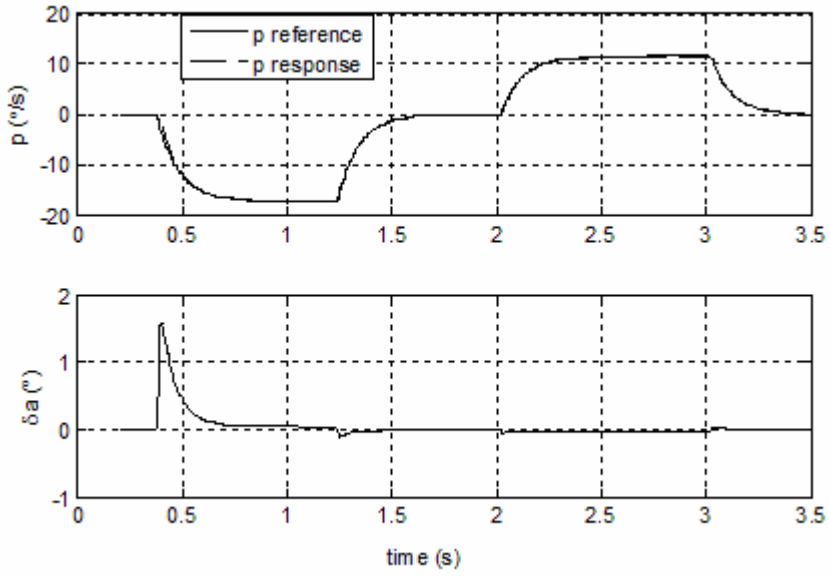

Figure 57 Roll Rate Reference and Response with Deflection Angle (Nonlinear)

5.3. Acceleration Autopilot

The autopilot structures till now are planned to be used in the midcourse guidance phase. However, acceleration autopilot is preferred for the terminal guidance. In order to use proportional navigation guidance, it will be beneficial to design

acceleration autopilot for the phase where pure aerodynamic control surfaces are used. The state space equation for the pitch plane integrated with actuator dynamics is:

$$\begin{bmatrix} \dot{\alpha} \\ \dot{q} \\ \dot{\delta} \end{bmatrix} = \begin{bmatrix} Z_\alpha - \dfrac{\dot{U}}{U} & 1+Z_q & Z_{\delta_e} \\ M_\alpha & M_q & M_{\delta_e} \\ 0 & 0 & -\omega \end{bmatrix} \begin{bmatrix} \alpha \\ q \\ \delta_e \end{bmatrix} + \begin{bmatrix} 0 \\ 0 \\ \omega \end{bmatrix} \delta_{e,c} \tag{4.26}$$

$$a_z = Z_\alpha \alpha + Z_{\delta_e} \delta_e \tag{4.27}$$

where actuator transfer function is

$$\frac{\delta_e(s)}{\delta_{e,c}(s)} = \frac{\omega}{s+\omega} \tag{4.28}$$

that can be written in the state space form as

$$\dot{\delta}_e(s) = \omega(-\delta_e + \delta_{e,c}) \tag{4.29}$$

To analyze the acceleration dynamics, pole-zero analysis is carried on. Figure 58 shows the pole and zeros of acceleration dynamics. As it is known, in this study, there is only one boost motor; so that after the boost phase is over velocity decreases quickly. Decrease in the velocity results a corresponding decrease in the stability of the acceleration dynamics as seen in Figure 58.

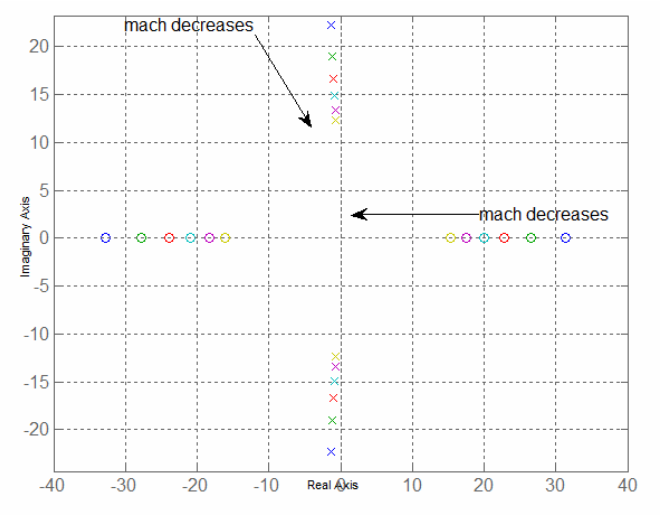

Figure 58 Pole Zero Map of Acceleration Dynamics

Before starting the design of the controller, some analyses have been performed. As mentioned previously, acceleration has also important effects on the acceleration dynamics [55]. There are two possible regions where $\dot{U}/U$ changes significantly. One is the boost phase where velocity increases rapidly as the first phase. Linearized systems scheduled with Mach and a deflection command is applied to compare the system results of linear and nonlinear systems. Deflection command and responses are presented at Figure 59. $\dot{U}/U$ effect for the boost phase is drastic where velocity is low. If this acceleration is not taken into account, acceleration dynamics will not be defined correctly.

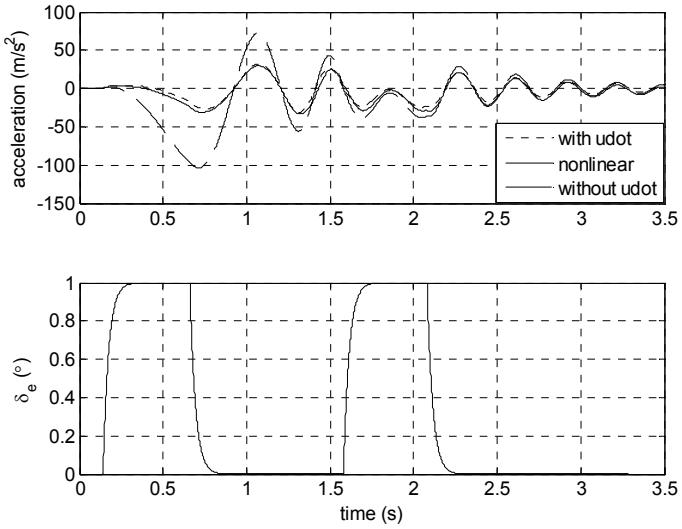

Figure 59 $\dot{U}/U$ Effect on Linear-Nonlinear System Comparison

The second condition where change in $\dot{U}/U$ is the terminal phase where high acceleration is needed for interception. In the terminal phase, this change has to be considered if needed. Trim points for the acceleration autopilot are given in Table 6. Acceleration autopilot design depends basically on classical 3 loop autopilot structure [57] with specified design parameters in Table 7. Structure of the three loop autopilot is also presented in Figure 60.

Table 6 Trim Points Used for Autopilot Design

Variables	**Trim Points**
Angle of Attack (deg.)	0º
Velocity (Mach)	2.41 2.09 1.87 1.69 1.55 1.43 1.32 1.23
Altitude (m)	1514 1929 3276 4462 5529 6502 7395 8222

Here is a transfer function of acceleration dynamics where velocity is 2.41 Mach and altitude is 1514 m:

$$\frac{a_z(s)}{\delta_e(s)} = \frac{-222s^2 - 302.5s + 2.542e5}{s^2 + 2.66s + 499.8}$$

and

$$\frac{a_z(s)}{\delta_e(s)} = \frac{-95.3s^2 - 74.49s + 3.425e5}{s^2 + 1.445s + 180.5}$$

where velocity is 419 m/s and altitude is 8222 m.

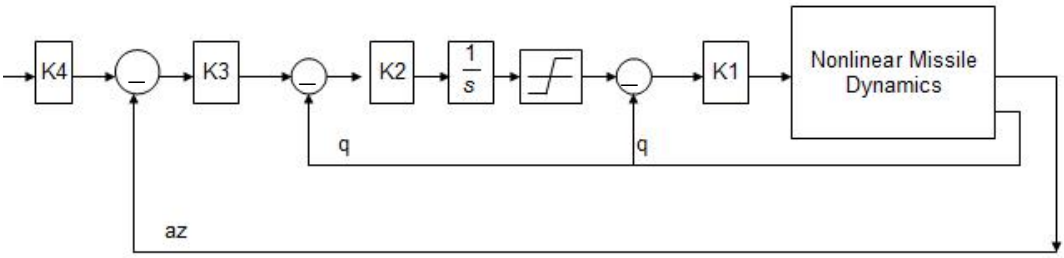

Figure 60 Three Loop Acceleration Autopilot Loop

Designed control structure is applied to linearized systems within the design criteria are given in Table 7. The controllers' gains are also given in Table 7 and they are changing between the given gains given for the first and last linearized system. Settling time and rise time is decided with respect to linearized systems natural frequencies and actuator bandwidths. The LTI responses for the linearized systems are presented in Figure 61. The autopilot structure and the gains are embedded into the nonlinear simulation and scheduled with velocity to examine its performance in the nonlinear model. Response to a 0.5 Hz 20 m/sn^2 square wave command is illustrated in Figure 62. The angle of attack change while performing the reference command is also given in Figure 63. As expected, deflection angle and angle of attack are increasing in order to achieve the desired acceleration command because missile's velocity is decreasing. The changing parameters, velocity and dynamic pressure, are also exhibited to come to a decision of autopilot

performance in Figure 64. As seen, acceleration commands are performed while velocity and dynamic pressure are changing very rapidly.

Table 7 Design Parameters and Gains

Settling Time (sec)	< 1.5
Rise Time (sec)	< 0.5
[K1 K2 K3 K4]	[0.1119 -0.0119 -20.4 1.035]- [0.0898 -0.0086 -22.7 1.0125]

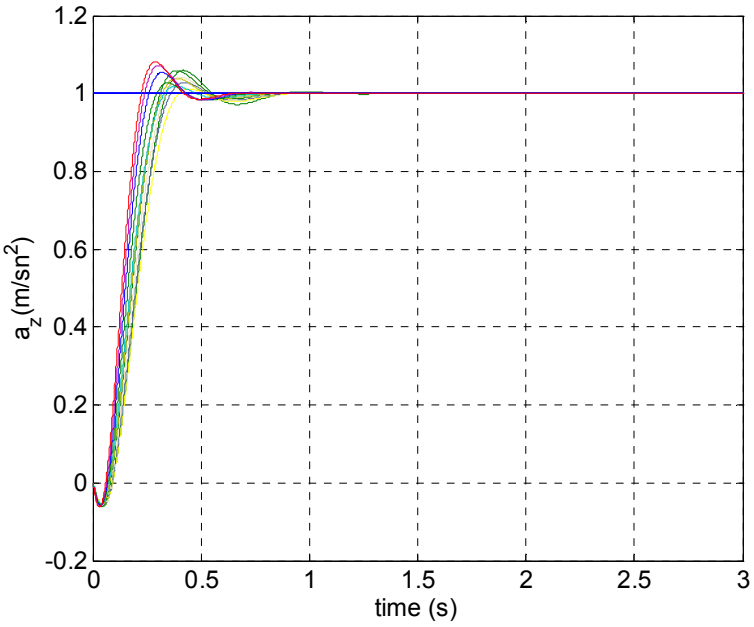

Figure 61 LTI Responses of Closed Loop Systems

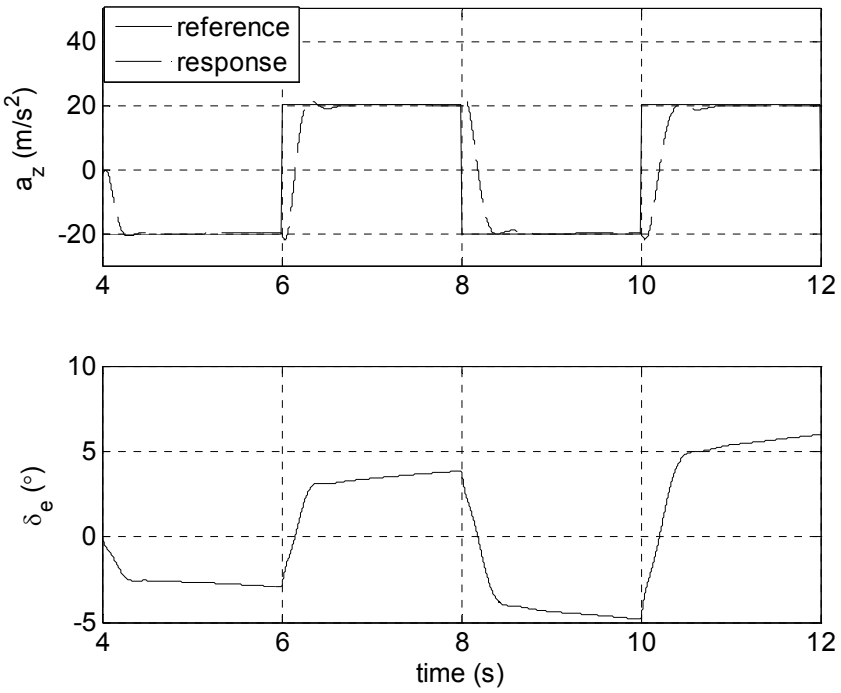

Figure 62 Nonlinear Simulation Response and Deflection Angle

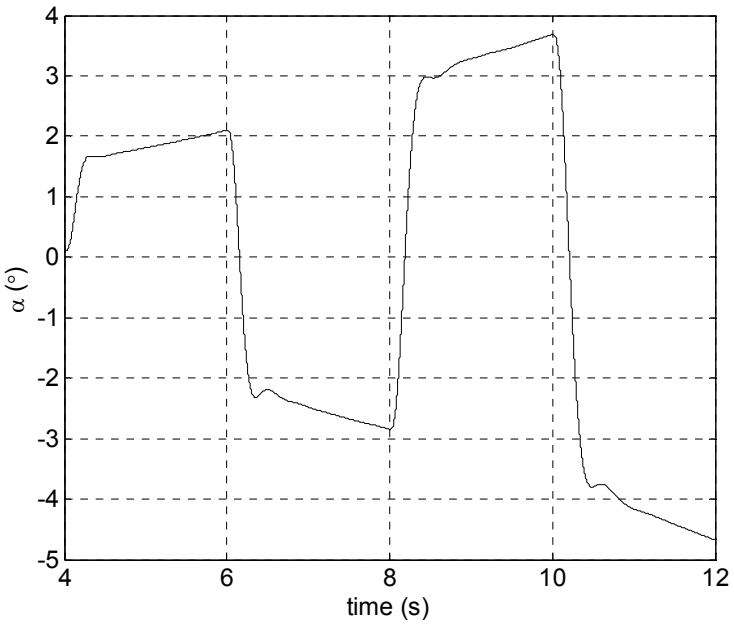

Figure 63 Angle of Attack During the Nonlinear Simulation

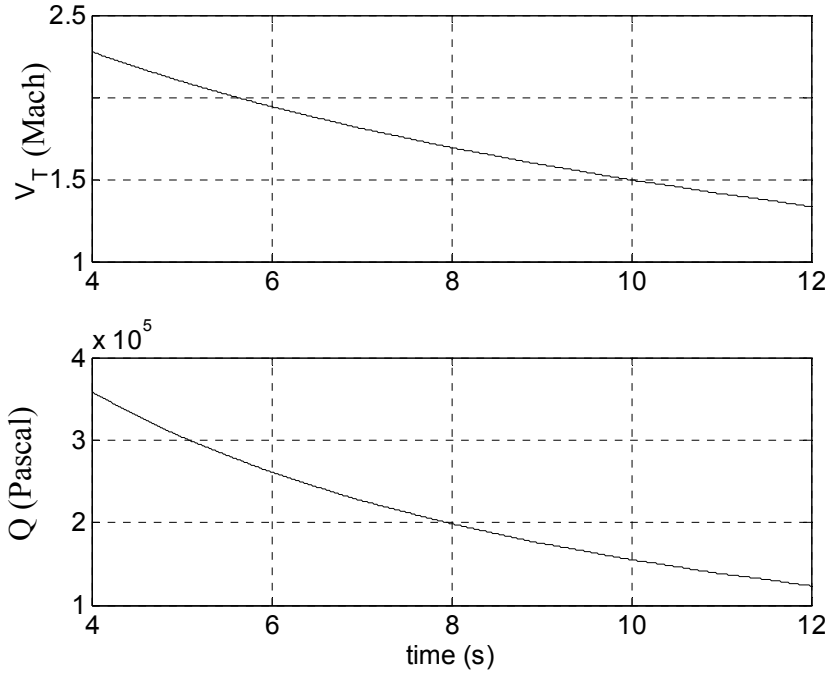

Figure 64 Velocity and Dynamic Pressure Change During Simulation

CHAPTER 6

CONVENTIONAL GUIDANCE DESIGN

Guidance refers to variety of methods to intercept a target. Guidance can be divided as target related guidance and non target related guidance. Figure 65 (adapted from [59]) shows the general block diagram of target related guidance. As there are many theoretical guidance methods, there are many concepts of guidance, too. Lock on before and after launch abilities are also related with missile capability. Indeed, all capabilities are related with requirements and sensor systems.

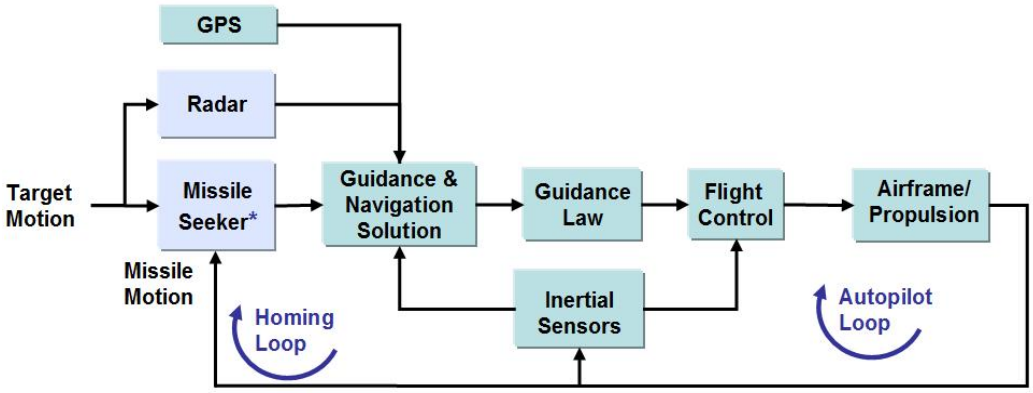

Figure 65 Integrated Guidance and Control Structure

Air defense missile systems may have inertial navigation systems, GPS, and tracking or surveillance radar systems. Air defense missiles' targets are aircrafts, missiles, helicopters and UAVs, as seen in Figure 66. As the target variety is large, there exist different guidance algorithms which need the information of target's position, velocity and type which can be supplied by radar systems. Guidance

algorithms may be designed integrated with autopilot system or separately [27], [49], [50], [65], and [66]. Mostly, autopilot and guidance algorithms are designed separately. In this thesis, guidance algorithms and autopilots are designed separately.

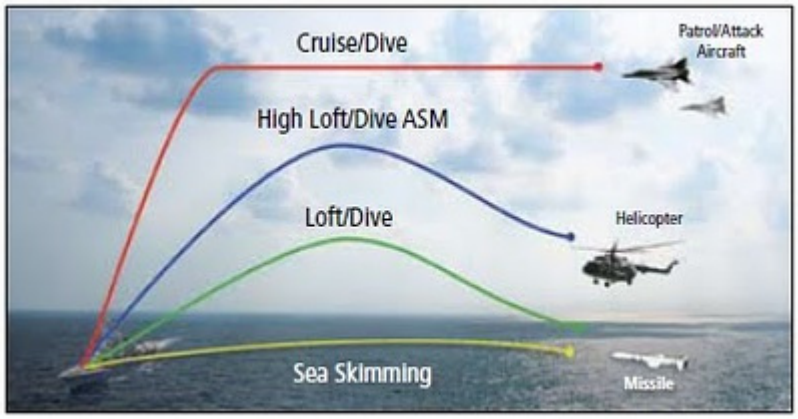

Figure 66 Targets of Air Defense Missile [11]

Guidance algorithms are generally divided into two phases as midcourse and terminal guidance. Midcourse guidance starts from launch phase lasts until terminal guidance phase. Midcourse guidance phase is a first step of guidance in order to decrease the effort of terminal phase. Also, in midcourse guidance phase most of the seeker systems do not usually work and, midcourse guidance is performed with inertial navigation instruments and/with radar systems. However, some vertical launch systems, as an example Figure 67 (adapted from [59]) divide guidance phase to three phases, as initial phase, midcourse and terminal phase. Thrust vector control strategies or capabilities usually force to define initial guidance phase. In the thesis, guidance phase is firstly divided into two sections, midcourse and terminal. In the following chapters, after maneuver optimizations, guidance phase will also be defined as initial, midcourse and terminal phase.

After brief introduction, switching conditions from midcourse guidance to terminal guidance has to be defined. These switch conditions are;

- field of view (FOV) angle less than ±3º and
- lock on range less than 3000 meters

which are used in all nonlinear simulations.

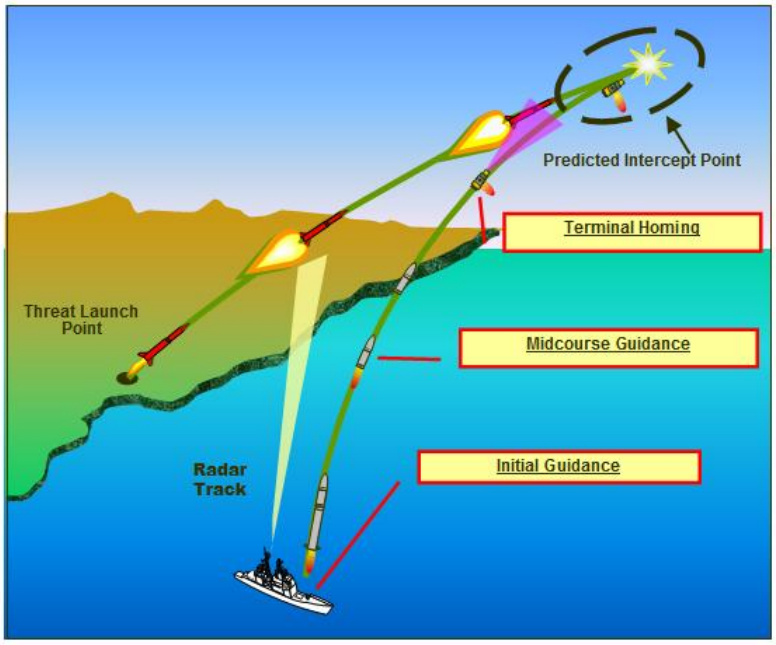

Figure 67 Guidance Concept

Here, guidance algorithms which are implemented are introduced. The traditional Proportional Navigation (PN) guidance methodology for terminal phase and midcourse phase are constructed. The guidance methods are implemented and performance analysis is considered on defined target sets.

6.1. Midcourse Guidance

Midcourse guidance phase starts from launch phase and lasts until terminal guidance phase. Firstly, relative position vector is found in earth frame coordinates, (5.1), then the relative position vector is expressed in body frame coordinates in Eq. (5.2). After then, unit vectorization process is held in Eq. (5.3).

$$\begin{aligned}\bar{P}_C^{(e)} &= \begin{bmatrix} X & Y & Z \end{bmatrix}^T{}_C \\ &= \begin{bmatrix} X & Y & Z \end{bmatrix}^T{}_{Missile} - \begin{bmatrix} X & Y & Z \end{bmatrix}^T{}_{Target}\end{aligned} \tag{5.1}$$

$$\bar{P}_C^{(b)} = \hat{C}^{(b,e)} \bar{P}_C^{(e)} \tag{5.2}$$

$$\bar{u} = \frac{\bar{P}_C^{(b)}}{\left\| \bar{P}_C^{(b)} \right\|} \tag{5.3}$$

$$\lambda_{AZ} = arctan\left(\frac{\begin{bmatrix} 0 & 1 & 0 \end{bmatrix} \bar{u}}{\begin{bmatrix} 1 & 0 & 0 \end{bmatrix} \bar{u}} \right) \tag{5.4}$$

$$\lambda_{EL} = -arcsin\left(\begin{bmatrix} 0 & 0 & 1 \end{bmatrix} \bar{u} \right) \tag{5.5}$$

Look angle is the angle between the line of sight and missile body angle which is

$$\varepsilon = arccos\left(\begin{bmatrix} 1 & 0 & 0 \end{bmatrix} \bar{u} \right) \tag{5.6}$$

Figure 68 illustrates the 2D midcourse engagement geometry. In the 2D geometry the look angle and the azimuth/elevation angles are the same. Defined midcourse guidance commands the difference between the body angle and the look angle in order to point the missile body to the target as body pursuit guidance approach.

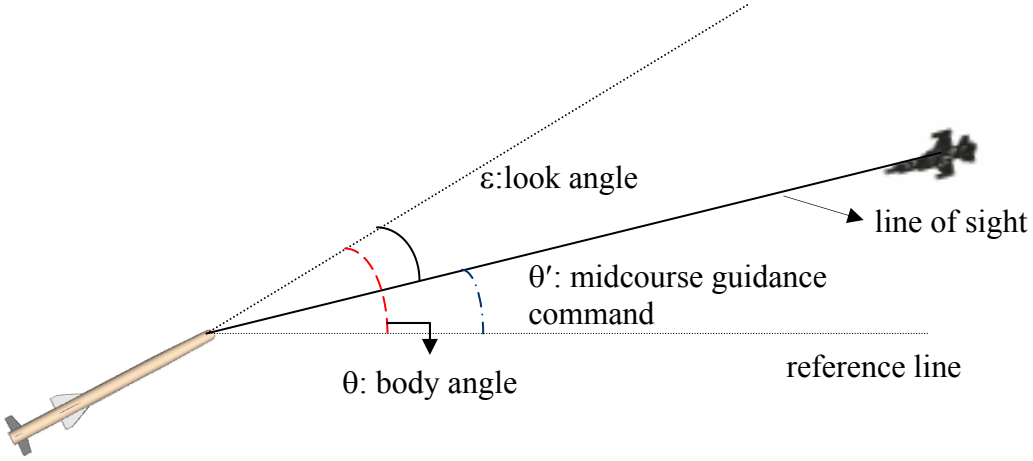

Figure 68 2D Midcourse Engagement Geometry

Generated azimuth and elevation angles are sent as guidance commands to angle autopilots. Advantage of this approach is that target is always in the field of view before terminal guidance phase. Figure 69 shows look angle change versus time for a target that its initial position is $\begin{bmatrix}7500 & 1500 & -2500\end{bmatrix}^T$ m and velocity is $\begin{bmatrix}-200 & 0 & 0\end{bmatrix}^T$ m/s. The figure confirms that the midcourse guidance phase steers the missile to the trajectory which provides target is in the field of view of missile. Figure 70 illustrates the angle commands generated with the defined midcourse guidance algorithm.

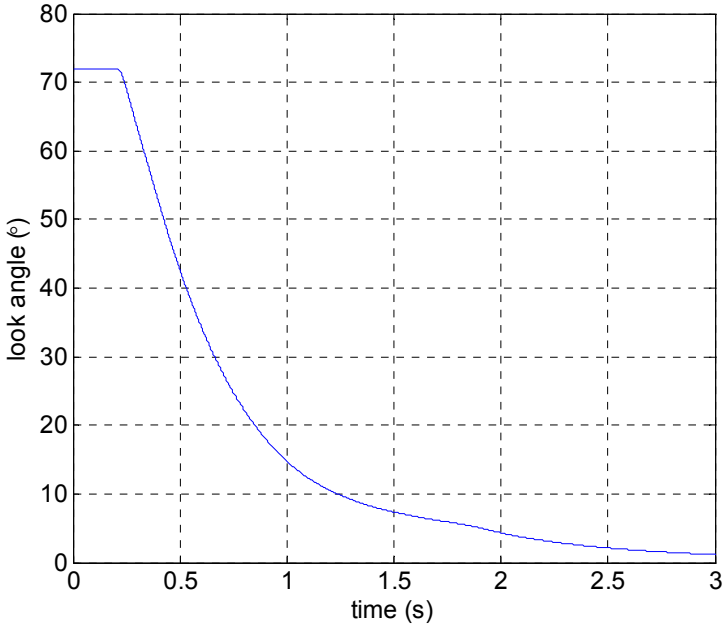

Figure 69 Look Angle Change During Midcourse Phase

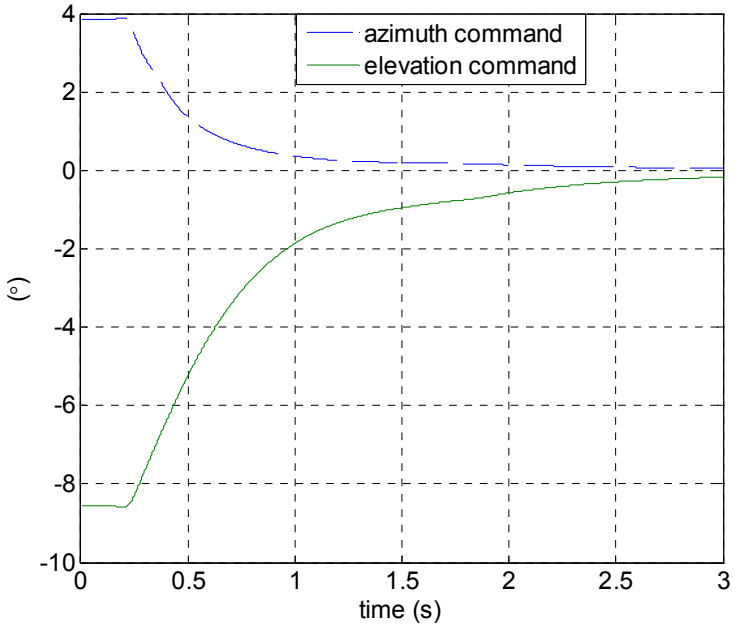

Figure 70 Azimuth - Elevation Command Profile

6.2. Terminal Guidance

After midcourse guidance, terminal guidance is applied to intercept the target. In general, proportional navigation is used because of its simplicity in terminal phase. Within the complexity of target maneuver, derived approaches of PN guidance can be preferred. Theoretically, PN guidance law issues acceleration command, perpendicular to the missile velocity or closing velocity [2]. Mathematically, the guidance law can be stated as

$$\vec{a}_c = N \cdot \vec{w} \times \vec{V}_M \tag{6.1}$$

where $\vec{a}_c$ is the normal acceleration command, N is a unitless, designer chosen gain (usually in the range of 3-5) known as the navigation ratio, $\vec{w}$ is the angular velocity of LOS and $\vec{V}_M$ is missile velocity.

6.3. Guidance and Control Simulation Results

In order to test the performance of guidance and control system in nonlinear simulation environment, two target sets are created. These two sets include 4 targets in total. The first target set includes a static target at low altitude, and a crossing target. The second target set includes maneuvering, and forthcoming targets. Forthcoming target dives to the launch point of the missile with PNG gain 3 and the other target starts weaving maneuver when distance between missile and itself is equal to 1500 meters. Maneuvering target accelerates with a 5g and 0.5 Hz sinusoidal acceleration.

The midcourse and PNG terminal guidance strategies defined in previous section are used as guidance strategies. The switching from midcourse to terminal guidance is a hard switch that whenever target is in the field of view of the missile ($\leq \pm 3^\circ$) and the closing range is less than 3000 meters, guidance algorithm switches to terminal guidance from midcourse guidance. Midcourse guidance algorithm produces guidance commands and these commands are reference inputs for angle

autopilots and terminal guidance commands are executed by acceleration autopilots.

6.3.1. Non Maneuvering Targets

The first target set is given in Table 8. Target 1 is a static target at very low altitude. Target 2 is a high velocity target at medium altitude and it is a crossing and diving target, its total velocity is 141 m/s.

Table 8 Target Set I Properties

	Target 1	**Target 2**
Initial Position (m)	$[6000 \quad 2500 \quad -30]$	$[3000 \quad 1500 \quad -3000]$
Initial Velocity (m/s)	Static	[0 100 100]

Time of flight, midcourse and terminal guidance durations and miss distances are listed in Table 9. It can be said that the guidance strategies and autopilots performances are quite acceptable. Miss distances are less than 1 meter in ideal conditions.

Table 9 Simulations Results for Target Set I

	Target 1	**Target 2**
Time of Flight (s)	12.5	8.07
Midcourse (s)	6.79	3.51
Terminal (s)	5.71	4.56
Miss Distance (m)	0.06	0.02
Final Velocity (Mach)	1.32	1.72

Figure 71, Figure 72, and Figure 73 illustrate the trajectory, angle of attack, sideslip and body angular rates during maneuver for target 1. Missile reaches about 350 meters altitude and gets closer to 30 meter altitude while it is getting to 6000 meters downrange. Less than 40 degrees of angle of attack and more than 10 degrees angle of sideslip and related body angular rates are obtained during the maneuver. As the turn type is skid to turn, very small amount of roll rate is taken by the missile which is related with the roll autopilot performance.

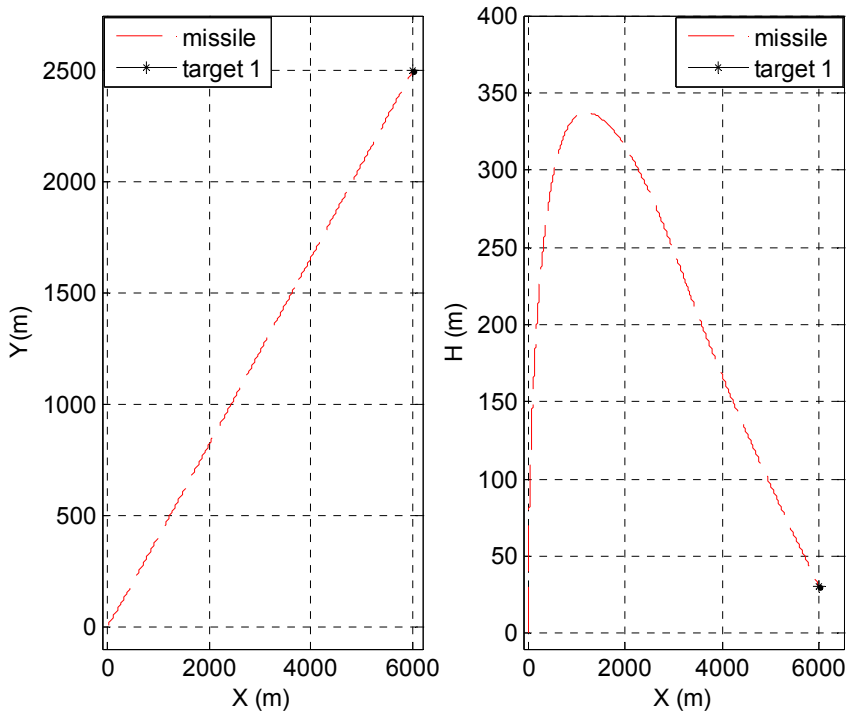

Figure 71 Missile-Target 1 Trajectory

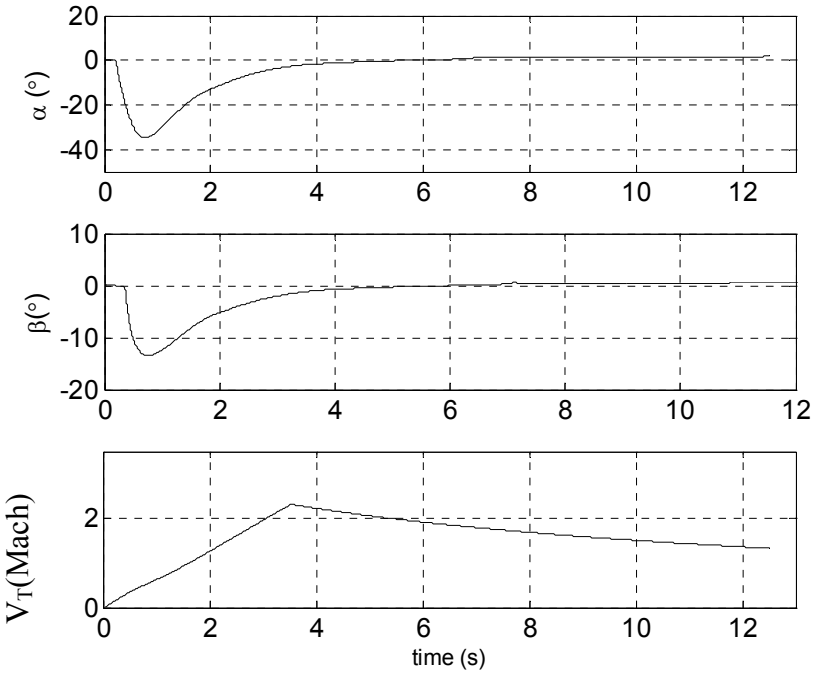

Figure 72 Velocity & Angles of Attacks for Target 1

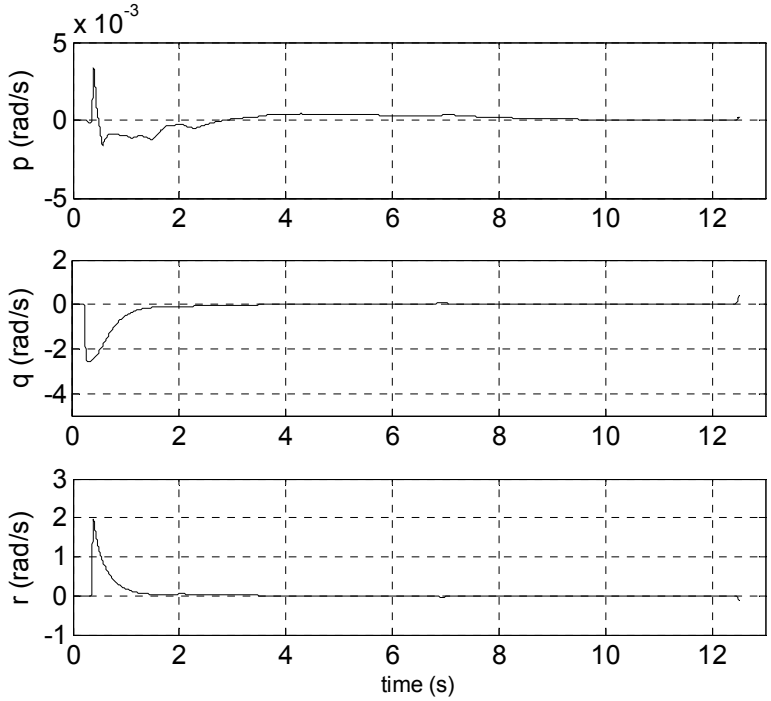

Figure 73 Body Angular Rates for Target 1

Figure 74, Figure 75, and Figure 76 present the same properties for the target 2. Trajectory is illustrated in Figure 74. Figure 75 shows angle of sideslip, attack and velocity of the missile during flight. As the missile is crossing, angle of sideslip is increasing in terminal guidance phase with respect to the angle of attack.

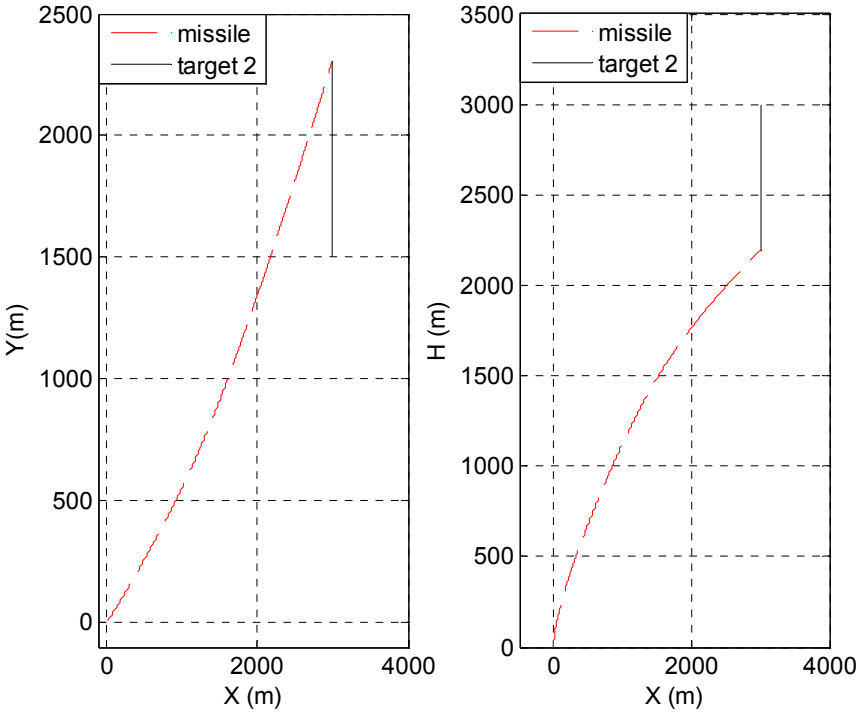

Figure 74 Missile-Target 2 Trajectory

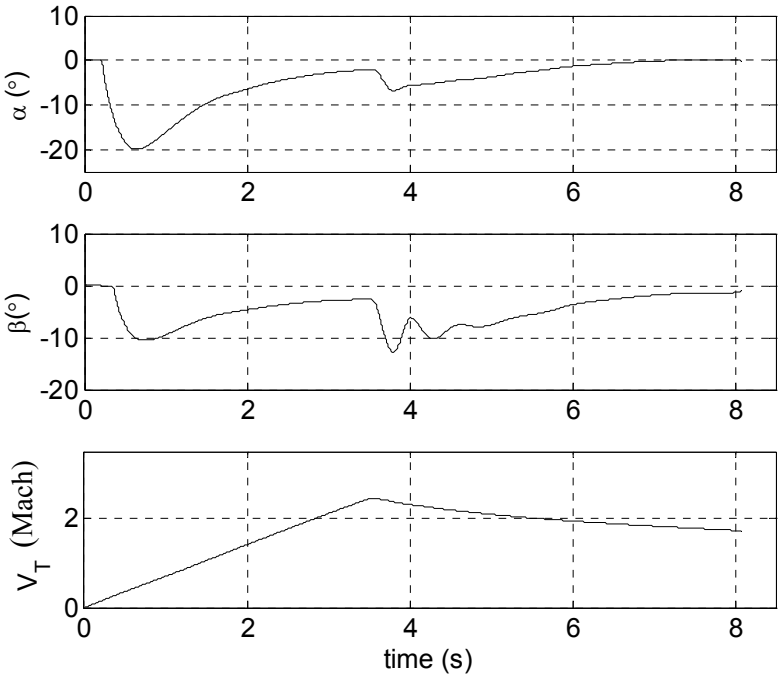

Figure 75 Velocity & Angles of Attacks for Target 2

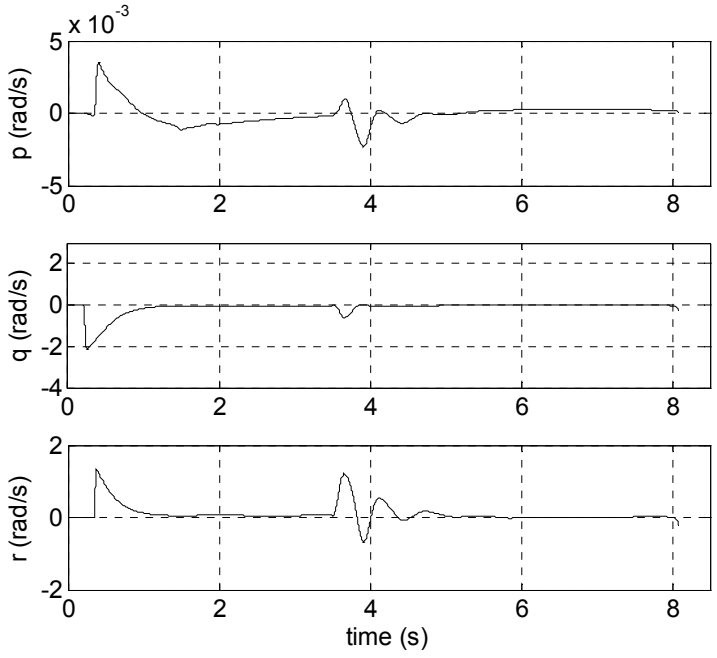

Figure 76 Body Angular Rates for Target 2

6.3.2. Maneuvering Targets

The second target set is presented in Table 10. Target 3 is demonstrating a tactical/strategic missile, attacking to the launch point of the missile. Its speed is 400 m/s and it is in its terminal phase guidance with navigation constant 3. Target 4 is a weaving target which has an importance in defining missile performance. This target starts weaving when it is close to missile.

Table 11 shows the time of guidance phases, miss distance and final velocity and as seen the miss distance for the weaving target is the worst which is 1.26 meters in ideal conditions. However, miss distance in such systems that is less than 5 meters is acceptable.

Table 10 Target Set II Properties

	Target 3	**Target 4**
Initial Position (m)	$[10000 \quad 1000 \quad -3000]$	$[7500 \quad 2500 \quad -500]$
Initial Velocity (m/s)	$[-400 \quad 0 \quad 0]$	$[-200 \quad 0 \quad 0]$
Maneuver	PNG to the missile launch point with N=3	Starts maneuvering at 1500 m closing distance the with acceleration $a_y=5.g.\sin(\pi.t)$

Table 11 Simulations Results for Target Set II

	Target 3	Target 4
Time of Flight (s)	11.26	11.29
Midcourse (s)	8.01	6.98
Terminal (s)	3.25	4.31
Miss Distance (m)	0.52	1.26
Final Velocity (Mach)	1.43	1.27

Figure 77, Figure 78 and Figure 79 show the trajectory of missile and target 3, angle of attack and sideslip, velocity profile and the body rates of the missile during flight.

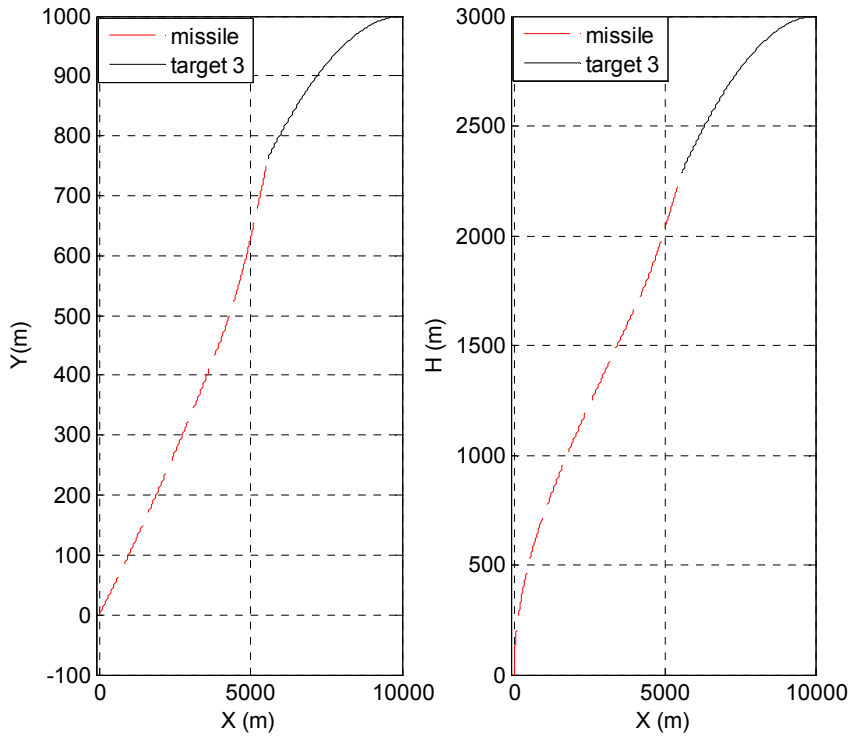

Figure 77 Missile – Target 3 Trajectory

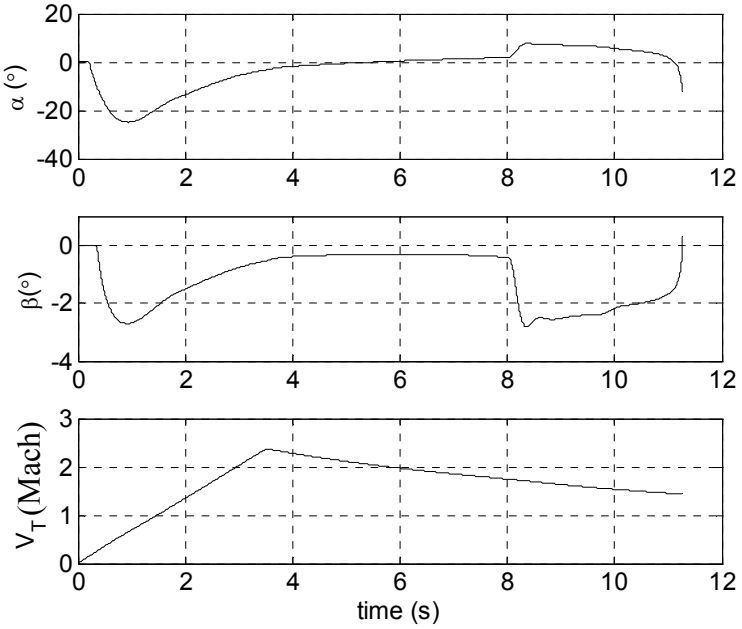

Figure 78 Velocity & Angle of Attacks for Target 3

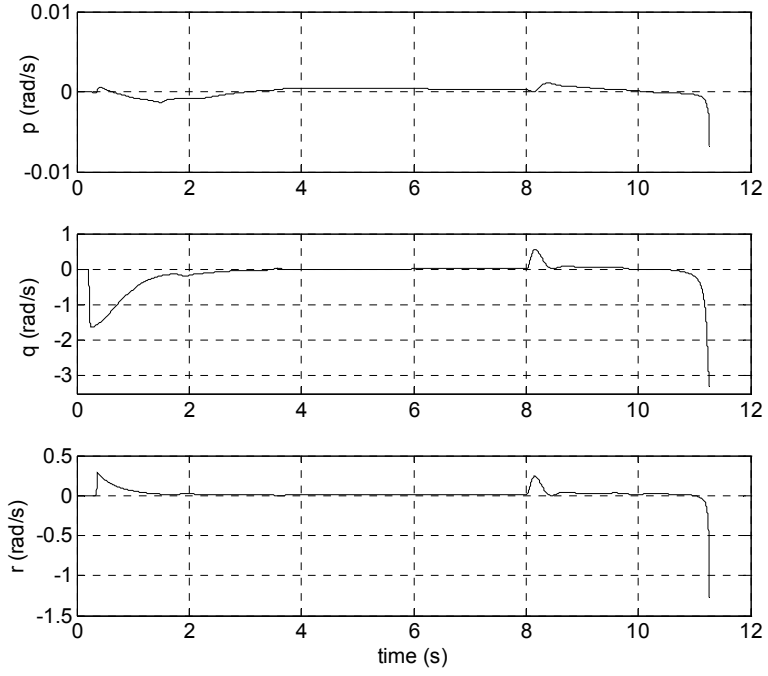

Figure 79 Body Angular Rates for Target 3

Figure 80 shows the trajectories of the missile and target 4 which is maneuvering for the last 1500 meters of closing range. Figure 81 and Figure 82 illustrate properties of flight during intercept with target 4. As the target is weaving, missile is also weaving in the terminal phase.

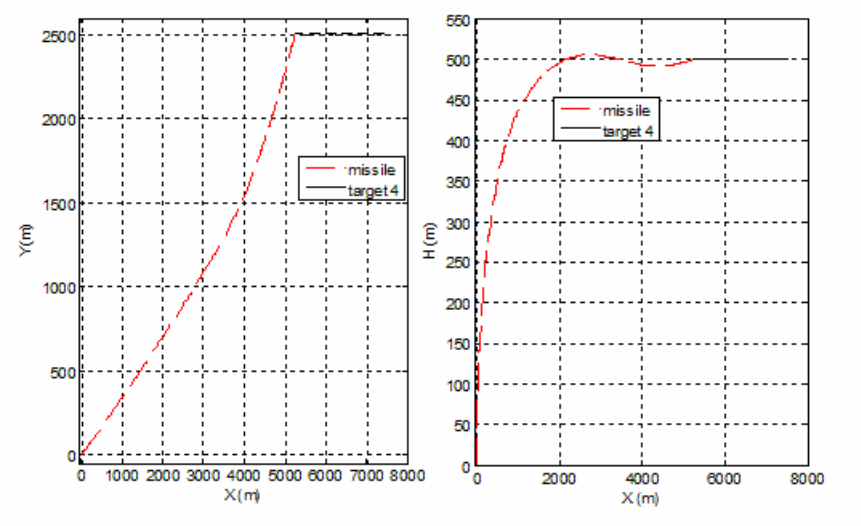

Figure 80 Missile – Target 4 Trajectory

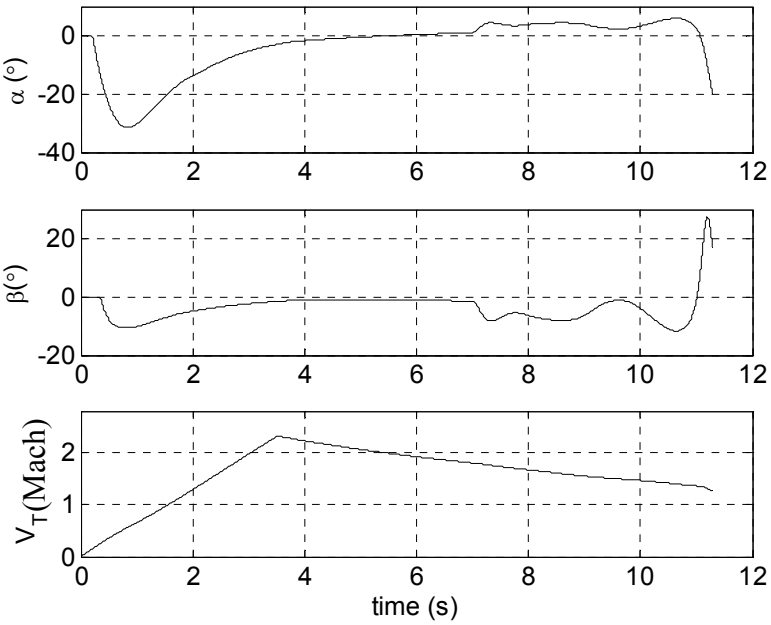

Figure 81 Velocity & Angle of Attacks for Target 4

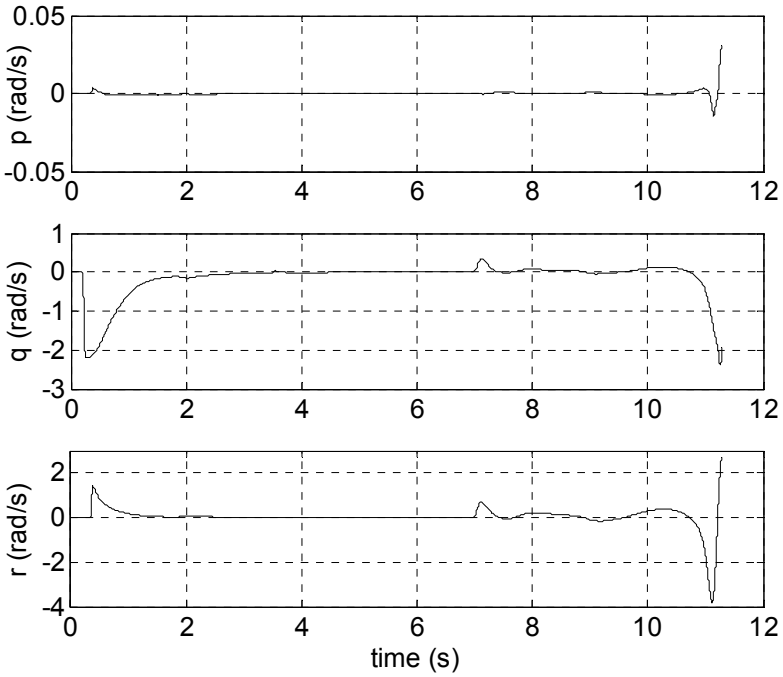

Figure 82 Body Angular Rates for Target 4

CHAPTER 7

TURNOVER STRATEGY ANALYSIS

In the previous section, in the vertical launch phase, the missile is controlled as it is skid to turn. In this section, an enhanced strategy will be studied especially for the turnover of the missile in short time. The proposed strategy is actually a mixed ascend and turnover maneuver composed of an initial roll and then skid to turn. That kind of maneuvering is also used for air to air missiles [3].

Figure 83 shows the expressed strategy. In vertical flight missile makes an initial roll maneuver and then starts turn over maneuver. The main point of the initial roll maneuver is that the pitch plane of the missile's body coordinates is placed in approximately the same vertical plane with the target. Hence, missile will need less lateral acceleration and reduce sideslip angle. The results are discussed in details in the following section.

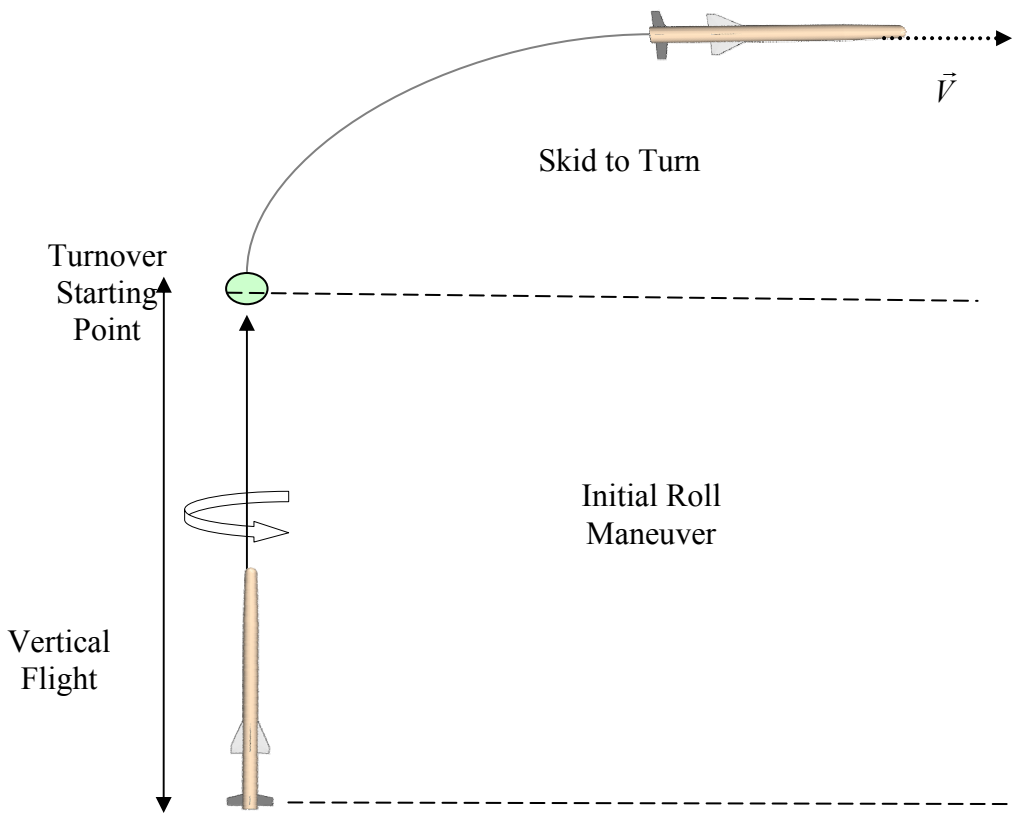

Figure 83 Turnover Strategy

7.1. Initial Roll Maneuver Comparison of the Aerodynamic and Thrust Vector Control

In this section, aerodynamic and thrust vector control over initial roll maneuver is performed. A static target at [3000, 3000,-300] is being tried to hit with two turnover strategy and with different control capabilities. The azimuth angle so the initial roll command is 45°. In order to prevent wrong decision of autopilot because of the Euler angles singularity at θ=90º, roll angle commands are generated with integral of the roll rate. During the initial roll maneuver, yaw channel is not controlled as it does not need control, the cross coupling terms do not result effective yaw motion at velocities close to 0. But after initial roll, the yaw channel and pitch channel control starts with respect to the guidance command profile.

As shown in the previous chapters, during vertical flight missile velocity is very low so the dynamic pressure, which means aerodynamic control, is insufficient and this roll maneuver can be achieved in a short time with thrust vector control, but the thrust vector control model described in section 3.4.2 cannot create axial moment. But it is possible that if all of the jet vanes turn into the same direction for the cruciform fin style and the resulting force can be multiplied with the distance from the center of pressure of jet vane to the center of nozzle to create axial moment (see Appendix). During the initial roll maneuver, all jet vanes are used for roll maneuver and this necessity brings a modeling convenience for roll moment created by thrust vector control system. As the nozzle and jet vane design is not the subject of this thesis, from the fact defined above, an axial moment can been taken into account linearly by aileron deflection. So, a look up table is implemented for axial force moment for thrust vector control. The maximum value of axial moment created with maximum jet vanes deflection is considered as 220 Nm which is a realistic moment value. For example, [28] describes the moments and forces created by jet vane thrust vector control system. In that study, large amount of lift forces so the moments are created with a low level of thrust. Also, a simple thrust vector control design is presented in the Appendix and the obtained maximum roll moment is 217 Nm.

In order to examine effectiveness of the two different control inputs, initial roll maneuver is commanded to place missile coordinates in approximately the same vertical plane with the target. Roll command starts with simulation run time, after 0.3 seconds pitch and yaw channel autopilots are active. Figure 84 shows the roll angle trend with two control technologies. As the roll moment created by TVC is more than aerodynamic roll moment at the early times of vertical launch (<0.3s), roll angle settles down quickly with TVC. Settling time of desired roll angle with TVC is <0.3 seconds and <1.6 seconds with aerodynamic control.

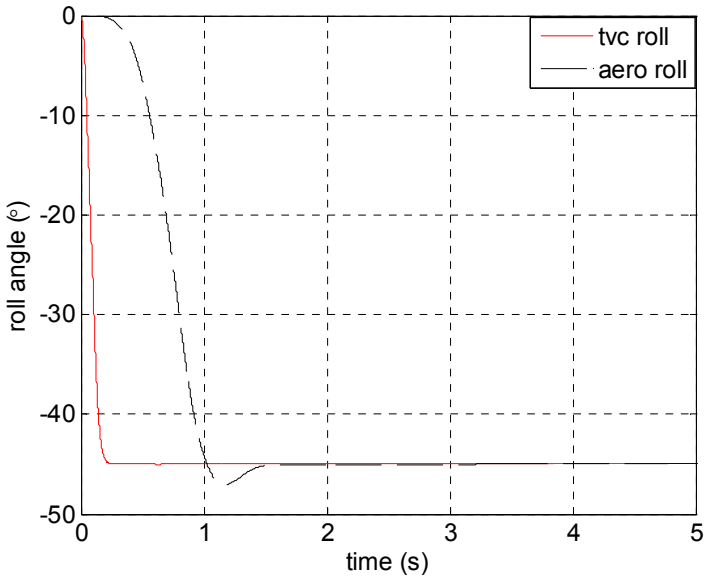

Figure 84 Roll Angle During Flight

Figure 85 and Figure 86 illustrate the trajectories, closing distance and velocity profile with two control methods. They show that there is not a major difference in the terms of flight time and closing distance. Angle of attack and sideslip profiles are given in Figure 87. As seen, roll maneuver with TVC does not cause angle of sideslip. Instead as missile is not at the same plane with the target with aerodynamic roll maneuver in desired time interval, it has quite enough angle of sideslip which is not different than skid to turn style.

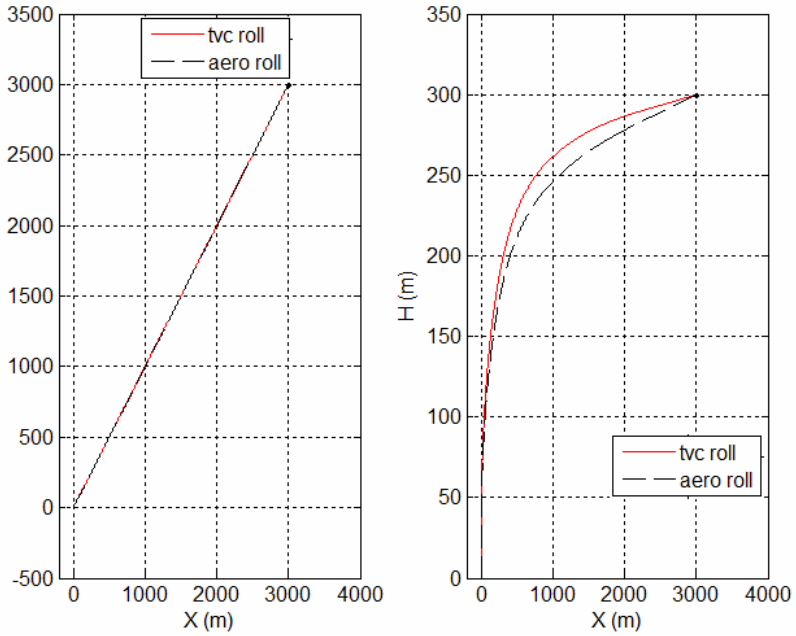

Figure 85 Engagement Trajectory Comparison During Flight

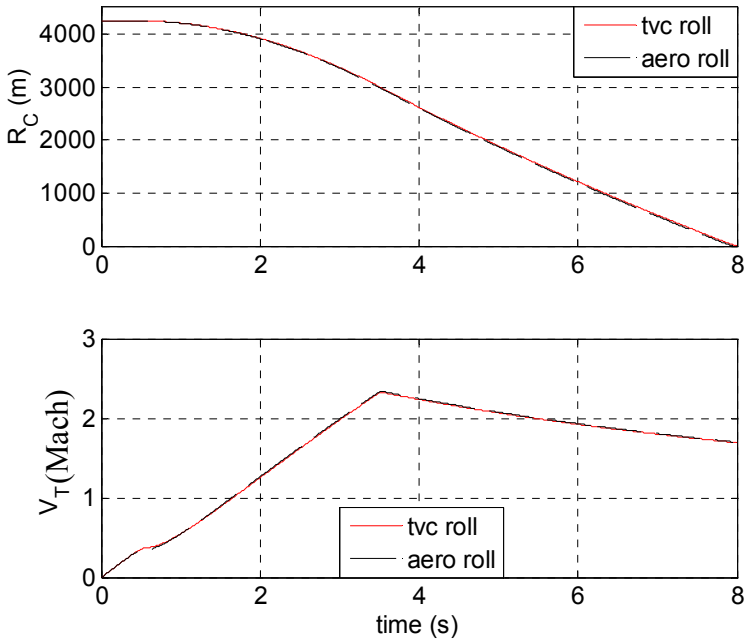

Figure 86 Closing Distance and Velocity Comparison During Flight

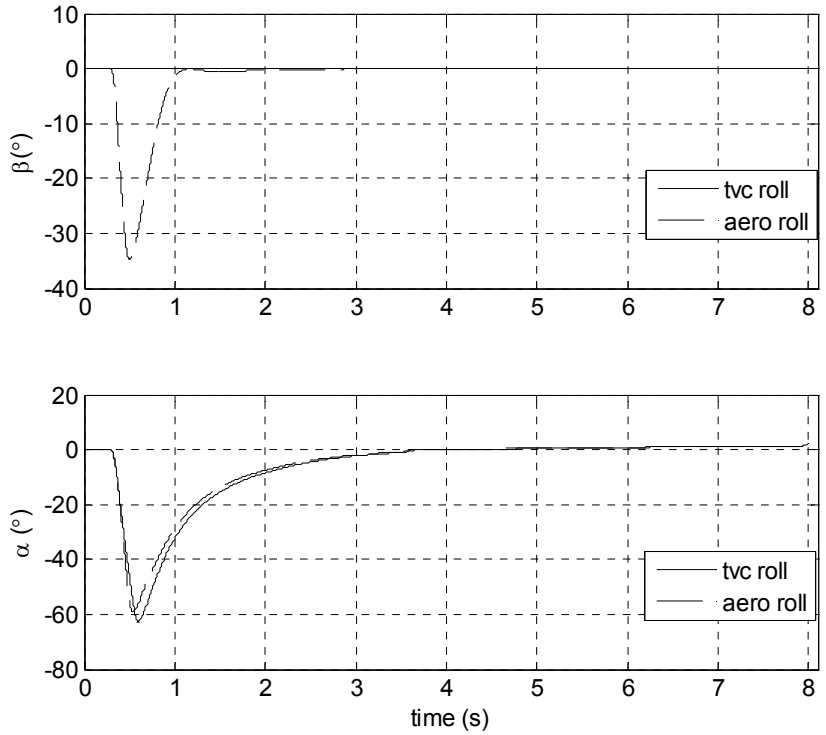

Figure 87 Angle of Sideslip and Attack Comparison During Flight

Figure 88 shows the body angular rates, as missile's velocity and dynamic pressure is not enough to create effective roll moment; the desired roll rate is developing lately for aerodynamic roll control. However with TVC, the desired roll rate develops quickly. Figure 89 shows the acceleration during flight. As the same behavior, a_y acceleration is used to turn towards the target, but there is very small amount of acceleration in the *Y* axis (10^{-3}) with initial roll control with TVC. As the coordinates of the missile and target is in the same plane, missile just has a_z acceleration to turnover to the target, which of all means, to have less lateral acceleration and initial roll maneuver needs roll control with TVC.

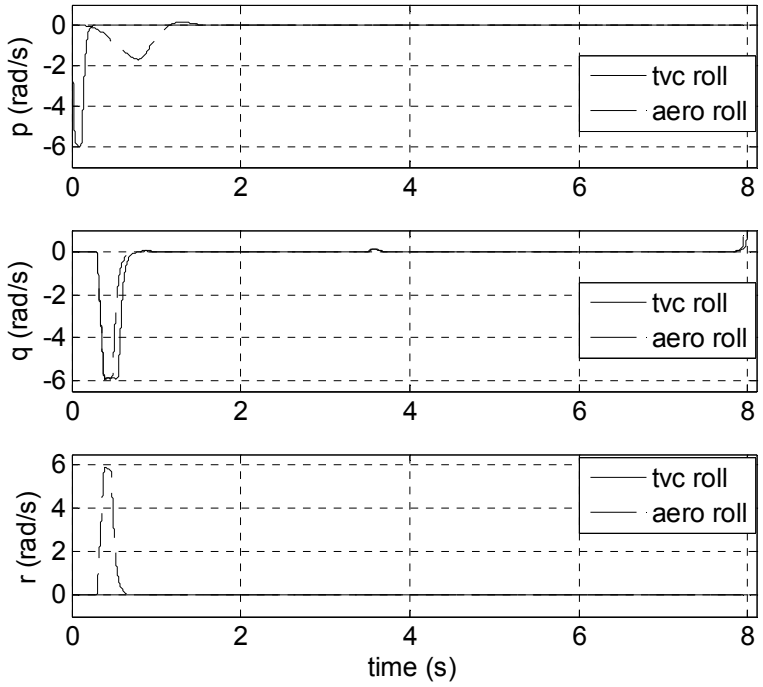

Figure 88 Body Rates (p ,q, r) Comparison During Flight

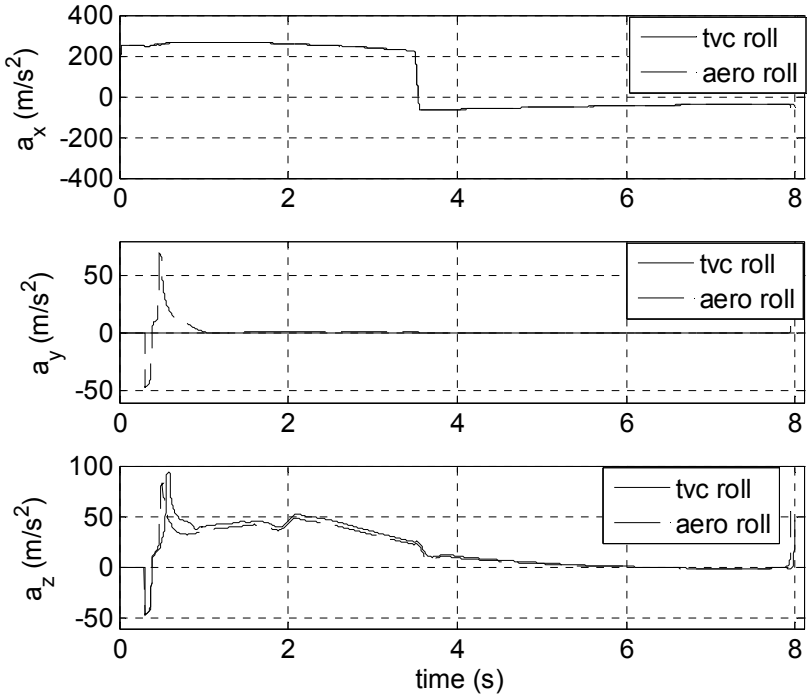

Figure 89 Accelerations Comparison During Flight

7.2. Skid to Turn and Skid to Turn with Initial Roll Strategy Comparison

As explained in the previous chapter, if target and missile is going to be in the same pitch plane, initial roll maneuver has to be performed quickly. After initial roll, missile will turnover towards to the target rapidly. There is one point that has to be considered, the results given in the previous sections are for static targets. A static target which has a component in Y axis can be hit with only the initial roll and pitch maneuver as seen. However, if target has a velocity with respect to the missile, initial roll will not be enough to hit the target. So that, missile needs to use its yaw channel autopilot as it is a skid to turn missile.

In order to analyze this maneuver, a target has been define at [5000,-2500,-500] m and with velocity [100,100, 0] m/s. the same critics to switch to terminal phase is used, FOV ± 3 degrees and lock on range is 3000 meters. If the simulations are analyzed, flight time lasts for 12.75 seconds, and 5.83 seconds for midcourse guidance phase. Desired roll angle and response of the system is given in Figure 90. Missile rolls and then it tries to hold that roll angle. Figure 91 shows trajectories of missile and target with the two turnover strategies. As seen, there is not much difference in the scope of trajectories. Figure 93 shows the closing distance and the velocity profiles through flight time. As seen, there is not even a major difference between two strategies, but there is a small different velocity trend during turnover because thrust loss is not defined for roll channel deflection. Full skid to turn strategy has much velocity loss during turn over than the suggested turnover strategies. The final velocities are very close to each other, because initial roll maneuver is performed where velocity is very low and the aerodynamic axial force has not yet produced in large amounts.

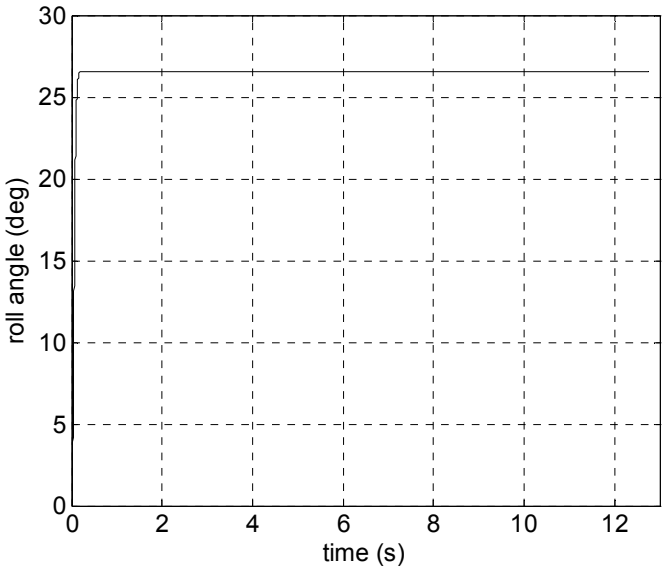

Figure 90 Roll Angle During Flight

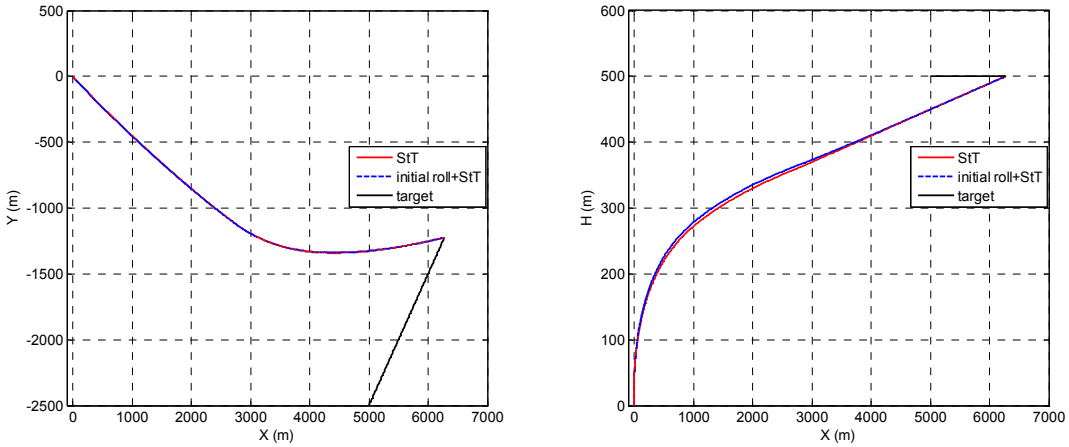

Figure 91 Engagement Trajectories Two Strategies

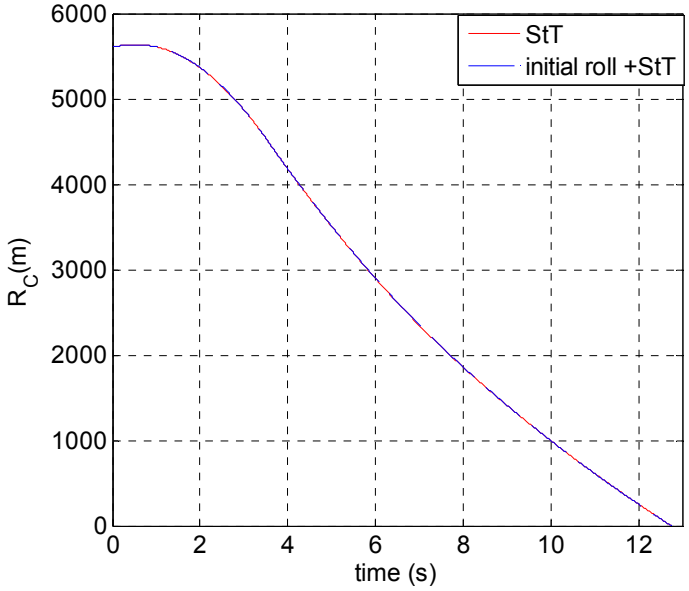

Figure 92 Closing Distance with Two Strategies

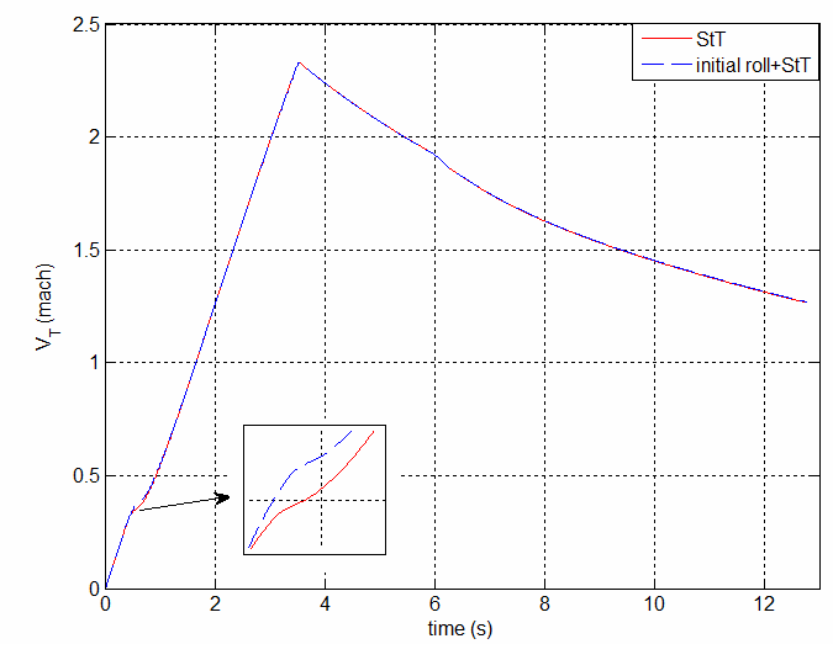

Figure 93 Velocity Profile with Two Strategies

Figure 94 is the angle of sideslip and attack during maneuvers. Skid to turn strategy's angle of side slip is approximately 25 degrees, but the suggested strategy does not need to have a side slip angle because of the initial roll maneuver, and this

roll maneuver does not have a significant effect in the terminal phase tendency. Angle of attack is approximately the same in the first phase (initial and midcourse), but in the terminal phase, mixed strategy need a little much angle of attack than the skid to turn. Maximum 4.6 degree of angle of attack for skid to turn and 1.6 degree of angle of attack for the mixed strategy is obtained. However, this change can be ignored with respect to the angle of sideslip difference.

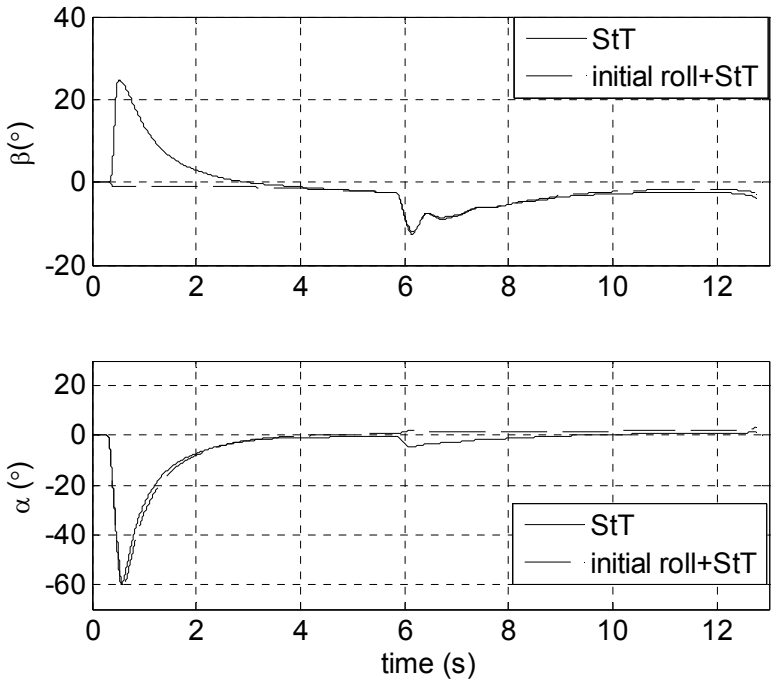

Figure 94 Angles of Sideslip and Attack with Two Strategies

Figure 95 explains one of the major differences between the two methods. In skid to turn, missile has to reach a higher velocity value to have a body rate for yaw maneuver; however in this strategy, missile rolls at a low velocity value and never has a yaw rate in this scenario. After midcourse phase is over, missile has the same trend in terminal phase. Figure 96 shows accelerations of missile during maneuver. Axial accelerations are closely the same, but lateral accelerations differ as seen. It is shown that skid to turn needs more lateral accelerations than the suggested strategy, so the yaw rate. This initial roll strategy simplifies the maneuver and reduces the required lateral accelerations, yaw or pitch plane, during the flight.

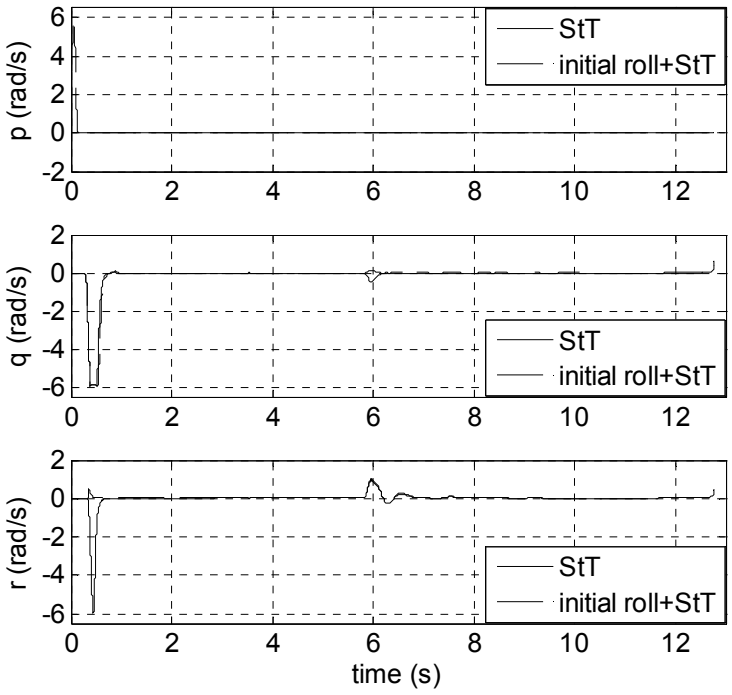

Figure 95 Body Rates (p, q ,r) with Two Strategies

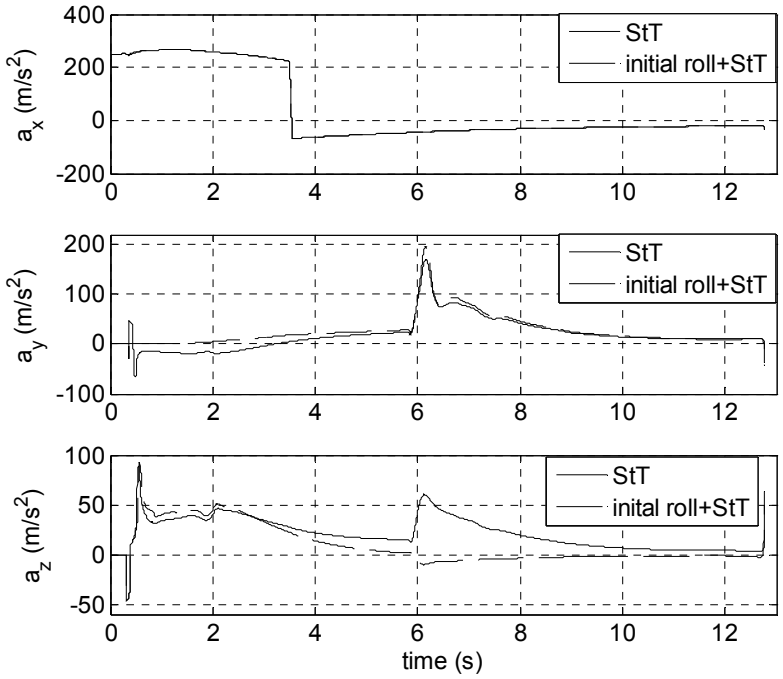

Figure 96 Accelerations with Two Strategies

CHAPTER 8

GUIDANCE DESIGN OPTIMIZATION

In this chapter, optimization via defined cost functions is applied to three chosen problems of vertical launch missiles. After all, guidance commands are generated as an output of the optimization. One of the main interests in this area is to analyze and define the capability of the missile during rapid turnover for low altitude targets. [60] is the only study found in literature on vertical launch missile turnover optimization with a simple mathematical model. It uses differential dynamical programming method and system is controlled with only thrust vector control.

In this thesis, the mentioned study is further enhanced and the optimization process is applied over a 6 DoF nonlinear mathematical model. Thus, the first guidance problem is based on the examination of the turnover capability of the missile. Hence, the "Rapid Turnover Maneuver for Low Altitude Intercept" is studied and the corresponding guidance commands are generated.

The second test case is cast in order to find a solution that gives an opinion on the hybrid control ratio which drives the mechanical design and reduction ratio between the thrust vector control and aerodynamic tail fins. The optimization is mainly studied for "Intercept" maneuver that drives the missile to a constant position within defense volume to intercept an attacking target.

The third test case is constructed to analyze the initial guidance phase which actually results in a desired target intercept. Thus, the "Engagement Initiation"

maneuver is studied and the look angle of the missile is minimized to successfully initiate the target intercept.

8.1. Real Coded Genetic Algorithm

Genetic algorithms, (GAs), are search methods based on the principles of natural selection and genetics. They were first introduced by [61], and were extensively explored by [62]. GAs have been proved to be efficient in many different areas such as image processing [63], and system identification [64]. It is also possible to see the application of genetic search methods in guidance and control, trajectory optimization applications such as [65], [66] and [67]. Unlike the conventional gradient based searching algorithms, GAs are inherently parallel, because they simultaneously evaluate many points in the parameter space, called search space.

Real-coded genetic algorithm (RCGA) differs from the traditional binary-coded GAs. It uses floating point representations in the searching procedure. The chromosomes are the arrays of unknowns instead of bit strings. It works without the need of coding and encoding procedures and reduces the computation time. The procedure of real coded genetic algorithm applied in this study is given in Figure 97. Algorithm has fitness function, ordering, selection, crossover, mutation and elitism algorithms for the best populations among the past and new populations.

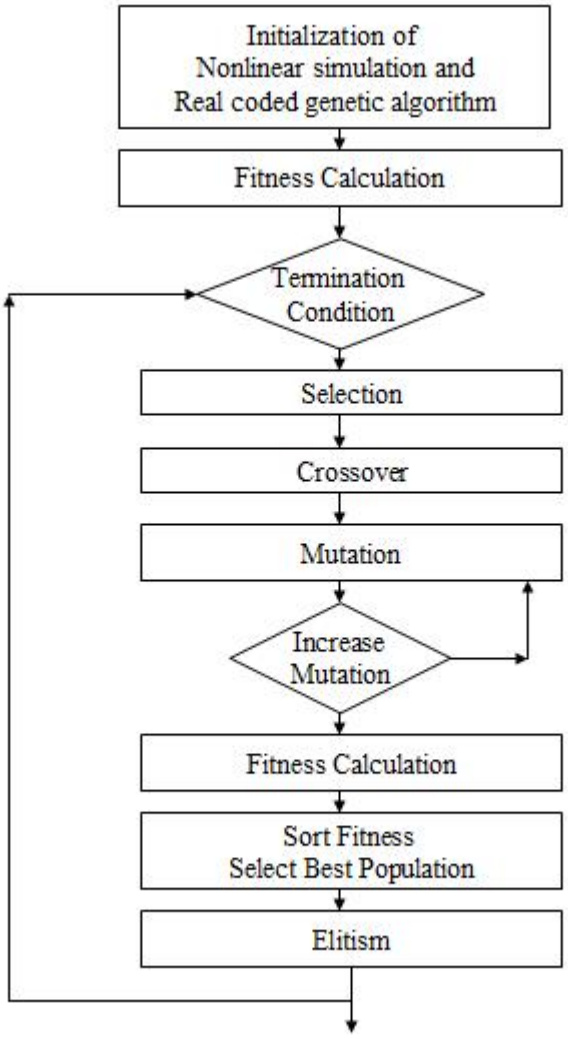

Figure 97 Genetic Algorithm Search Procedure

Initialization: The initial population of candidate solutions is usually generated randomly across the search space. However, domain specific knowledge or other information can be easily incorporated. In this study, initial populations are generated on basic knowledge of guidance commands generated from the midcourse method mentioned in midcourse guidance section. Basic guidance commands are then formed with random data production process. After then, guidance commands are processed by a masking system which saturates the high level guidance commands. Guidance commands are filtered with a low pass filter in order to satisfy a guidance command frequency components at the end and the time lag caused because of the filter is negligible.

Evaluation: Once the population is initialized or an offspring population is created, the fitness values of the candidate solutions are evaluated.

Selection: Selection allocates more copies of those solutions with higher fitness values and thus imposes the survival of the fittest mechanism on the candidate solution. The main idea of the selection is to prefer better solutions to worse ones. Roulette Wheel, stochastic universal, ranking and tournament selection are some of the methods which are used generally. In this search algorithm, a linear function mapping is used. The best and the worst fitness values are mapped to 0 and 1. The other fitness functions so the populations are mapped in between them.

Crossover: Crossover combines parts of two or more parental solutions to create new, possibly better solutions. The selected populations are chosen with Roulette Wheel method). The number of crossover is predefined. Crossover procedure is given in (8.1) where α is an algorithm parameter which is taken as 0.65 and *s,p,s´* are vectors (chromosomes).

$$s' = \alpha.s + (1-\alpha).p \tag{8.1}$$

Mutation: While crossover operates on parents, mutation locally but randomly modifies a solution. Again there are many variations of mutations, but it is usually involves one or more changes made to an individual's traits. In addition to classical mutation processes, the search algorithm increases both the search area and the amplitude of mutation if the best fitness value is the same for last two or more times of the generation.

Elitism: The method is also 1 elitist so the top performing individual of each generation is assured to be included in the next population.

Replacement: The offspring population created by selection, crossover, mutation and elitism replaces the original parental population. Many replacement techniques

such as elitist replacement, generation-wise replacement and steady state replacement methods are used in genetic algorithms. Here, elitist replacement method is used.

Decision Variables: In the construct optimization problem two decision variables are considered. They are maximum generation number and fitness value. If the maximum number of generation or the minimum fitness value is obtained, search algorithm stops.

Cost Function to Fitness Function: There are several methods for calculation fitness function over cost function. In this study, two methods are used. One of the methods is normalizing the cost function and scaling it to a maximum and minimum function values. Then minimum cost is converted maximum fitness and vice versa. The second method is subtracting cost function from a very larger number. As the cost function is minimized, result of the subtraction is increases.

8.2. Rapid Turnover Maneuver for Low Altitude Intercept

Rapid turnover maneuver requires high angle of attack capability. As seen in Figure 98, missile launches vertically and starts to turn over at a safety altitude for rapid turnover maneuver. At the end of the maneuver, missile velocity vector is desired to be parallel to the inertial ($\gamma_f = 0^\circ$) X axis which means missile can go horizontally to the X axis. This maneuver usually defines missile critic requirements. In order to analyze the designed missile turnover capability and analyze the missile rapid turnover capability, an optimization algorithm is implemented with real coded genetic search method.

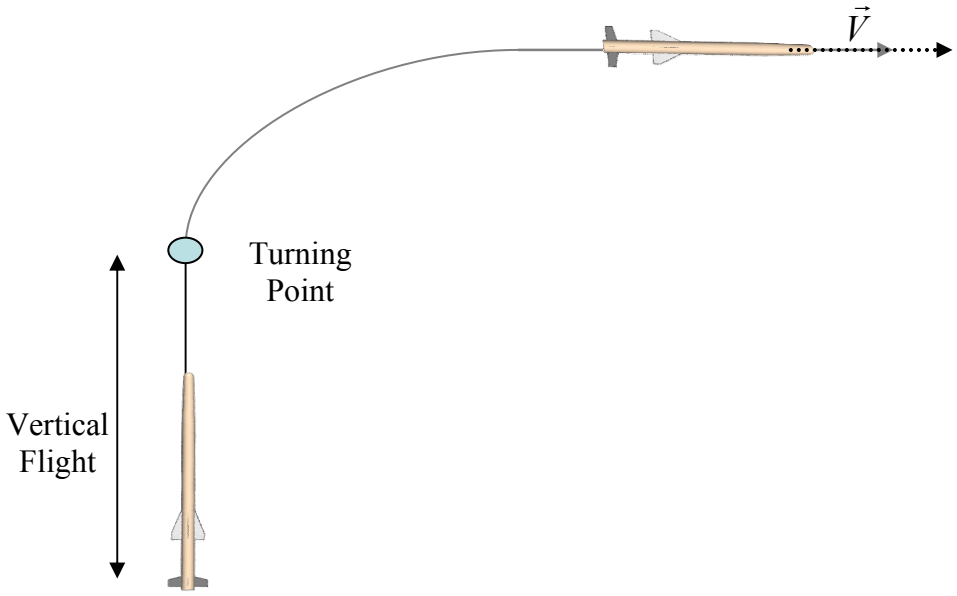

Figure 98 Rapid Turnover Maneuver

Problem formulation can be defined as;

1- Minimize the rapid turnover altitude at minimum time with the constraints that missile velocity vector is horizontal at this altitude
2- Minimize the rapid turnover maneuver time

So, the cost function is formulated as;

$$minimize\ J$$
$$J=\xi_1 \frac{t_f}{t_{f\,max}} + \xi_2 \frac{h}{h_{max}} \tag{8.2}$$

where ξ_1 and ξ_2 are weighting coefficients. h_{max} and $t_{f\,max}$ are the maximum values of turning altitude and time. Results are normalized with respect to these maximum values which are given in Table 12.

Table 12 Parameters for Rapid Turnover Maneuver Optimization

Variable	Value
h_{max}	300 m
$t_{f\,max}$	3.5 s
ξ_1	0.5
ξ_2	0.5

Final condition of the simulation is $\gamma_f = 0^\circ$ that means velocity vector is parallel to the X axis. The constraints in the optimization are:

$$\begin{aligned} &-20^\circ \le u \le 20^\circ \\ &-350^\circ / s \le q \le 350^\circ / s \\ &-90^\circ \le \alpha \le 90^\circ \\ &\gamma_f = 0^\circ \end{aligned} \tag{8.3}$$

Figure 99 and Figure 100 show the best fitness values and optimal guidance command. Figure 101 illustrates the deflection command throughout the maneuver. Figure 102 presents trajectories through generations. The maximum fitness value is 0.94 for the last 10 generations which lead us to at least a local optimal point. It shows fitness values of improved populations. Elite population of the first generation can only reach to altitude higher than 80 meters, however the 3rd, 6th and 14th generations elite populations can reach to 70 to 60 meters altitude with flight path angle 0 degree. Through generations, the turnover range also decreases. The range decreases from 250 meters to 50 meters.

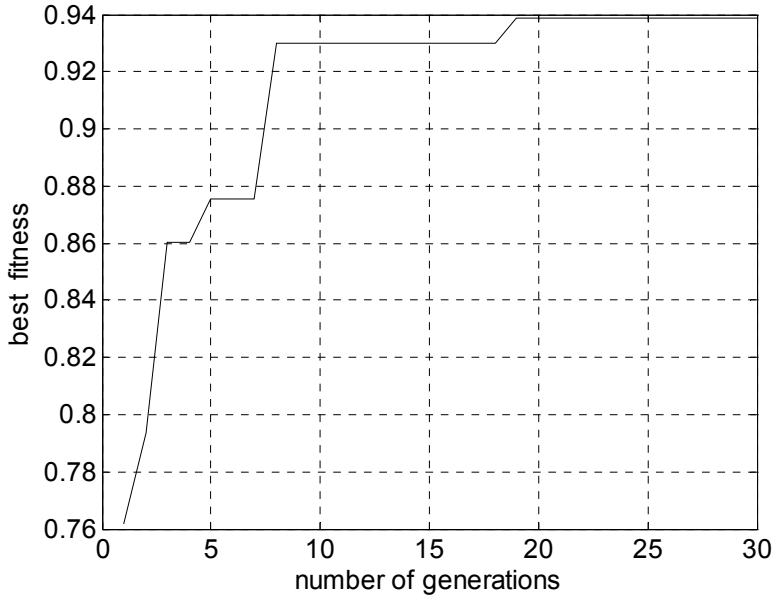

Figure 99 Best Fitness Values for Elite Populations Through Generations

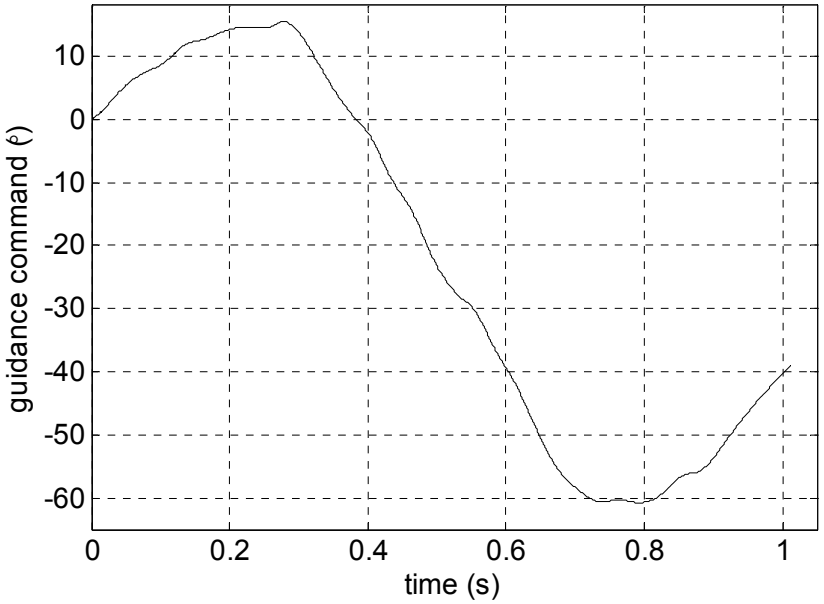

Figure 100 Guidance Command

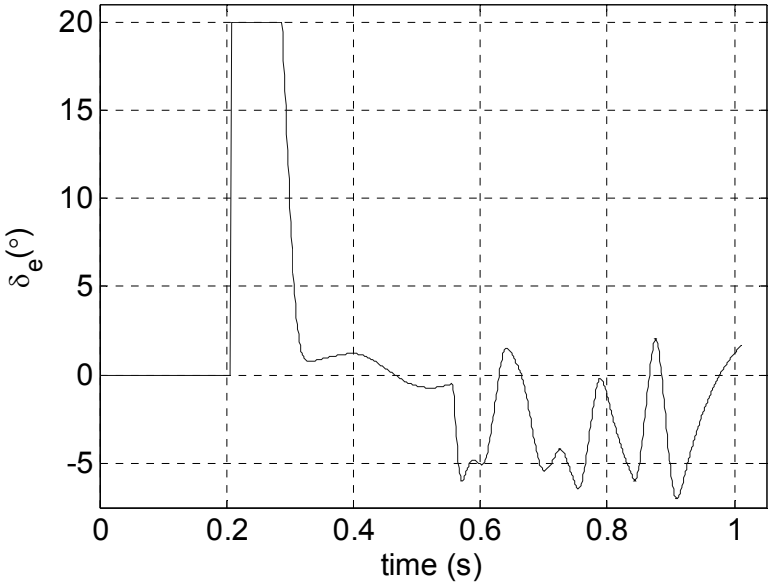

Figure 101 Deflection Throughout the Maneuver

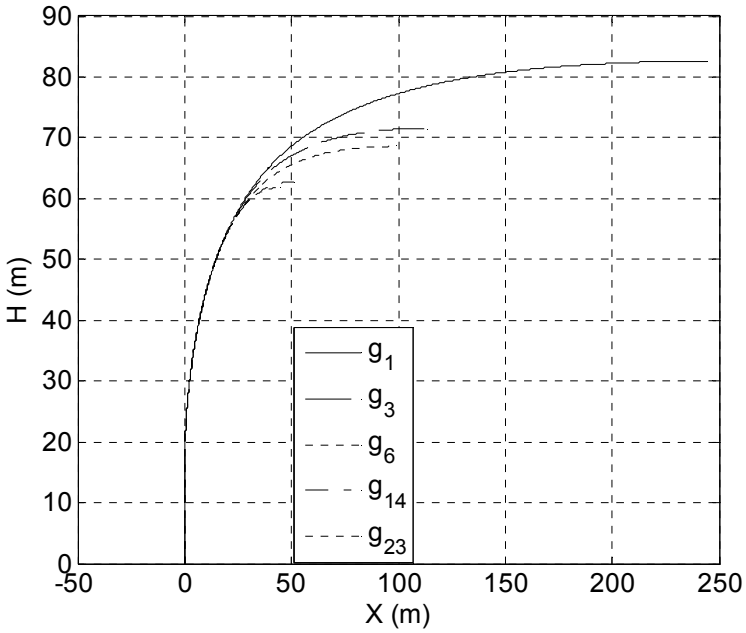

Figure 102 Trajectories for Elite Populations Through Generations

Figure 103 shows the velocity profile during rapid turnover maneuver. The first elite population maneuver lasts for about 1.8 seconds and its last velocity is much more than 1 Mach and the last generation's elite population maneuver lasts for about 1 second and finishes the maneuver less than 0.4 Mach. Also, the best elite

population linearly decreases flight path angle form 90 degrees to 0 degree in about 1 second, see Figure 104.

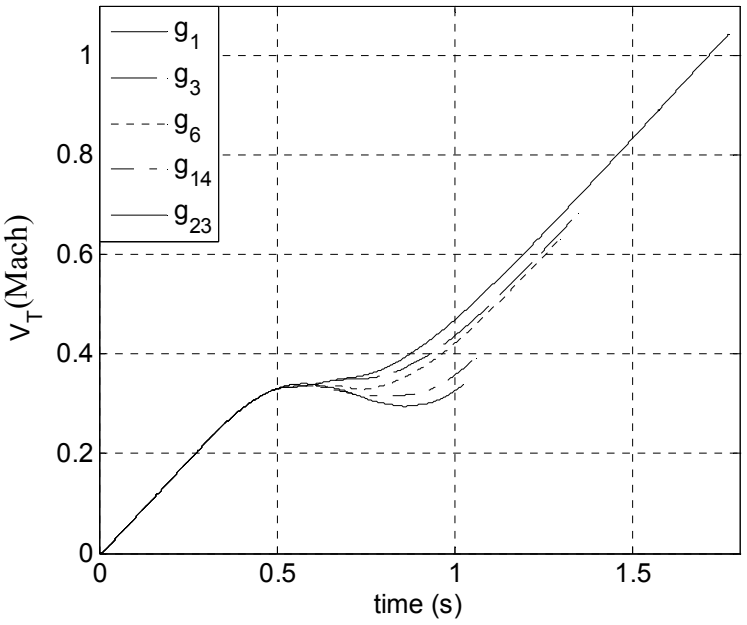

Figure 103 Velocities for Elite Populations

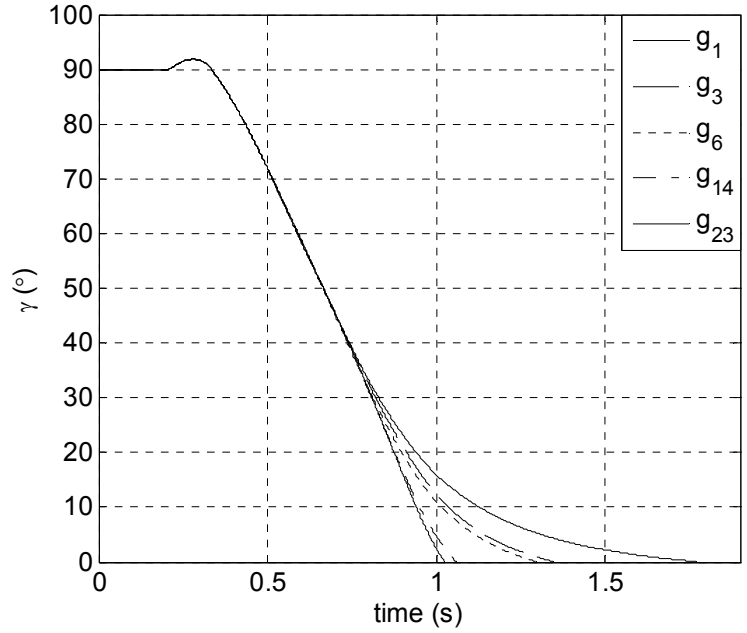

Figure 104 Flight Path Angle for Elite Populations

8.3. Intercept Maneuver Analysis with Hybrid Control Ratio

As mentioned in the 3.4.2 the hybrid control ratio between aerodynamic control and thrust vector control is a design decision. This ratio is the mechanical coupling ratio of the control inputs, and it is not being changed during flight. For the sake of simplicity, the hybrid control ratio had been decided according to the control effectiveness of the two control inputs. As seen at Figure 21, the ratio of the control inputs are close to each other after the velocity becomes higher than 1 Mach. To have the same control effectiveness with aerodynamic control and use less thrust vector control, the ratio had been taken 0.87. In order to analyze the chosen ratio's effectiveness and give an idea to hybrid control ratio decision, an optimization process has been supplied. The optimization algorithm finds the optimal hybrid control ratio K which couples both of the control inputs given at (8.4) and optimizes its trajectory during the flight. Here, (8.4) is given to simplify the problem and remind the term hybrid control ratio. However, the hybrid control ratio is changed in the nonlinear simulation.

$$\begin{aligned} \dot{x} &= Ax + B_A u_1 + B_T u_2 \\ \dot{x} &= Ax + (B_A + KB_T)u \end{aligned} \tag{8.4}$$

where A is system matrix, B_A is the control input of aerodynamic control, B_T is the thrust vector control input matrices and the K is hybrid control ratio defined in section 4.6.

In order to find an optimal hybrid control ratio, different points are defined. Missile is trying to reach the desired points and optimization algorithm is trying to find a feasible trajectory and hybrid control ratio. So, problem formulation of the optimization can be given as;

- Minimize maneuver time
- Minimize miss distance
- Minimize control effort which of all define the cost function below:

$$minimize\ J$$
$$J = t_f + R_c^2 + \left(\int_0^{tf} \|u\|^2 dt\right) \tag{8.5}$$

The constraints are;

$$\begin{aligned} -20^\circ \le u \le 20^\circ \\ -350^\circ / s \le q \le 350^\circ / s \\ -90^\circ \le \alpha \le 90^\circ \end{aligned} \tag{8.6}$$

As seen from the Table 13, hybrid control ratio increases whenever missile needs to get close to a lower altitude. This result was an expected result, because missile needs more acceleration to go a critical point such as 50 meters above ground which means more control power requirement. Another result is the increase in the final time of the maneuvers; on the contrary initial distance to the desired point is decreasing. This result is also a result of a critical maneuver needs more time to be successful. Miss distances are all less than 1 meter which is quite well. This result remarks that an optimal trajectory is also found with real coded genetic algorithm search method. Figure 105, Figure 106, Figure 107 and Figure 108 shows the best trajectories and velocities of each point at each generation. Throughout generations, miss distance is decreasing, but a generalization for final time cannot be made directly, because at each flight the traveled distance is changing.

In conclusion, if a vertical launch missile control system will be a hybrid control, the mechanical coupling ratio has to be considered with respect to the critical maneuver. In this study, the ratio has been changed between 0.5 and 2.5. This optimization study says that, the chosen ratio which was taken into account at the early stages of the thesis is quite proper which defines the critical maneuver between 100 and 300 meters altitude.

Table 13 Optimization Results for Trajectory and Hybrid Control Ratio

Desired Positions (m)	Miss Distance (m)	t_{final} (s)	Hybrid Control Ratio
[1000;0;-50]	0.60	3.23	0.957
[1000;0;-100]	0.74	3.17	0.909
[1000;0;-300]	0.56	3.11	0.81
[1000;0;-500]	0.33	3.18	0.673

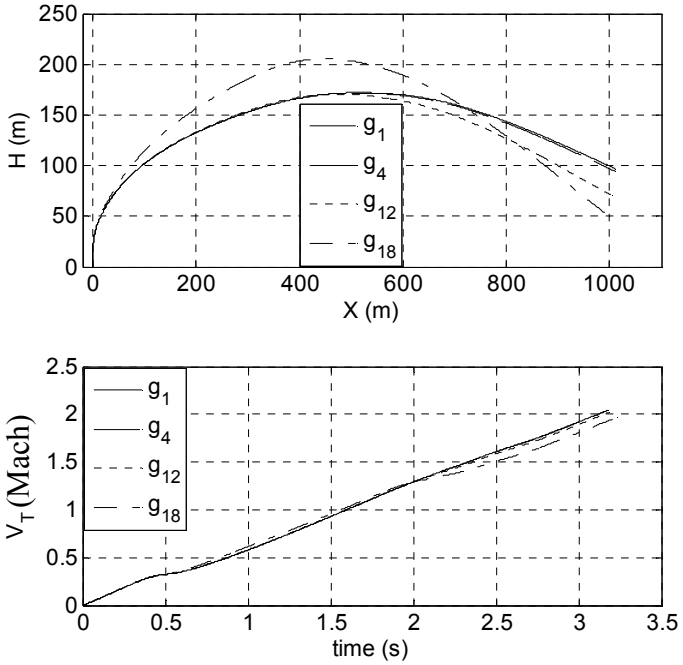

Figure 105 Trajectories and Velocities for Position 1

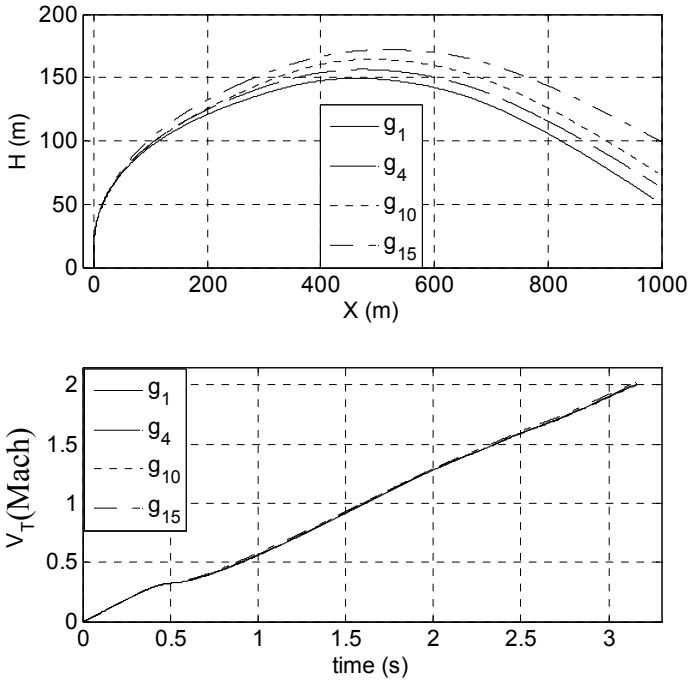

Figure 106 Trajectories and Velocities for Position 2

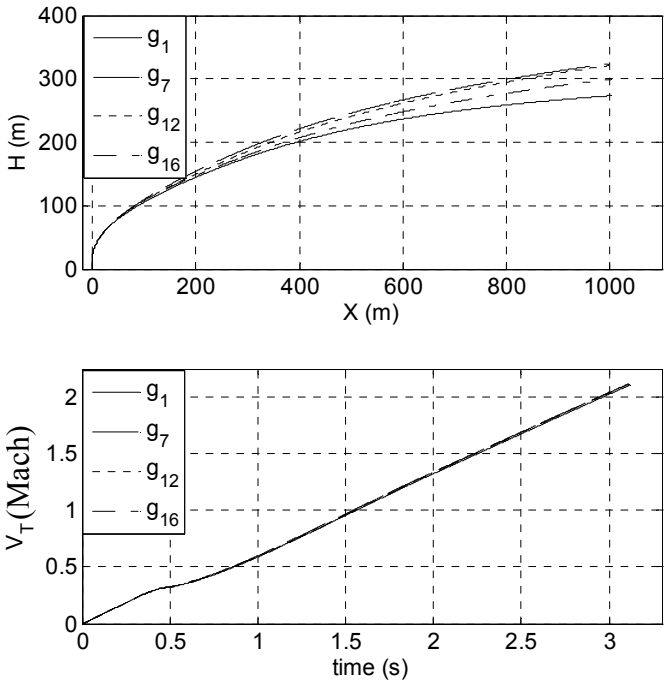

Figure 107 Trajectories and Velocities for Position 3

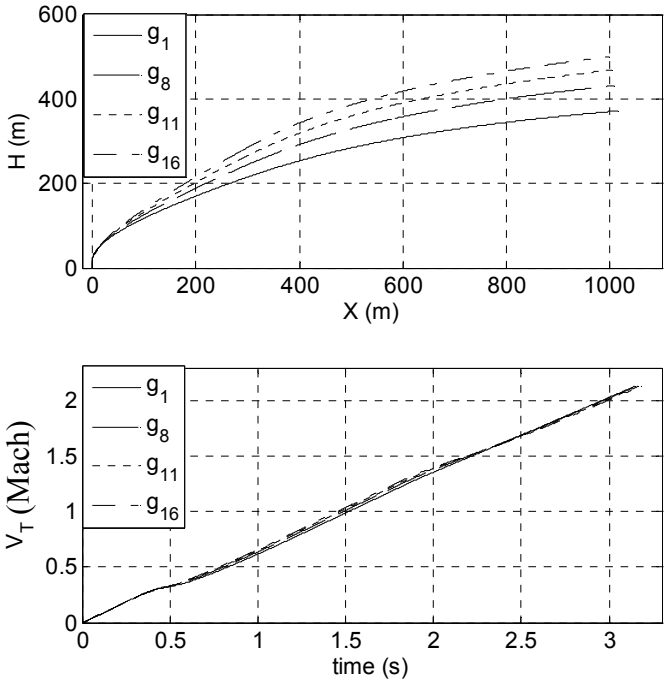

Figure 108 Trajectories and Velocities for Position 4

8.4. Engagement Initiation Maneuver Optimization

In the initial phase where missile is not yet pointed to the target, an initial guidance can be defined that missile will be pointed to the target at the end of the initial guidance that the maneuver in this phase is the engagement initiation maneuver. After missile is pointed to the target, midcourse and terminal phase guidance algorithms will be active. This pointing procedure is quite similar to trainable launcher application, but here pointing missile to the target is a part of missile guidance and control system not launcher's mission and it is much more applicable rather than trainable launcher. Launcher needs more space to turn 360º; however missile can be pointed in any direction with its guidance and control system without increased space need. There may be also other reasons for defining engagement initiation maneuver; for example jet vanes may erode or thrust vector control section is thrown away after turnover maneuver in order to inherit thrust loss and extra weight of thrust vector control unit and because of these reasons, initial guidance will be critical.

In the section, guidance of a vertical launch missile has been divided into three phases; initial which is for engagement initiation, midcourse and terminal phases, illustrated in Figure 109, and an optimization algorithm is applied in order to have an optimal engagement initiation. In such an algorithm, elapsed time for maneuver and successful pointing will be very critical. After engagement initiation, it is important that missile can see or track the directed point and lock on the target. Another critical parameter is the control effort, in other words energy optimization has to be taken into consideration. To sum up, the cost function used for initial guidance, the expressions are formulated in Eq. (8.7). Cost function is normalized with maximum time, control effort and κ defined in Eq. (8.8). κ includes the maximum term and also the square of look angle in order to have more effect. In Eq. (8.7), ξ_1, ξ_2 and ξ_3 are weighting coefficients, ε is look angle, u is control effort. $t_{f\max}$ and $\varepsilon_{f\max}$ are the maximum values of maneuver time and look angle. $U_{Normalize}$ is the maximum value for the energy cost. Results are normalized with respect to these maximum values.

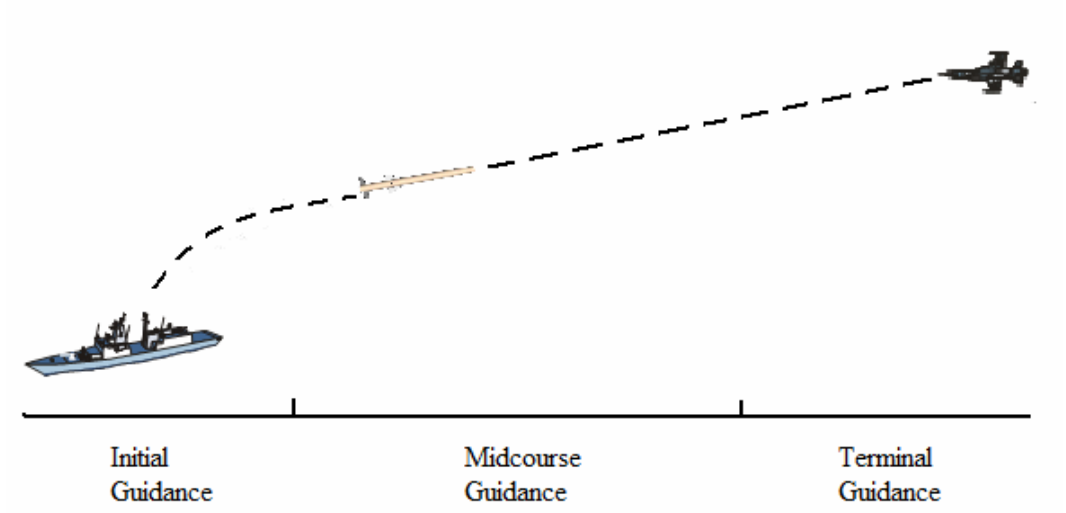

Figure 109 Guidance Strategy

$$minimize\ J$$

$$J = \xi_1 \frac{t_f}{t_{f\,max}} + \xi_2 \frac{\kappa}{\kappa_{max}} + \xi_3 \left(\frac{\int_0^{tf} \|u\|^2\, dt}{U_{Normalize}} \right) \tag{8.7}$$

$$\begin{aligned} k &= max\ \begin{bmatrix} 0 & 3-\varepsilon & -3-\varepsilon \end{bmatrix} \\ \kappa &= k + \|\varepsilon\|^2 \end{aligned} \tag{8.8}$$

Constraints of dynamical systems are obliquely the constraints of the optimization algorithm which are given in Eq. (8.6).

Table 14 Parameters for Engagement Initiation Maneuver Optimization

Parameter	Value
$t_{f\,max}$	1.5 s
κ_{max}	12
$U_{Normalize}$	0.2
ξ_1	0.4
ξ_2	0.3
ξ_3	0.3

Optimization results are summarized in Table 15. Some positions are defined and some initial look angles related with the given positions are presented as example look angles. Maximum fitness function, final time and velocity at the final time are also shown in order to make comparison. Time to point the missile to a direction that target is in the field of view, is decreasing as initial look angle is decreasing and maximum velocity is decreasing as a consequence of this result. Look angles progress for each example throughout generations are presented in Figure 110, Figure 111 and Figure 112. Progress trend of each example differs, because of wide range of initial condition of populations and mutation success. If Figure 112 is analyzed carefully, initial guidance problem turns into initial guidance command

problem. For initial look angle less than 50 degrees, an optimal guidance command for maximum 0.2 seconds is optimal initial guidance starting command.

Table 15 Optimization Results for Several Look Angles

Example	Initial Look Angle (°)	Position (m)	Max. Fitness	t_{final} (s)	Velocity (Mach)
1st	83	[1000;0;-30]	4.94	0.525	0.329
2nd	73	[1000;0;-300]	4.94	0.522	0.33
3rd	63	[2000;0;-1000]	4.92	0.445	0.308
4th	53	[2000;0;-1500]	4.93	0.414	0.294
5th	26.6	[2000,0;-4000]	4.95	0.335	0.246

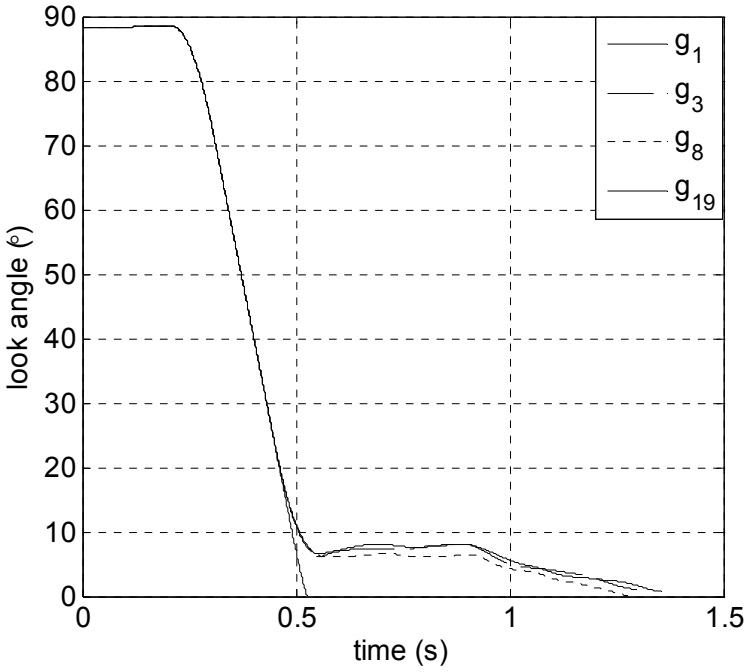

Figure 110 Look Angle Progress of the 1st Example

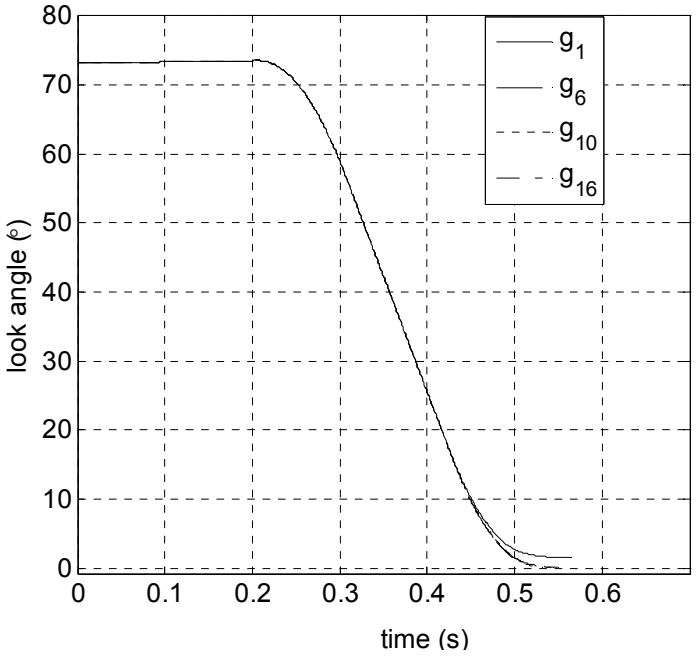

Figure 111 Look Angle Progress of the 2nd Example

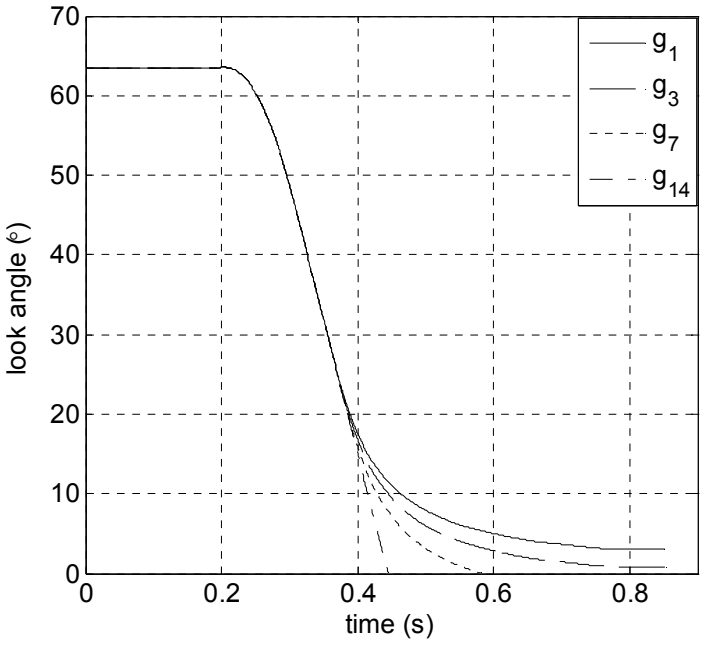

Figure 112 Look Angle Progress of the 3rd Example

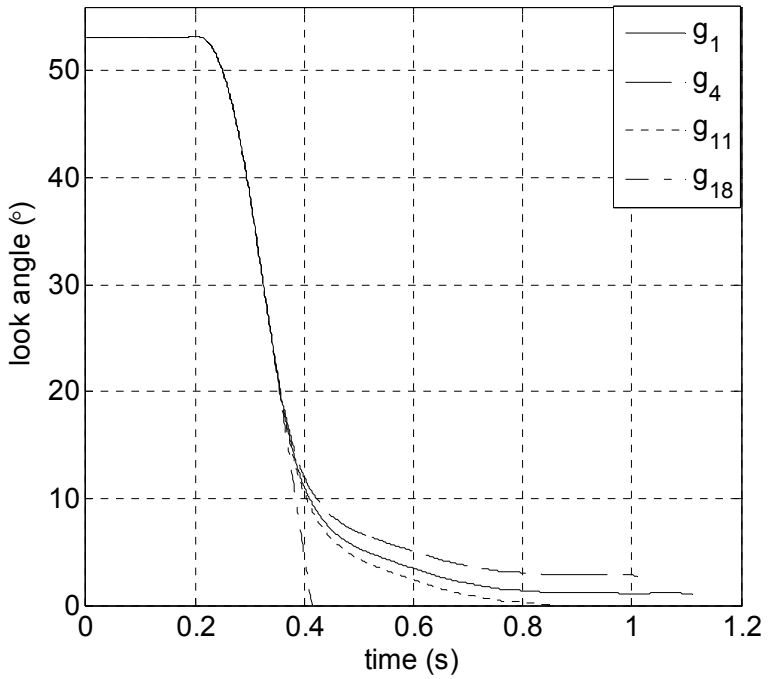

Figure 113 Look Angle Progress of the 4th Example

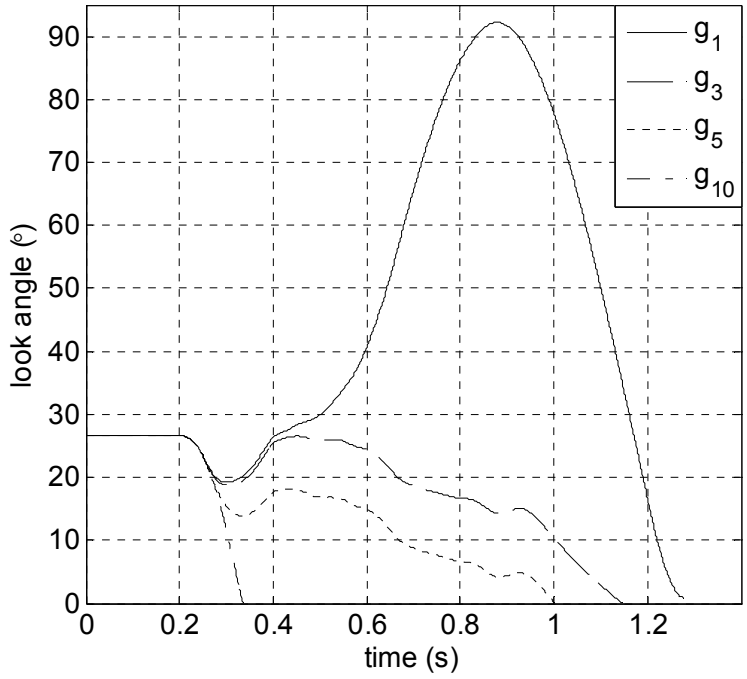

Figure 114 Look Angle Progress of the 5th Example

8.5. 3D Engagement with Sub-Optimal Initial Guidance

In this section the guidance commands obtained from optimizations, which are calculated for the engagement initiation, are used within a 3D engagement scenario considering the 6 DoF motion of the missile. In order to apply this test case, the calculated optimal guidance commands, that steers the missile towards to the targets defined in the previous section, are defined as a discrete function of look angle. In order to calculate the command values with respect to the instantaneous look angles a look up table is constructed using the results of the previous section. Thus, the pre-determined optimal guidance commands are constructed to cover the possible defense volume of the missile in a "sub-optimal" fashion.

Since the optimal guidance commands are already generated for pitch plane, if the missile rolls initially to orient its body pitch plane motion to the same plane with the target, this proposed that sub-optimal engagement initiation strategy can be applied. After sub-optimal guidance phase with initial roll maneuver, midcourse and terminal guidance algorithms, proposed in the Chapter 6, are applied with the same switching criteria. Figure 115 shows the suggested guidance strategy. An example scenario is applied for this guidance strategy. The target's properties are given in Table 16. This target has maneuver weaving maneuver in pitch and yaw planes.

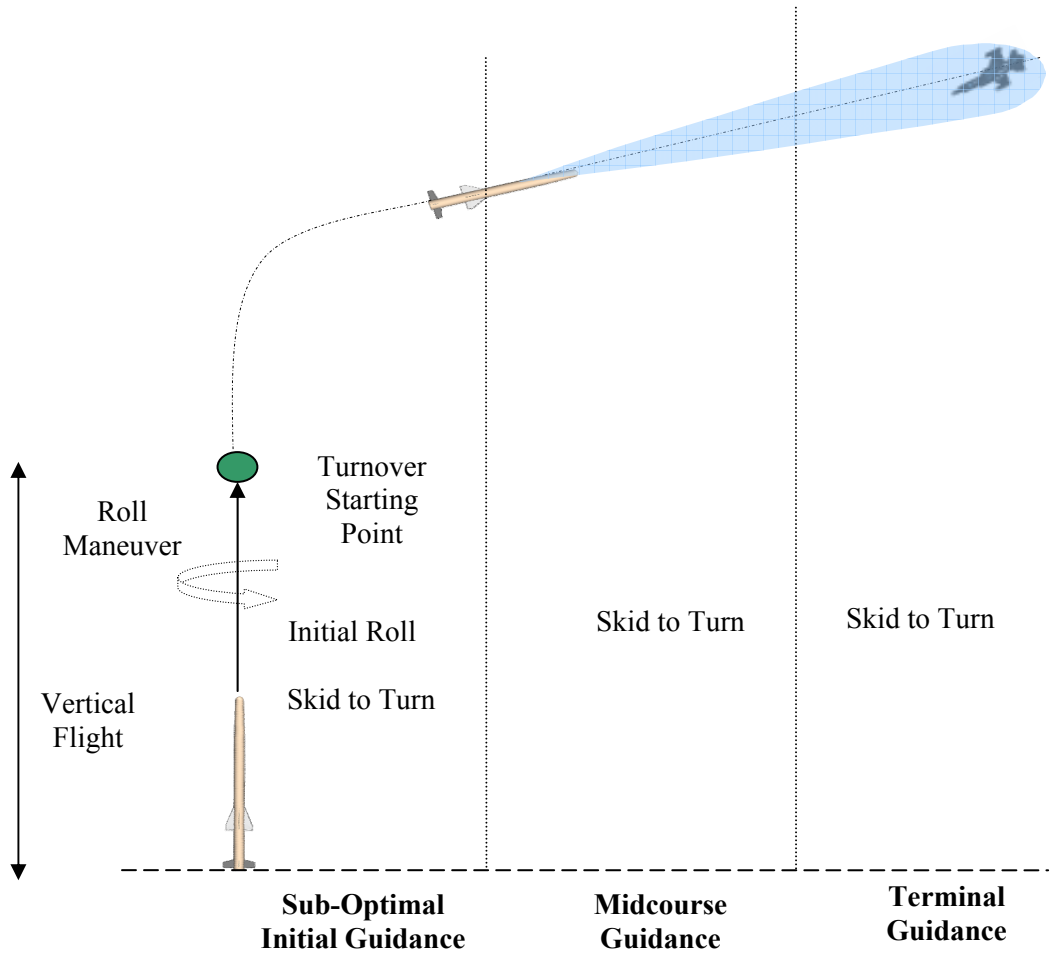

Figure 115 Guidance Strategy for 6 DOF Motion

Table 16 Target Properties for the Suggested Guidance Strategy

Initial Position (m)	[6000; -3000; -2500]
Initial Velocity (m/s)	$[-200 \quad 0 \quad 0]$
Maneuver	Starts maneuvering at 2000 m closing distance the with acceleration $a_y=5.g.\sin(0.1.\pi.t)$ $a_z=5.g.\sin(0.1.\ \pi.t)$

Figure 116 presents the missile and target trajectory, as target has maneuver both in pitch and yaw planes, and a constant velocity, all of the combinations of motion at

each plane is given. Figure 117 shows velocity, angle of sideslip and attack. In the midcourse phase missile has not a significant angle of side slip because of initial roll maneuver. More than 20 degrees of angle of attack is seen in the optimal initial guidance and midcourse guidance phases. Figure 118 illustrates the body rates of the missile during flight. Although at the end of midcourse, body rates are quite inconsiderable, as the guidance switches to terminal guidance body rates again increase. Miss distance is 0.815 meters. Figure 119 illustrates the roll angle during flight and Figure 120 shows the initial guidance command the look angle during the initial guidance command.

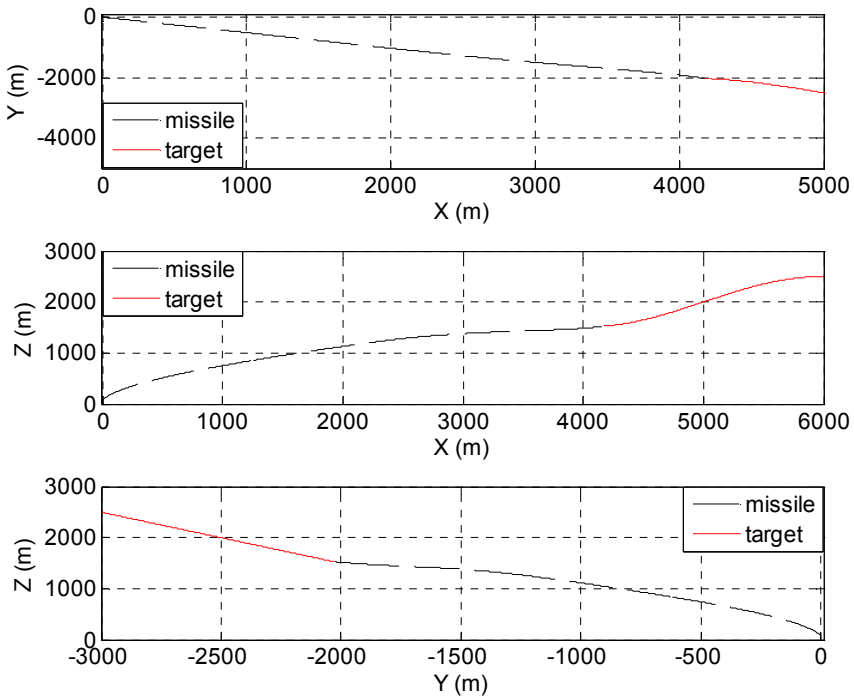

Figure 116 Missile Target Trajectory

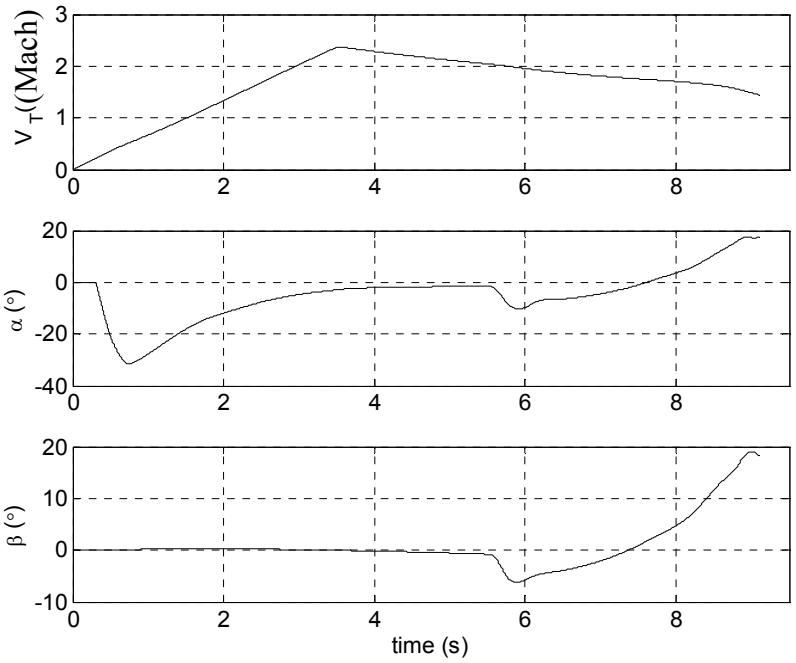

Figure 117 Velocity, Angle of Attack and Sideslip Angles

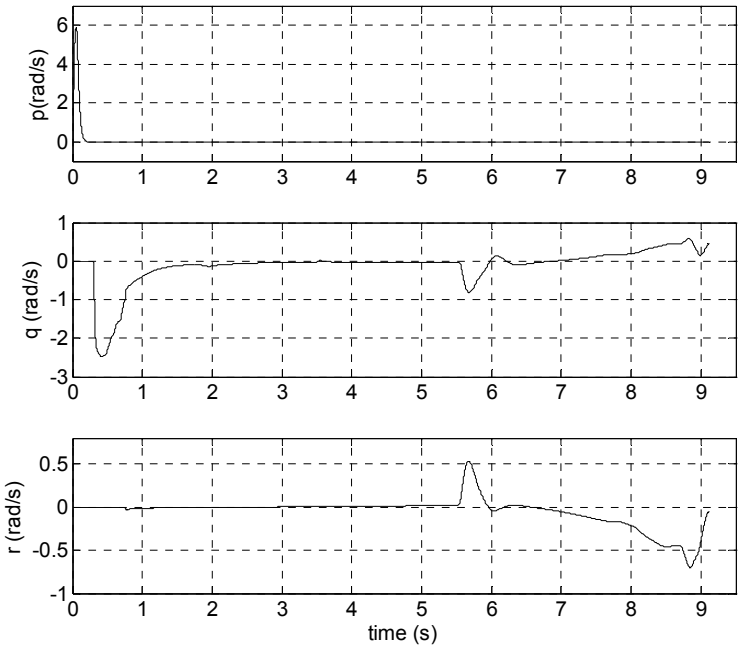

Figure 118 Body Rates of the Missile

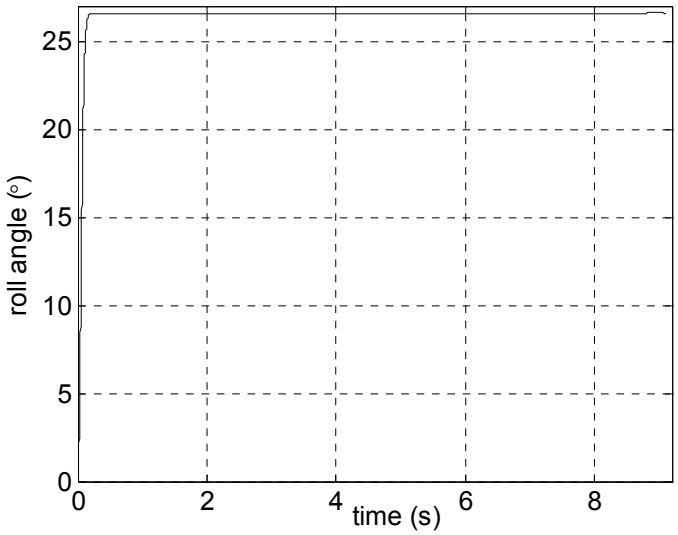

Figure 119 Roll Angle

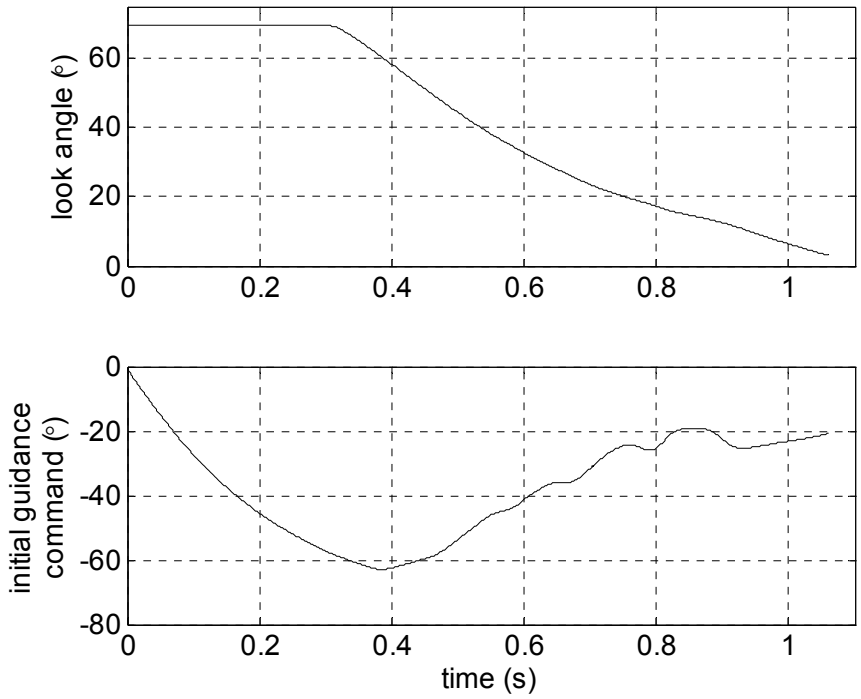

Figure 120 Sub-Optimal Guidance Command and Look Angle

CHAPTER 9

DISCUSSION AND CONCLUSION

The aims of this study is to obtain a nonlinear model for a generic hybrid controlled VLSAM, and analyze the constructed system under the effect of high angle of attack flight characteristics by 6 DoF simulations and linearization.

The dynamic modeling of VLSAM is carried out by implementing the well-known Newton-Euler equations with rigid body assumptions including thrust vector forces and moments. This is followed by aerodynamic data construction. On the contrary to the investigated literature, in which there is limited aerodynamic data with limited numerical parameters due to confidentiality purposes, a new and complete aerodynamic data base over a wide range of angle of attack values is generated. This is generally done by using a semi-empirical aerodynamic data estimation tool, Missile DATCOM. However, in order to complete the aerodynamic data set, the generated set is tailored and extrapolated to $\alpha \leq 90°$ flight regime. The general tendencies of the aerodynamic coefficients with respect to different velocities are presented and analyzed. Static stability and aerodynamic characteristics are analyzed and results are discussed. After then, the accuracy and validity of the constructed VLSAM model is investigated by 6 DoF nonlinear simulations.

In order to design autopilot a linearization algorithm is carried on. Since the system under study has two different flight phases as the first phase where there is thrust and the second phase without thrust, which are different from each other, the linearization of the missile dynamics is separated in two different categories. Since

time is the most dominant parameter that affects the thrust, impulse, and, the mass, inertia, center of gravity of the missile and the velocity variation of the missile in that phase, the scheduling is done with respect to time for the boost phase. Linearization scheduling is done with respect to velocity as it is done in the in the conventional systems, for the second phase. After the linearization study, the accuracy and validity of the linearized model are tested. This is done by comparing the outputs of the linear system model with the outputs of the nonlinear system model, under the effect of the control input commands, jet vanes and tail fins. The nearly perfect match of the linear and nonlinear system outputs showed that the scheduling with respect to time for the first phase and scheduling with respect to velocity for the second phase of the flight can be used reliably for the linear system models. Following the linearization of the nonlinear dynamics, with the proposed scheduling methods, control sensitivity and stability analysis of the missile for the vertical launch phase is carried out. This analysis showed that the kinetic energy of the missile decreases with decreasing velocity. This causes the eigen values of the linear system move to the right hand side of the imaginary axis.

Missile dynamics are separated into three planes, pitch, yaw and roll after linearization. Controllers are designed as the missile is a skid-to-turn missile. Controllers design is also challenging as the system parameters are changing rapidly. Body rate, angle and acceleration autopilots are designed with classical approaches. The reasons behind the different autopilot types are to examine different dynamic behaviors and to be adaptable to guidance requirements. As autopilot design phase is considered before the design of guidance algorithms, autopilot has to respond the guidance command and/or conversion logic has to be designed. Autopilot performances are tested in the nonlinear model. According to the outputs, designed autopilots have different performance characteristics. Angle autopilot has the best performance than rate autopilots. This autopilot is compensating the fast dynamics in the inner loop, and the outer loop compensates the relatively slow dynamics. Moreover, the other autopilot types can also be used with proper guidance algorithms.

Next, body pursuit guidance as midcourse guidance and proportional navigation guidance for terminal guidance are studied and implemented. Switching conditions from midcourse to terminal are determined. For yaw and pitch planes, angle autopilots are chosen for the midcourse guidance phase and acceleration autopilot is used for the terminal phase. In the roll plane body rate autopilot is preferred for all of the flight time. After guidance algorithms are implemented, target sets are defined and categorized into two sets as non maneuverable and maneuverable. The first target set includes a low altitude static target and a target which is crossing and diving with constant velocities is chosen. The second target set consists of maneuverable targets, one is an oncoming target and the other is a target that has a weaving maneuver in the terminal phase. The nonlinear simulations with the designed autopilots and guidance algorithms have successful results on the target sets. Some critical parameters such as angle of attack and side slip, body rates, accelerations and trajectories are also presented.

In addition to guidance and autopilot algorithm development, a different turnover strategy is suggested. Here, missile has an initial roll maneuver in order to be in the same vertical plane with the target during vertical launch and so, missile has less acceleration in yaw plane and has significantly less angle of side slip. The comparison of initial roll maneuver with thrust vector control or aerodynamic control is also examined. Differences of the roll maneuver with aerodynamic and thrust vector control surfaces are shown and conclusions are presented, then. As it is not possible to control the missile with aerodynamic control surfaces when the missile velocity is close to 0, initial roll maneuver with aerodynamic control causes nothing but very close skid-to-turn mode and missile has angle of sideslip because of that. However, initial roll maneuver with thrust vector control does not have any angle of sideslip for the same target. This result was an expected results and the importance of thrust vector control in the initial phase of the missile is thus exhibited.

The last part of the thesis includes some critical maneuver optimizations. All of the optimization algorithms produce guidance commands. Open loop guidance

commands are performed by autopilots. In this section, a rapid turnover maneuver optimization is carried on firstly. The aim of this is to optimize the most critical maneuver for a very low altitude target. The second optimization problem is studied for suggesting a methodology to define the hybrid control ratio which is a mechanical coupling and has a preset value. In this methodology, some critical positions are chosen and the missile is guided to these points optimally. Miss distance and hybrid control ratios are presented. In this search, it is obtained that for a critical maneuver missile needs more control power as expected. So, it can be clearly said that hybrid ratio can be pre-set with respect to the desired tactical requirements. Lastly, engagement initiation maneuver optimization is studied and initial guidance commands are generated. The first aim of this optimization is to search for the optimal guidance commands to direct the missile to the target. The second aim is to define criteria for thrust vector usage. As it is well known, in some applications jet vanes are not in use for the whole flight time. As the jet vanes are the cause of extra drag, they result in some decrease in velocity. Thrust vector control unit may be preferred to be erodable or they may be jettisoned during flight. The problem is to determine the maximum duration that the jet vanes have to be effective. Here, the guidance commands are found which yields answers to the problems above implicitly. In order to merge the open and closed loop guidance, the optimal open loop guidance commands are generated for some initial look angles and interpolated. The different turnover strategy and the open loop guidance command set is implemented for the nonlinear simulation. Open loop guidance commands are scheduled with respect to the look angle. This strategy is performed with a maneuvering target. A miss distance less than 1 meter is obtained.

We think that the present study needs some improvements in the following issues:

1. Intercept maneuvers can be enlarged to cover all the space with a varying hybrid control ratio (two actuators for two control surfaces as in some applications) and it can be developed for intercept positioning instead of body pursuit midcourse guidance.
2. Full range guidance algorithms can be developed by merging the initial TVC regime with the aerodynamic tracking guidance regime.

3. Developed controllers / autopilots can be improved by using more advanced controller design techniques such as adaptive control.
4. Controllers are going to be developed which utilizes all the control surfaces at the same time.

We plan to continue our academic work in these topics and a set of publications will be prepared.

REFERENCES

[1] M.J. Hemsch, "Tactical Missile Aerodynamics: General Topics", Vol. 141, Progress in Astronautics and Aeronautics, AIAA, Washington DC. 1992.

[2] P. Zarchan, "Tactical and Strategic Missile Guidance", Vol. 124, Progress in Astronautics and Aeronautics, AIAA, Washington DC. 1990.

[3] K. A. Wise, D. J. Broy, "Agile Missile Dynamics and Control", Journal of Guidance, Control and Dynamics, Vol. 21, No. 3, June 1996.

[4] A. Thukral, M. Innocenti, "A Sliding Mode Missile Pitch Autopilot Synthesis for High Angle of Attack Maneuvering", J. Propulsion, Vol. 6, No. 3, May 1998.

[5] A. Facciano, K. Seybold , T. Kutz ,D. Widmer, "Evolved Seasparrow Missile Jet Vane Control System Prototype Hardware Development", J. Spacecraft and Rockets, Vol. 39, No. 4, pp. 522-531, 2002.

[6] R. Solis, "An Analysis of the Vertical Launch Phase of a Missile Concept", AIAA, Aerospace Sciences Meetings, January 1983.

[7] C.Y. Kaya, "Thrust Vector Control of a Rocket Vehicle Associated with Aerodynamic Control", M. S. Thesis Mechanical Eng., METU, October 1989.

[8] E. Erdem, "Thrust Vector Control with Secondary Injection", M. S. Thesis Mechanical Eng., METU, September 2006.

[9] Ö. Atesoglu, "High Alpha Maneuvering and Stabilization Control of Flight Vehicles", Phd. Thesis Mechanical Eng., METU, July, 2007

[10] http://en.wikipedia.org/wiki/Vertical_launching_system_20_05_2010.

[11]http://defense-studies.blogspot.com/2010/07/hmasnewcastle-and-hmas warramunga.html

[12] http://en.wikipedia.org/wiki/File:Buk-M1-2_9A310M1-2.jpg.

[13] www.en.wikipedia.org/wiki/IRIS-T, 12 January 2010.

[14]http://www.deneldynamics.co.za/brochures/Broc0266_Umkhonto-IR%20external.pdf.

[15] www.en.wikipedia.org/wiki/MBDA_MICA, 14 January 2010.

[16] http://en.wikipedia.org/wiki/LFK_NG, 14 October 2009.

[17] www.en.wikipedia.org/wiki/Umkhonto, 1 February 2009.

[18] Control Actuation System Workshop/System Analysis Reference, Martin Marietta Training Notes, Martin Marietta Inc., 1993.

[19] R.F.H. Woodberry, R.J. Zeamer, "Solid Rocket Thrust Vector Control", NASA-SP-8114, 1974.

[20] http://www.armscontrolwonk.com/images/1472.jpg.

[21]http://www.knovel.com/web/portal/browse/Thrust_Vector_Control.

[22] P. H. Reisenthel, "Development of a Nonlinear Indicial Model for Maneuvering Fighter Aircraft", AIAA Aerospace Sciences Meeting, 1996.

[23] M. Y Park, W. Kim, S. Kim, S. H. Park and J. W. Lee, "Asymmetric Vortices Around a Body in a High Angle of Attack Supersonic Flow" Journal of the Korean Physical Society, Vol. 55, No. 5, November 2009.

[24] H. Sadeghi, M. Mani, M. A. Ardakan, "Effect of Amplitude and Mean Angle of Attack on Wake of an Oscillating Airfoil", World Academy of Science, Engineering and Technology, 2008.

[25] E. Abney, M. McDaniel, "High Angle of Attack Aerodynamic Predictions Using Missile Datcom", AIAA Applied Aerodynamics Conference, June 2005.

[26] Ö. Ateşoğlu, "Different Autopilot Designs and Their Performance Comparison for Guided Missiles", M .S. Thesis Aerospace Eng., METU, December 1996.

[27] P.K. Menon, E. J Ohlmeyer," Integrated Design of an Agile Missile Guidance and Control Systems", Proceedings of the 7th Mediterranean Conference on Control and Automation (MED'99), June 1999.

[28] E. Orbekk, "Thrust Vector Model and Solid Rocket Motor Firing Validations", 44th AIAA/ASME/SAE/ASEE Joint Propulsion Conference and Exhibit, July 2008.

[29] A. I. El-Sharkawy, "Experimental Studies on Thrust Vector Control in Solid Propellant Rockets", 13rd AIAA/SAE Propulsion Conference, July 1977.

[30] G. Sung, Y. S. Hwang, "Thrust-Vector Characteristics of Jet Vanes Arranged in X-Formation within a Shroud", Journal of Propulsion and Power, Vol. 20, No. 3, 2004.

[31] E. Orbekk, “Novel TVC System Utilizing Guide Vanes With Jet Flap’s İnto A High Efficiency Compact Nozzle”, 41st AIAA/ASME/SAE/ASEE Joint Propulsion Conference and Exhibit, July 2005.

[32] P.A Giragosian, “Theoretical and Experimental Aerodynamic Correlation of Jet Vane Control Effectiveness, AIAA Atmospheric Flight Mechanics Conference, August 1981.

[33] V. Harrisson, A. deChamplin, D. Kretschmer, R. Farinaccio, R. A. Stowe, “Force Measurement Evaluating Erosion Effects on Jet Vanes for a Thrust Vector Control System ”, 39th AIAA/ASME/SAE/ASEE Joint Propulsion Conference and Exhibit, July 2003.

[34] R. Tekin, Ö. Atesoğlu, K. Leblebicioğlu, “Modeling and Vertical Launch Analysis of an Aero- and Thrust Vectored Surface to Air Missile”, AIAA GNC/AFM/MST/ASC/ASE Conference, August 2010.

[35] http://www.scribd.com/doc/12515933/Tactical-Missile-Design-Presentation-Fleeman, 02_17_2009.

[36] L. H. Smith, R. H. Nunn, “Aerodynamic Characteristics of an Axisymmetric Body Undergoing a Uniform Pitch Motion”, J. Spacecraft, Vol. 13, No. 1, January 1976.

[37] J. E. Fidler, M. C. Bateman, “Asymmetric Vortex Effects on Missile Configurations”, J. Spacecraft, Vol. 2, No. 11, November 1975.

[38] A. B. Wardlaw Jr., A.M. Morrison, “Induced Side Forces on Bodies of Revolution at High Angle of Attack”, J. Propulsion, Vol. 3 No. 10, October 1976.

[39] H. Jorgensen, “Reduction of Static Aerodynamic Characteristics for Slender Bodies with Lifting Surfaces at very High Angle of Attack”, NASA TR R-474, September 1977.

[40] J. Nielsen, “The Present Status and the Future of Missile Aerodynamics”, NASA N88-29773, January 1988.

[41] Martin Marietta, “Aerodynamic Stability Technology for Maneuverable Missiles”, AFFDL-TR-76-55 Vol. 1, March 1979.

[42] P. Giragosian, “Aerodynamic Considerations in the Design of a Vertically Launched, Advanced Interdiction Missile”, AIAA Atmospheric Flight Mechanics Conference, August 1982.

[43] D. E Lesieutre, J. Love, M. Dillenius, “High Angle of Attack Missile Aerodynamics Including Rotational Rates-Program M3HAX”, Atmospheric Flight Mechanics Conference, July 1996.

[44] P. Liu, X. Deng, “Experimental Investigation of Aerodynamic Characteristics on Slender Bodies at High Angle of Attack”, Vol. 49, No. 1, March 2003.

[45] E. Smith, S. Hebbar, M. Platzer, “Aerodynamic Characteristics of a Canard Controlled Missile at High Angle of Attack”, Journal of Spacecraft and Rockets, Vol. 31, No. 5, October 1994.

[46] R. Tekin, Ö. Ateşoğlu, K. Leblebicioğlu, “Bir Hava Savunma Füzesinin Dikey Fırlatma Fazının ve Etkin Dönme Manevralarının İncelenmesi”, 5. Savunma Teknolojileri Kongresi, June, 2010.

[47] S. Wassom, L. Faupell,” Integrated Aerofin/Thrust Vector Control for Tactical Missiles”, J. Propulsion, Vol. 7, No. 3, June, 1991.

[48] E. Devaud, H. Siguerdidyane, S. Font, “Some Control Strategies for a High Angle of Attack Missile Autopilot”, Control Engineering Practice 8, pp. 885-892, 2003.

[49] H. Buschek, M. McDaniel, “Design and Flight Test of a Robust Autopilot for IRIS-T Air to Air Missile”, Control Engineering Practice 11, pp. 551-558, 2003.

[50] H. Buschek, “Full Envelope Autopilot Design Using Gain Scheduled Robust Control”, Journal of Guidance, Control and Dynamics, Vol. 22, No. 1, pp. 115-122, 1999.

[51] R. Tekin, Ö. Ateşoğlu, K. Leblebicioğlu, “Hibrit Kontrollü - Dikey Fırlatılan Bir Hava Savunma Füzesinin Dinamiği ve Hızlı Dönüş Manevrası için Otopilot Tasarımı”, Otomatik Kontrol Ulusal Toplantısı, September 2010.

[52] C. Song, “Adaptive Control of Linear Time Varying Systems with Applications to Missile Autopilots”, Phd. Thesis, University of Florida, 1989.

[53] A. Tsourdos, B. A. White, Adaptive Flight Control Design for Nonlinear Missile”, Control Engineering Practice,Vol. 13, No. 3, pp.373-382, 2005.

[54] T. B. Mull, “Use of Minimum Time Controllers in Vertically Launched Surface to Air Missiles “, Master Thesis, Naval Postgraduate School, June 1992.

[55] K. S. Erer, R. Tekin, “İleri Hız Değişiminin Füze Yanal Dinamiğine Etkileri Üzerine Bir İnceleme“, Otomatik Kontrol Ulusal Toplantısı, September 2010.

[56] K. Ogata, “Modern Control Engineering”, Prentice Hall, 4th Edition, 2002.

[57] A. Arrow, D. E. Williams, “Comparison of Classical and Modern Missile Autopilot Design and Analysis Techniques”, J. Guidance, Vol. 12, No.2, pp. 220-227, 1987.

[58] R. Tekin, Ö. Ateşoğlu, K. Leblebicioğlu, “ Çevik Füze Dinamiği ve Denetimi Üzerine Temel İncelemeler”, Ulusal Havacılık ve Uzay Konferansı, September 2010.

[59] http://acgsc.org/Meetings/Meeting_97/General%20Session/4.2.2.1.ppt.

[60] H.O. Jonnson, G. Malmberg, “Optimal Thrust Vector for Vertical Launch of Tactical Missiles”, Journal of Guidance, Control, and Dynamics, Vol. 5 No. 1, pp: 17-21, 1982.

[61] J.H. Holland, “Adaptation in Natural and Artificial Systems“, University of Michigan Press, Ann Arbor, MI, 1975.

[62] D.E Goldberg, “Genetic Algorithm in Search, Optimization, and Machine Learning”, Addison-Wesley, Reading, MA, 1989.

[63] D.M. Etter, M.J. Hicks, K.H. Cho, “Image Registration by Genetic Search” Proc. IEEE Soueastcon’84, pp. 460–464, 1984.

[64] K. Kristinsson, D.A Dumont, “Genetic Algorithms in System Identification”, 3rd IEEE Int. Symp. Intell. Contr., Arlington, VA, pp. 597–602, 1988.

[65] L.S Crawford, V.H.L Cheng, P.K. Menon, “Synthesis of Flight Vehicle Guidance and Control Laws Using Genetic Search Methods”, AIAA Guidance and Navigation Conference, August 1999.

[66] C.L. Lin, R-M. Lai, “Parameter Design for a Guidance and Control System Using Genetic Approach”, Aerospace Science Technology 5, pp: 425–434, 2001.

[67] A. H. Kasem, “Trajectory Optimization via Simulation Using Incremented Genetic Algorithms”, the Canadian Aeronautics and Space Journal, Vol. 52, No. 1, March 2006.

APPENDIX

THRUST VECTOR CONTROL MODELING

Jet vanes are fins mounted at the exit of a rocket nozzle, Figure 121. The purpose is to deflect part of the flow, thus providing side force. In order to give an idea of the lift force created by a jet vane, a simplified analytical model is presented.

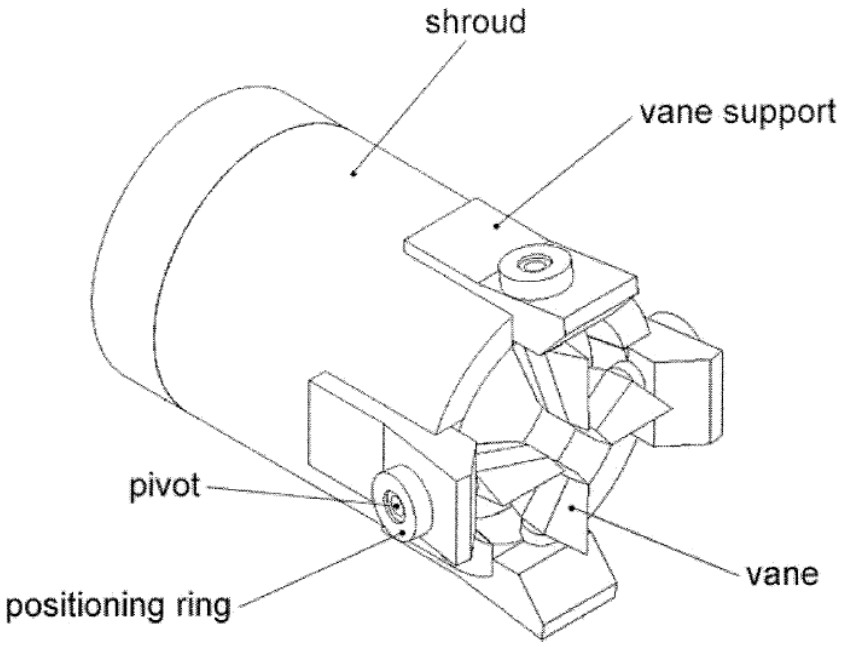

Figure 121 Jet Vane

The simplified model is for jet vanes that are not in a shroud but at the end of the nozzle exit and the position of the jet vanes are important. The lift force produced by jet vanes corresponds to the side force that jet vane system generates. 2D analysis overestimates the lift force generated by a real jet vane. This is caused by wing effects in the supersonic flow. In some references, a constant value is

suggested as a correction factor. In many cases, linear theory is enhanced with experiments and a correction factor is determined for the specific case. However, in order to give a brief idea about thrust vector modeling, these assumptions are not taken into account and basic thrust vector modeling is expressed.

To determine the lift force calculations from linear theory, the following equations can be directly applied. The lift and drag forces on a jet vane is

$$L = \frac{1}{2} P C_L \gamma M_\infty{}^2 S$$

$$D = \frac{1}{2} P C_D \gamma M_\infty{}^2 S$$

where

- P : Pressure
- M_∞ :Velocity at the exit of the nozzle
- S : Reference surface
- γ : Specific heat ratio
- C_L and C_D : Lift and drag coefficients of the jet vane
- L : Lift
- D : Drag

and

$$S = c.s$$

where s is span and c is chord of the jet vane.

It is also possible to define S, the reference surface as function of time as there is erosion on the surface of the vane with respect to the vane material and motor output materials.

The lift and drag coefficients are

$$C_L = \frac{4\delta}{\sqrt{M_\infty{}^2 - 1}}$$

$$C_D = \frac{4}{\sqrt{M_\infty{}^2 - 1}}\left(\delta^2 + \left(\frac{t_k}{c}\right)^2\right)$$

where

δ is deflection of the jet vane, c is chord and t_k is thickness.

Forces generated on the vane opposite of the flow are the cause of the drag force. Total drag force is the sum of the each drag force of each jet vane and it can be expressed as below:

$$T_{loss} = F_{drag1} + F_{drag2} + F_{drag3} + F_{drag4}$$

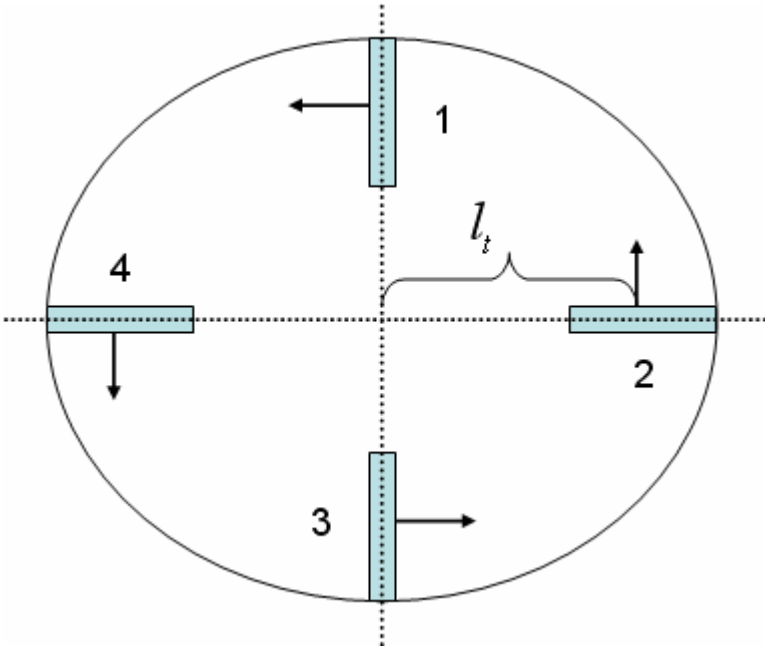

Figure 122 "+" Form Jet Vane Configuration

Thrust forces and moment equations for "+" form jet vane configuration illustrated in Figure 122 is given below:

$$\begin{bmatrix} F_x^T \\ F_y^T \\ F_z^T \end{bmatrix} = \begin{bmatrix} T - T_{loss} \\ F_{Lift1} - F_{Lift3} \\ F_{Lift4} - F_{Lift2} \end{bmatrix}$$

$$\begin{bmatrix} L^T \\ M_y^T \\ M_z^T \end{bmatrix} = \begin{bmatrix} (F_{Lift1} + F_{Lift2} + F_{Lift3} + F_{Lift4}).l_t \\ F_y^T.l_T \\ F_z^T.l_T \end{bmatrix}$$

where T is the main thrust. In this equation, the moments created by drag forces are neglected.

Moment arm in the equation of roll moment created by thrust vector control system is l_t and it is the distance from nozzle center to the center of pressure on the jet vane. The moment arm of roll moment can be expressed as;

$$l_t = d/2 - coP$$

where d is the nozzle exit diameter and coP is the center of pressure.

The moment arm for pitch and yaw moments is, l_T, the distance between center of gravity of the missile and center of gravity of thrust vector control system which is:

$$l_T = x_{cg} - x_{cg\_tvc}$$

Total side force is defined as:

$$T_{side} = \sqrt{F_y^2 + F_z^2}$$

Total thrust deflection angle is

$$\theta = arctan\left(\frac{T_{side}}{T - T_{loss}}\right).$$

Table 17 shows the parameters for a simple jet vane system design for the thesis.

Table 17 Motor and Jet Vane Parameters

Thrust	35000 N
Pressure	368417 Pa
Mach	2.9
Chord, c	0.084 m
Span, s	0.041m
Gamma, γ	1.17
Thickness, t_k	0.009
Roll moment arm, l_t	0.018 m

Table 18 shows the lift and drag forces of one jet vane at 10 and 20 degrees of deflection. 3012 N lift force and 362 N drag force is obtained at 20 degrees of deflection. It is obvious that lift force is a linear function of jet vane deflection but not the drag force.

Figure 123 shows the lift and drag force trend from 0 to 20 degrees of jet vane deflection.

Table 18 Lift and Drag Force Results from Linear Theories

Deflection (°)	Lift(N)	Drag(N)
10	1506	362
20	3012	1150

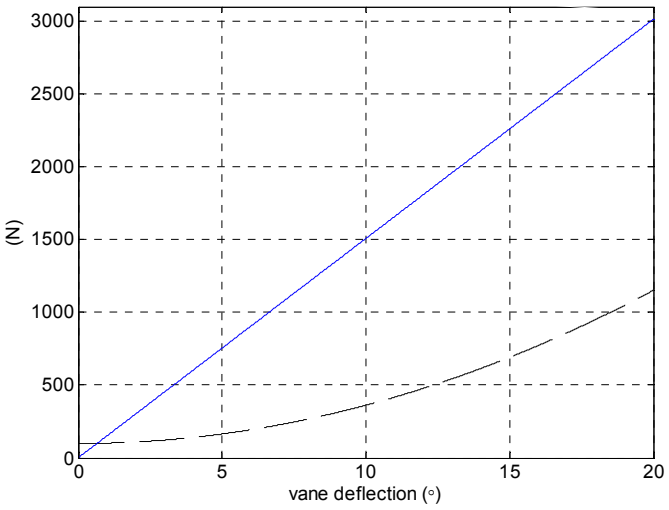

Figure 123 Lift and Drag Force of the Jet Vane

Critic design specifications of this system are given in Table 18. In this system at least, maximum %13.15 of the main thrust is lost because of drag forces. Maximum side force is 8520 N. Maximum roll moment is 217 Nm when if all the jet vanes are deflected for roll motion. Maximum azimuth and elevation angles are 11.21 degrees. The relation between azimuth or elevation deflection and jet vane deflection is $\theta_T = 0.56\delta_{tvc}$. These results are outputs of the linear theory; as it is well known these results are overestimated values. However, a better motor and jet vane can be designed. But this is out of the aim of this thesis.

Table 19 Critical Results from Linear Theories

Thrust Loss	%13.15
Max. Side Force	8520 N
Max. Roll Moment	217 Nm
Azimuth, θ_T	11.21°
Elevation, ψ_T	11.21°